The role of the environmental stress response in aneuploid and cell cycle-arrested budding yeast

by

Allegra Louise Terhorst

B.A. Biology
Cornell University, 2016

SUBMITTED TO THE DEPARTMENT OF BIOLOGY IN PARTIAL FULFILLMENT
OF THE REQUIREMENTS FOR THE DEGREE OF

DOCTOR OF PHILOSOPHY IN BIOLOGY
AT THE
MASSACHUSETTS INSTITUTE OF TECHNOLOGY

SEPTEMBER 2021

Signature of the Author: _____
Department of Biology
May 28, 2021

Certified by: _____
Matthew Vander Heiden
Director, Koch Institute for Integrative Cancer Research
Professor of Biology
Thesis Supervisor

Accepted by: _____
Amy Keating
Professor of Biology and Biological Engineering
Co-Director, Biology Graduate Committee

The role of the environmental stress response in aneuploid and cell cycle-arrested budding yeast

by

Allegra Louise Terhorst

Submitted to the Department of Biology

On May 28th, 2021 in Partial Fulfillment of the
Requirements for Degree of
Doctor of Philosophy in Biology

Abstract

Size matters in eukaryotic cells. Inability to maintain cell size homeostasis, or the coordination between growth and division, has direct consequences on cellular functions and fitness. Eukaryotic cells have developed mechanisms to ensure proper coordination of biomass accumulation and cell cycle progression. Cell growth can regulate cell cycle progression, and cells are required to grow to a "critical size" before entrance into the cell cycle. Much less is known about how cell cycle progression affects biomass accumulation, specifically, what happens to cell growth when cell cycle progression is slowed or halted. Here, I investigate this question using two models of cell cycle delay and arrest in *S. cerevisiae*: aneuploidy and temperature sensitive *cdc* (*cdc-ts*) mutants.

I first show that the environmental stress response (ESR) a gene expression pattern that represses ribosome biogenesis, is activated in both heterogeneous populations of aneuploid cells as well as complex aneuploid strains with one or more additional or lost chromosomes. Although my results here contradict a previous study using heterogeneous aneuploid populations, I show that their heterogeneous aneuploid populations did exhibit the ESR, but their euploid control population was grown into stationary phase, tainting their analysis. I see that in complex aneuploid strains, growth rate correlates to ESR strength and ribosomal fraction of the proteome, but this correlation is lost when strains are grown in a nutrient-limiting chemostat. Furthermore, there is a similar loss of ribosomes in the heterogeneous aneuploid populations. Next, I study size regulation in *cdc-ts* mutants, which arrest in the cell cycle at the restrictive temperature, and also see ribosome downregulation and ESR activation. Similar ESR activation and ribosome loss occurs in cells when either the TORC1 pathway or Ras/PKA pathway is inhibited. When I hyperactivate the Ras/PKA pathway during *cdc-ts* arrests, cells no longer exhibit the ESR and have significant loss of viability. I show that these strains no longer downregulate ribosomes and attenuate cell size growth. These studies have profound insights into how the ESR helps coordinate cell growth and cell cycle progression when the two are uncoupled.

Thesis supervisor: Matthew Vander Heiden
Title: Director, Koch Institute for Integrative Cancer Research; Professor of Biology

For my mentor, Professor Angelika Amon – who endlessly inspires me.

"If I have seen further, it is by standing on the shoulder of giants"

–Sir Isaac Newton

Acknowledgements

First and foremost, I would like to thank my thesis advisor, Angelika Amon. Her brilliance and passion for science kept me on my path toward discovery despite disappointments and failed experiments. She always knew what to say to encourage me, and I miss her dearly.

I was incredibly lucky to have such a supportive thesis committee. Thank you to Matthew Vander Heiden, Gene-Wei Li, and Iain Cheeseman for listening to my work countless times and offering valuable feedback. Thank you to Mike Tyers for participating in my thesis defense and for helping pave the way in the cell size field. Thank you to Frank Solomon who, although not an official member of my thesis committee, has been a wonderful mentor and neighbor.

I would also like to thank the entire Amon Lab, including all past and present members. Thank you to Monica Boselli for providing guidance and support through the most difficult times. Thank you to Gabriel Neurohr and Arzu Sandikci for your contributions to my project. The Amon Lab is an incredibly special group of people that have changed my life for the better.

My friends motivate me to be the best version of myself. Thank you to my lab friends – Becca, Cassie, Summer, Wendy, Teresa, Franny, and Juliet – with whom I've laughed and cried. Thank you to my cohort friends who made me feel welcome at MIT. Thank you to my friends from Cornell who, although spread across the country, are always there for me. And thank you to my oldest friend, Hannah, who somehow still isn't tired of me after a decade of friendship.

Finally, I could not have completed this work without my family. Thank you to my pets – Charlie, Fred, Riley, and Colby. Thank you to my sisters – Isabella and Natasha. And a huge thank you to my parents – Karen and Cox. I love you all with my whole heart.

Table of Contents

Chapter 1: Introduction

Eukaryotic cell size regulation

Among the many fascinating qualities of eukaryotic cells, one particularly remarkable characteristic is their extreme diversity in size (1, 2). Phytoplankton can have a diameter as small as 1 μm, while frog oocytes can grow to a diameter of approximately 1 mm, resulting in a cell volume a billion-fold larger than the phytoplankton (1). Cell size dictates how organisms are organized, proliferate, and function within their surrounding environment (1, 2). Eukaryotic cells have a distinctive challenge of providing space for various sub-compartments, or organelles, within their cytoplasm and therefore have evolved to be larger in volume than cells without membrane-bound organelles (3, 4). Ploidy, or the number of genomic copies within a cell, varies among eukaryotes and also dictates cell size. Cell size has been repeatedly shown to scale with ploidy, and imbalances between cell volume and ploidy greatly disrupt cell physiology, division, and survival (5). These intrinsic characteristics of the cell establish cell size.

External cues have an important role in controlling cell size as well. Eukaryotic cells can compose unicellular or multicellular organisms, and these two contexts provide different cell environments and, therefore, differing regulation and roles of cell size (1, 2). Unicellular organisms are vulnerable to environmental changes and must be able to rapidly adapt to their surroundings in order to proliferate. A unicellular organism's main obstacle in cell growth is sufficient nutrient uptake from the environment through transporter proteins that span the cell membrane, but cell growth itself can cause challenges in nutrient uptake (1, 2). As a cell grows, the ability to transport nutrients scales with increasing surface area of the cell, but its metabolic requirement scales with cell volume and therefore increases much faster than its nutrient transport capacity. If cells become too large, the surface area-to-volume ratio may be unable to

support cellular metabolism, and cells can experience starvation even if essential nutrients are readily available in the surrounding environment (1, 2, 4).

Cells within multicellular organisms do not often experience nutrient limitation and live in a more constant environment than unicellular organisms. Instead of nutrient availability, signals within the surrounding environment regulate cell proliferation. Two important types of messages that regulate cell size are growth factors and mitogens, which control when a cell grows and divides, respectively (1, 2). Depending on where and when these signals act, cell size may vary throughout an organism, which can establish organ and entire organism size. In the context of multicellular organisms, cell size has implications on the function and organization of the entire organism and the structures within (1, 2, 4).

Because correct cell size is vital to both unicellular and multicellular organisms, there are mechanisms in place to control cell growth in response to cues from the surrounding environment (1, 2). Size regulation varies between organisms, but the universal basis is the coordination of biomass accumulation and cell division. Simply, cells need to produce enough biomass to create an entirely new cell but must divide before becoming too large (2, 4). The effects of cell growth on cell cycle progression have been thoroughly studied, but, in contrast, little is known about the effects of cell cycle progression on the ability of cells to accumulate biomass. Unicellular budding yeast, or *S. cerevisiae*, is a particularly useful model organism for studying how eukaryotes regulate their size due to its thoroughly studied genome, structural simplicity, and ease of use. In this introduction, I will describe how biomass accumulation and cell division are coordinated to regulate cell size in *S. cerevisiae* and ultimately pose the question: how do cells regulate biomass accumulation when cell division slows or halts?

Biomass accumulation

The growth rate of a cell depends on its ability to accumulate biomass and subsequently increase its volume (4). The biomass of proliferating budding yeast is composed of 50% proteins, 32% carbohydrates, 8% minerals, 8% nucleic acids (mainly RNA), and 4% lipids by weight (6, 7). The ability of cells to synthesize proteins can drastically effect biomass accumulation and therefore growth rate. Proteins are created by transcription of genes into messenger RNA (mRNA), which are subsequently translated into proteins by ribosomes. All translated proteins within the cell constitutes the proteome, and the composition of the proteome is dynamic and has dramatic effects on how cells grow and function. Specifically, the ribosomal proportion of the proteome has been shown to correlate with growth rate in budding yeast (8, 9). To summarize, cell growth rate relies on biomass accumulation through protein synthesis, which in turn is controlled by the number of ribosomes able to translate mRNA into proteins.

Protein synthesis in *S. cerevisiae*

S. cerevisiae relies on protein synthesis for biomass accumulation as half of its biomass is composed of protein (6, 7). Protein synthesis begins in the nucleus with the transcription of DNA into RNA. The budding yeast genome is composed of over 6,000 protein-encoding genes organized into 16 chromosomes with haploid yeast containing one copy of the genome and diploid yeast containing two copies of the genome (10). Many components of transcription are conserved throughout eukaryotes, including the machinery required. RNA polymerase II reads each nucleotide of DNA in a gene and synthesizes a complementary nucleotide to form a single-stranded dynamic messenger RNA (mRNA) (11, 12). There are also genes that encode RNA required for biogenesis of the ribosome organelle, termed ribosomal RNA (rRNA), and rRNA is

transcribed by either RNA polymerase I or RNA polymerase III, two other forms of RNA polymerase. A third form of RNA involved in protein synthesis is transfer RNA (tRNA), which is transcribed by RNA polymerase III and involved in protein translation (12).

Transcription is mainly regulated through transcription factors, which can either be transcriptional activators or transcriptional repressors. Transcriptional activators bind to specific DNA sequences upstream of a protein-coding gene, known as upstream activation sequences (UASs), and promote the recruitment of machinery required for transcription. Transcriptional repressors bind to upstream repression sequences (URSs), recruit repression complexes, and prevent transcription. Some transcription factors can co-regulate many genes simultaneously, integrating cell signaling into a coordinated response (11).

During and after transcription by RNA polymerase II, mRNA experiences a series of processing events. First is the addition of a modified guanine nucleotide cap to the 5' end of the mRNA, which will help a ribosome find and bind to the molecule of mRNA (12, 13). The mRNA is next spliced, a process in which RNA sequences not needed for protein coding are removed from the mRNA strand (12). Finally, a poly-A tail is added to the 3' end of the mRNA to stabilize the mRNA strand (12). After completion of these processing steps, the strand of mRNA exits the nucleus (12).

All cells accumulate biomass by translating processed mRNA into proteins using the ribosome, a machine of RNA and proteins that decodes mRNA and catalyzes the peptidyl transferase reaction that forms peptide bonds between amino acids to create proteins (13). Ribosomes are able to recognize and bind mRNA at their 5' caps with the help of translation initiation factors. Ribosomes then scan the mRNA for the initial AUG codon, which signals translation initiation and corresponds to a methyionyl-tRNA (13). The loading of the tRNA with

14

an amino acid, assembly of the aminoacyl-tRNA-ribosome-mRNA complex, and formation of

each peptide bond require extensive energy expenditure in the form of ATP and GTP hydrolysis.

As translation continues, the ribosome scans along the mRNA for each codon, associates with

the corresponding aminoacyl-tRNA, and catalyzes the peptidyl transferase reaction to form a

peptide bond between the incoming amino acid and the nascent protein strand (13). As the

protein strand is synthesized, it begins to fold into a functional protein. When the ribosome

reaches a stop codon that signals translation termination, translation ends, and the folded protein

is released from the ribosome. Final folding and processing events occur to ensure that the

protein is functional (13). Translation is an energetically expensive process, and the ribosome

has evolved to produce proteins as fast and accurately as possible (13, 14).

Structure of the yeast ribosome

Ribosomes synthesize all of the cell's proteins and therefore drive cell growth. In

proliferating budding yeast, there are approximately 190,000 ribosomes per cell, 75% of which

are actively translating proteins (14, 15). Ribosomes are structurally remarkable, containing both

protein and RNA, and the composition of ribosomes is relatively conserved among eukaryotes. *S.*

cerevisiae is no exception, and budding yeast ribosomes are made of 79 unique ribosomal

proteins (RPs) and 4 unique rRNA molecules of over 5,400 total nucleotides (16, 17). The

ribosomal fraction of the proteome has been measured to be approximately 30% in proliferating

budding yeast, and approximately 80% of all cellular RNA encodes rRNA (14).

The larger structural components of the ribosome were originally isolated through

sedimentation centrifugation and therefore are named by units of sedimentation rate, Svedbergs

(S). Proteins are translated by the 80S ribosome, which is composed of two subunits, the 60S

subunit and 40S subunit (16, 17). The 80S ribosome contains many universally conserved sites that are important for the function of the ribosome in all eukaryotes but is only assembled and functional interacting with mRNA and specific initiation factors (13, 17).

As suggested by the name, the 40S subunit is the smaller of the two subunits and contains the 18S RNA and 33 RPs (16, 17). The RPs are embedded in and wrap around the 18S RNA core. When the 80S ribosome is assembled, the 40S subunit is responsible for decoding mRNA and binding the correct corresponding aminoacyl-tRNA (17). The large subunit is known as the 60S subunit and is composed of the 25S RNA, 5.8S RNA, and 5S RNA plus 46 RPs (16, 17). It has a similar structure to the 40S subunit with a core of rRNA surrounded by RPs. The 60S subunit is the site of peptide bond formation between amino acids through the GTP-hydrolyzing peptidyl transferase reaction (17). Together, these ribosomal components function in symphony to create proteins.

Ribosome biogenesis

Producing ribosomes requires a significant portion of cellular resources and is energetically expensive. Ribosomal biogenesis involves extensive transcription and translation, employing all three forms of RNA polymerase and many ribosomes, and consumes nucleotides, amino acids, ATP, and GTP (14, 17). This process occurs frequently; in a proliferating budding yeast cell, more than 2,000 ribosomes are synthesized per minute (14, 17). To produce ribosomes at this rate, 60% of total transcription is devoted to rRNA, and 50% of RNA polymerase II transcription and 90% of mRNA splicing are devoted to RPs (13). The production of ribosomes is a key driver of cell growth rate, and therefore, when ribosome biogenesis has significant consequences on cellular and organismal fitness (17).

As previously mentioned, ribosomes are composed of rRNA and ribosomal proteins, both of which require tuned biogenesis and precise stoichiometric assembly. The process of ribosome biogenesis is described in Figure 1. All three RNA polymerases are required for ribosome biogenesis. There are 137 genes responsible for ribosomal proteins scattered throughout the genome (17). Ribosomal proteins (RPs) are transcribed by RNA polymerase II and translated by ribosomes in the cytoplasm (17). 150 rRNA genes are required for ribosome biogenesis and are encoded on chromosome XII in tandem repeats of the four rDNA genes. Transcription of the rDNA genes occurs in the nucleolus, a non-membrane bound compartment of the nucleus (17). RNA polymerase I transcribes the 35S pre-rRNA molecule, which requires a series of processing and cleavage events to form the 18S, 5.8S, and 25S RNAs (12, 17, 18). The 5S RNA is transcribed by RNA polymerase III (17, 18). Alongside rRNA and RPs, 200-250 co-regulated genes encode proteins that aid in the processing and formation of the ribosome without becoming part of its structure. These are known as ribosome biogenesis (Ribi) genes and are transcribed and translated by the same processes as RPs (18, 19). The transcription of rDNA, RP, and Ribi genes are all essential in ribosome biogenesis.

After being translated in the cytoplasm, a large number of RPs are transported into the nucleus. Many 60S RPs assemble with the 5S RNA. Aided by Ribi factors, the 35S pre-RNA complex assembles with the small subunit (SSU) processome and additional RPs associated with the 40S subunit. The 90S SSU processome, including the 35S RNA and RPs, is cleaved, and the pre-40S and pre-60S subunits are further processed and exit the nucleus into the cytoplasm. Final RPs associate with each subunit, which then release bound Ribi factors (18). When mRNA is present to be translated, these two subunits can assemble to form the intact 80S ribosome (18).

Pol III   Pol I   rDNA cluster

5S   18S   5.8S   28S

5S RNA   35S pre-RNA

Nucleolus   RPs

90S SSU
processome

Pol II   Ribi genes

pre-
60S   Ribi

Pol II   RP genes

Nucleus   pre-
60S   pre-
40S   RP

RP and Ribi mRNA

Cytoplasm   pre-
40S   RPs   Ribi
factors

Nuclear pore
complexes

pre-
60S   60S

mRNA   60S   RPs   40S
pre-
40S   60S
40S   Translating
80S ribosome

Translating   40S   RPs
80S ribosome   Ribi
factors

Figure Key

RNA Pol   RPs

DNA   Gene   Ribi

RNA

40S   Nuclear   SSU
pore   proces-
60S   complex   some

18

Figure 1. Eukaryotic ribosome biogenesis involves synthesis and association of rRNA and ribosomal proteins (RPs). Ribosomal DNA (rDNA) transcription occurs in the nucleolus. RNA Polymerase I transcribes the rDNA genes for the 18S, 5.8S, and 28S RNAs into the 35S pre-RNA molecule. RNA Polymerase III transcribes the 5S RNA. RNA Polymerase II transcribes ribosomal protein (RP) and ribosomal biogenesis (Ribi) genes in the nucleus. The RP and Ribi mRNAs then exit into the cytoplasm where they are translated by ribosomes. The majority of RPs re-enter the nucleus once translated. RPs of the 60S subunit bind to the 5S RNA. The 35S pre-RNA, RPs, and Ribi factors assemble with the SSU processome. The 90S SSU processome is cleaved to form the pre-40S subunit, containing the 18S RNA, RPs, and Ribi factors, and the pre-60S subunit, containing the 28S, 5.8S, and 5S RNAs, RPs, and Ribi factors. Further processing occurs in the nucleus, and then both subunits exit into the cytoplasm where they bind final RPs and disassociate from Ribi factors. The 40S and 60S subunits create the translating 80S subunit when mRNA is present to be translated.

Ribosome biogenesis is primarily regulated at the transcriptional level by a variety transcription factors, some likely yet to be discovered. rRNA transcription is regulated by four general transcription factors, while there are many more transcription factors involved in RP and Ribi synthesis (17). Some of these transcription factors, such as Sfp1, Abf1, and Rap1, are involved in both RP and Ribi gene transcription (19, 20). Changes in the amount or activity of these transcription factors and subsequent alterations of ribosome biogenesis have been shown to have profound effects on cell physiology and growth rate (1, 2). For example, Jorgensen & Tyers (2004; 2) showed the effects of altering *SFP1* expression (Fig. 2). Cells unable to produce *SFP1*

(Fig. 2, *sfp1Δ,* left) appeared to be much smaller than cells that overexpressed *SFP1* (Fig. 2,

SFP1 OE, right). This experiment exhibits the direct effect of ribosome biogenesis on cell size.
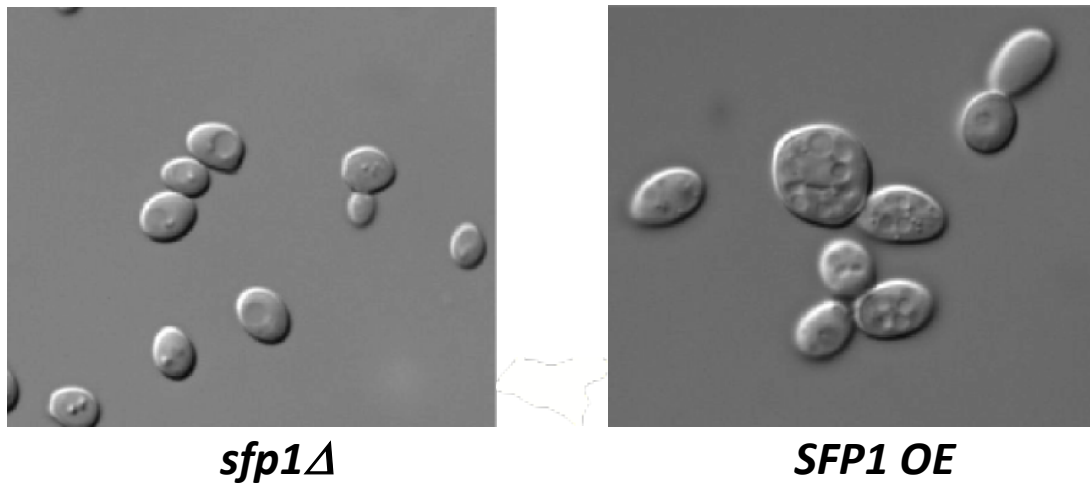
sfp1Δ   **SFP1 OE**

Figure 2. The effect of *SFP1* expression on cell size. Adapted from Jorgensen & Tyers (2004; 2). Images of proliferating *S. cerevisiae* cells lacking *SFP1* (s*fp1Δ* , left) and overexpressing *SFP1* (*SPF1 OE*, right). Cells with the *sfp1Δ* mutation are much smaller than cells that overexpress *SFP1*.

Regulation of ribosome biosynthesis through nutrient sensing pathways

Cells can regulate the rate of ribosome biosynthesis based on growth conditions, such as availability of key nutrients (21). Overlapping nutrient sensing pathways, including the TORC1 pathway and the Ras/PKA pathway, have been shown to regulate ribosome biosynthesis by affecting the activity of ribosomal biogenesis transcription factors (2, 19, 20). This is intuitive because when nutrients are depleted, cells must reduce biomass accumulation coordinately to

preserve resources. Therefore, nutrient availability is a main effector of biomass accumulation and cell growth rate (22, 23).

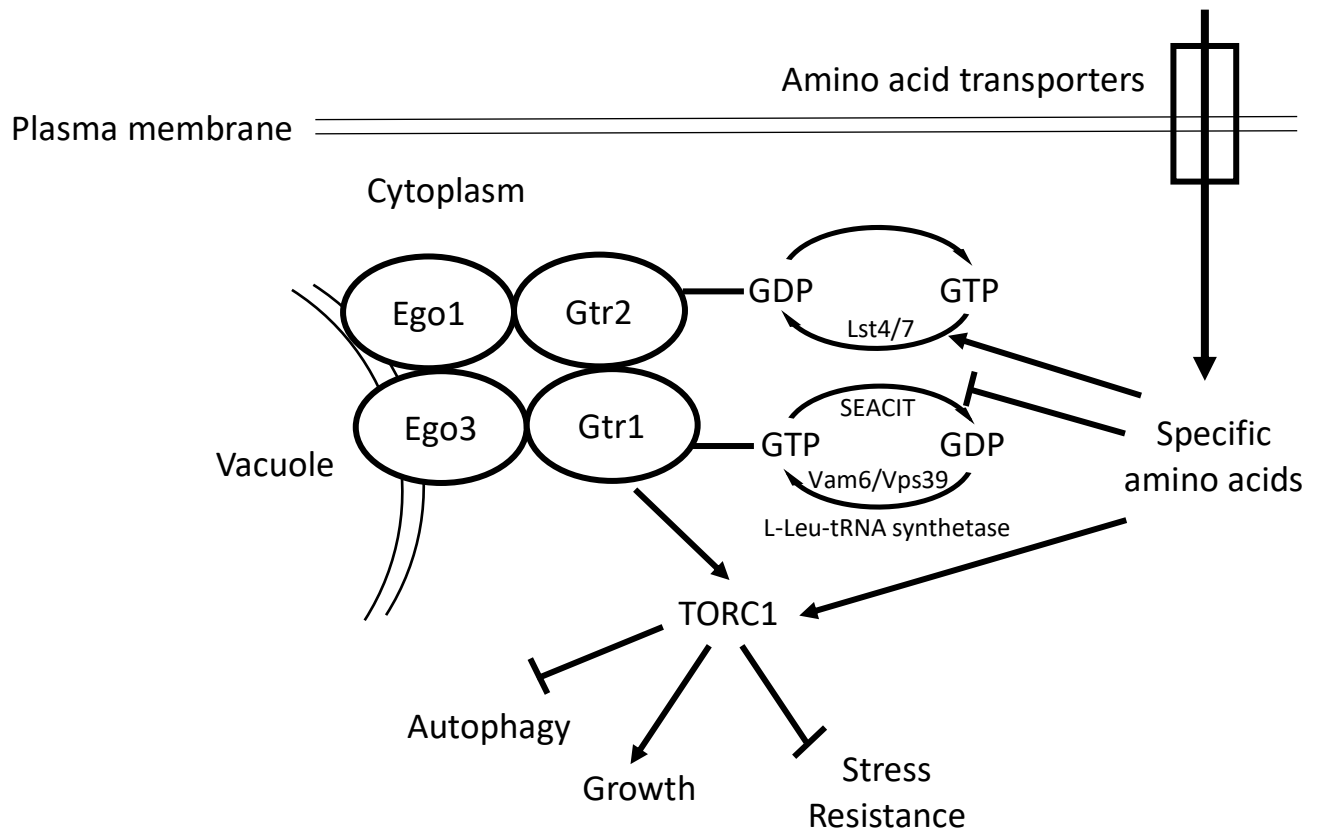**Nitrogen sensing through the TORC1 pathway**

The target of rapamycin (TOR) pathway was first discovered in *S. cerevisiae* with the characterization of the TOR protein (23, 24, 25). Upon rapamycin addition, cells stopped proliferating in a manner similar to nitrogen starvation, and researchers uncovered that rapamycin was directly inhibiting the TOR protein, which could also sense nitrogen availability within a cell, particularly the presence of nitrogen-containing amino acids (23, 24, 25). In response to intracellular nitrogen availability, the TOR pathway increases activity of anabolic processes, such as synthesis of lipids, nucleotides, and proteins, and decreases activity of catabolic processes, such as autophagy, in order to stimulate cell growth and proliferation (24).

The TOR protein is able to form two structurally unique complexes that have different roles within the cell: the TOR complex 1 (TORC1) and the TOR complex 2 (TORC2) (24). TORC1 has roles in protein and ribosome synthesis, cell cycle progression, nutrient uptake, and autophagy, while TORC2 is involved in actin cytoskeleton organization, endocytosis, lipid synthesis, and cell survival. Only TORC1 is sensitive to rapamycin (23, 24). Here, I will focus on the TORC1 pathway because of its role in protein synthesis and ribosome biogenesis. Yeast TORC1 is composed of the proteins Kog1, Lst8, and one of two very similar TOR proteins: TOR1 or TOR2 (24). TOR1 and TOR2 are 67% similar in sequence and have the same essential features (23). The TORC1 complex resides in the cytoplasm and is tethered to the vacuole membrane, inside which excess amino acids are stored (23).

Nutrients, growth factors, and cellular energy control TORC1 activity. In unicellular

organisms, nutrients are sufficient to activate TORC1. The mechanisms of the TORC1 pathway

are described in Figure 3. The EGO complex directly regulates TORC1 and consists of four

proteins: Ego1, Ego3, Gtr1, and Gtr2 (23, 24). Gtr1 and Gtr2 are small GTPases, while Ego1 and

Ego3 tether the EGO complex to the vacuole membrane (24). In the presence of amino acids,

Gtr1 is bound to GTP, while Gtr2 is bound to GDP (23). Gtr1 is in turn regulated by the GTP-

activating protein (GAP) SEACIT and the guanine nucleotide exchange factors (GEFs)

Vam6/Vps39 and the L-Leu-tRNA synthetase. Gtr2 is regulated by the GAP Lst4/Lst7. Many

amino acid control TORC1 activity through unique mechanisms that are still being studied (24).

TORC1 can phosphorylate many different proteins, which in turn directly or indirectly

regulate many cellular processes, such as glutamine and glutamate biosynthesis, stability of the

general amino acid transporter Gap1, nitrogen catabolite repression (NCR), and ribosome

biogenesis (23). TORC1 can only phosphorylate these proteins when active. In the presence of

rapamycin or absence of carbon, nitrogen, phosphate, or specific amino acids, TORC1 is

inactivated, and many of its target proteins are dephosphorylated (23). Sch9 is one of the proteins

downstream of TORC1 and also interacts with other nutrient-sensing pathways. It has roles in

autophagy, response to stress, entry into quiescent non-proliferating state of G0, translation

initiation and elongation, ribosome biogenesis, mitochondrial function, sphingolipid homeostasis

and signaling, and aging (23). The specific transcription factors altered by TORC1 activity are

extensive and are still a topic of research. Some worth noting are Msn2 and Msn4, which are

involved in stress responses, and Sfp1, Fhl1, Ifh1, Stb3 and Dot6/Tod6, which involved in

rRNA, RP, and Ribi transcription. By being able to affect these transcription factors, TORC1

activity has profound consequences on ribosome biosynthesis, and therefore, cell growth (2, 23, 24, 25).

Figure 3. The TORC1 pathway of *S. cerevisiae* senses intracellular nitrogen availability.

Nitrogen can enter the cell in the form of amino acids through amino acid transporters. Specific amino acids can alter the GTP-state of the EGO complex in various ways that are still being studied, and some amino acids even seem to activate TORC1 directly. The EGO complex is composed of four proteins (Ego1, Ego3, Gtr1, and Gtr2) and directly regulates TORC1. The roles of Ego 1 and Ego 3 are to tether the EGO complex to the vacuole membrane. Gtr1 and Gtr2 are small GTPases. Gtr1 is regulated by the GEFs Vam6/Vps39 and the L-Leu-tRNA synthetase

and the GAP SEACIT. Gtr2 is regulated by the GAP Lst4/Lst7. In the presence of amino acids, Gtr1 is bound to GTP, while Gtr2 is bound to GDP, and the EGO complex is able to activate TORC1. Active TORC1 induces growth and proliferation, while repressing stress resistance and autophagy.
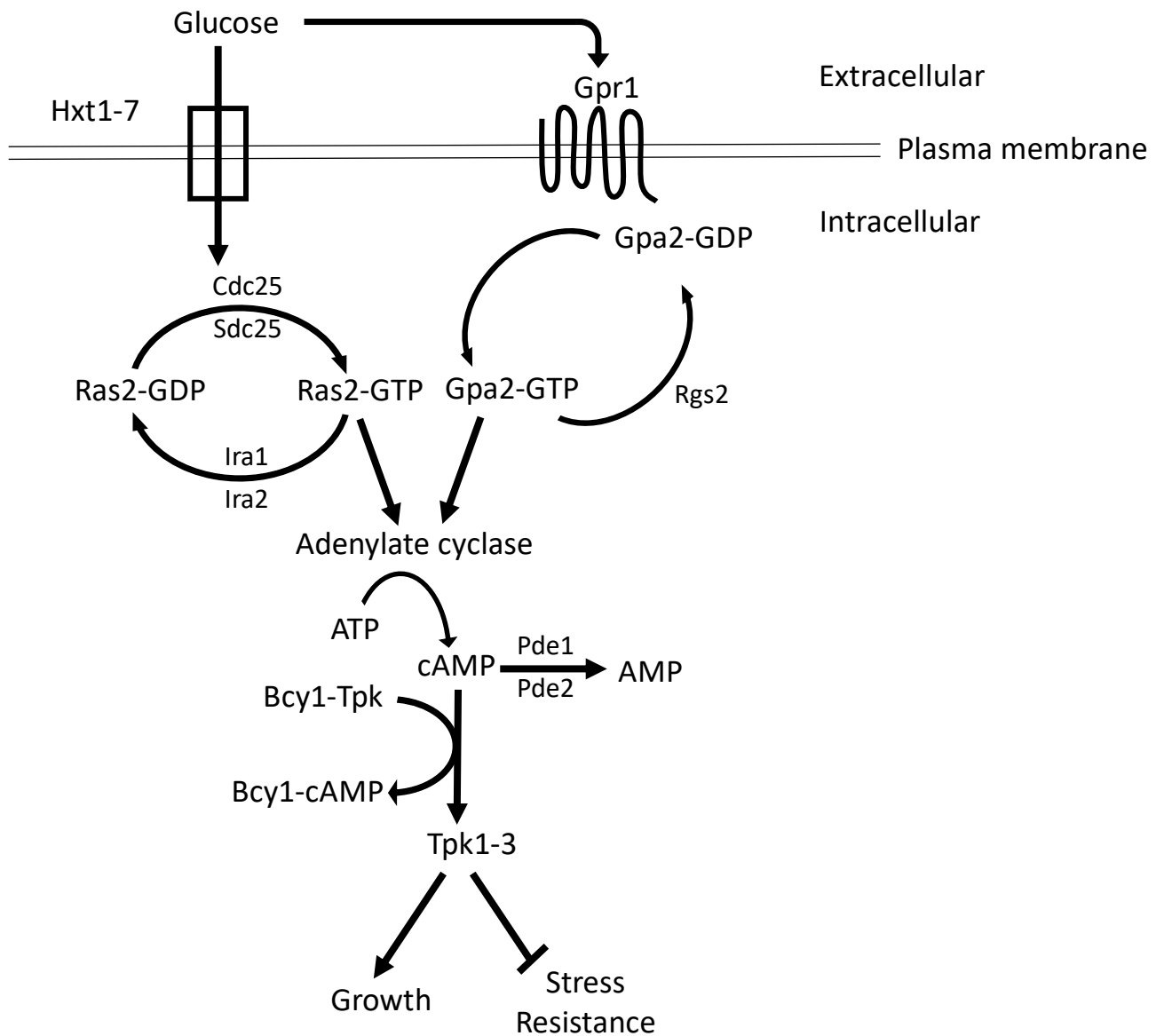

Glucose sensing through the Ras/PKA pathway

The Ras/PKA pathway senses intracellular and extracellular glucose in budding yeast (1, 2, 23, 25, 26). When glucose is readily available, the Ras/PKA pathway stimulates fermentative cell growth and represses stress tolerance. When glucose is absent, the Ras/PKA pathway forces cells into stationary phase, a quiescent non-proliferating G0 phase (1, 2, 23, 25, 26). Ras/PKA pathway activity is also regulated by the availability of other nutrients required for yeast growth, such as nitrogen and phosphorus. When cells are starved for one of these essential nutrients, the Ras/PKA pathway downregulates growth and promotes entrance into enter stationary phase regardless of glucose abundance (23).

An overview of the Ras/PKA pathway is shown in Figure 4. As suggested by its name, the main signaling component of the Ras/PKA pathway is PKA, which is composed of Tpk1-3 and two molecules of inhibitor Bcy1 in budding yeast. PKA can be activated through two glucose-sensing branches of the pathway. Extracellular glucose is sensed by a G-coupled protein receptor (GPCR) system that is made up of Gpr1 (the GPCR) and Gpa2 (the associated Gα protein). Intracellular glucose sensing requires cells to uptake glucose through glucose transporters Hxt1-7, and the presence of intracellular glucose subsequently activates the small GTPase Ras, a homolog of the Ras oncogene in mammals (23). Either Gpa2 or Ras can activate adenylate cyclase, which in turn promotes synthesis of cyclic-AMP (cAMP), a small secondary

messenger produced from ATP. When glucose is abundant, cAMP binds to Bcy1, releasing it

from Tpk1-3 and activating PKA (23).

Active PKA has many targets involved in a variety cell processes. Notably, PKA

promotes fermentative growth and represses stress tolerance and entrance into stationary phase

(23). PKA has many of the same downstream targets as the TORC1 pathway, including Sch9,

Msn2/4, and, importantly, many transcription factors involved in rRNA, RP, and Ribi

transcription (Sfp1, Fhl1, Ifh1, Stb3 and Dot6/Tod6) (23, 25, 26). The TORC1 and Ras/PKA

pathways appear to be highly intertwined and affect almost all ribosome and protein synthesis

genes, making them the direct link between nutrient availability and cell growth in *S. cerevisiae*

(2, 23, 25, 26, 27).

Figure 4. The Ras/PKA pathway of *S. cerevisiae* senses intracellular and extracellular glucose. When readily available, glucose can enter the cell through the Hxt1-7 glucose transporters. Intracellular glucose is sensed by unknown mechanisms but results in the activation of the small GTPase Ras. Ras is regulated by GAPs Ira1 and Ira2 and GEFs Cdc25 and Sdc25. Extracellular glucose can bind to the GPCR Gpr1, which activates its associates Gα protein

Gpa2. The GAP of Gpa2 is Rgs2. Either G proteins can then activate adenylate cyclase, which

hydrolyzes ATP into the secondary messenger cyclic-AMP (cAMP). cAMP levels can further be

regulated by Pde1 and Pde2, which convert cAMP to AMP. In budding yeast, the PKA complex

is composed of Tpk1-3 and two inhibitory subunits of Bcy1. The presence of glucose causes

cAMP to bind and relocalize Bcy1 and allows for Tpk1-3 activity, which promotes fermentative

growth and inhibits stress resistance.

The environmental stress response

Limiting nutrients cause dramatic changes to the proteome that begin with the regulation

of transcription. As described above, Ras/PKA and TORC1 have numerous similarities,

particularly concerning their downstream effectors. Shown in Figure 5, Gasch et al. (2000; 28)

used DNA microarrays to study how transcription changed under a variety of extracellular

stresses: temperature change, hydrogen peroxide, hyper- and hypo-osmotic shock, amino acid

starvation, nitrogen depletion, entrance into stationary phase, and addition of drugs menadione,

diamide, and dithiothreitol. Under almost all of these conditions, including inhibition of

Ras/PKA and TORC1 through glucose and amino acid depletion, respectively, approximately

900 genes responded similarly, but the amplitude and duration of the gene expression changes

differed based on the severity of the stress imposed on the cell (28). This common transcriptional

response was termed the environmental stress response (ESR).

Within these ~900 genes, ~300 were upregulated, and ~600 were downregulated. The

induced ESR (iESR) is composed of the ~300 upregulated genes. Only 40% of these genes were

characterized when the ESR was initially described (28). The functions of iESR genes hint of

how cells can survive stresses and are involved in processes such as protein folding and

degradation, various redox reactions, carbohydrate and fatty acid metabolism, DNA damage repair, cell wall modification, function of the vacuole and mitochondria, autophagy, and signaling within the cell (28). The repressed ESR (rESR) is composed of the ~600 downregulated genes. Many of these genes are part of metabolic processes, including RNA processing, mRNA splicing, tRNA synthesis, nucleotide synthesis, initiation and elongation of translation, and secretion. Many genes encoding ribosomal proteins and ribosome biosynthesis factors are also downregulated but with a mild delay (28).

There are many genomic changes that occur in cells that are specific to the stress applied. The ability of cells to survive certain stressors can be more deeply understood by studying the differences in their genomic changes. Many of these condition-dependent changes are mediated by the transcription factors Yap1, Msn2, and Msn4 (28). Furthermore, ESR genes are regulated by different transcription factors under different conditions (28). For example, upregulation of the ESR genes *GPD1*, *HSP12*, and *CTT1* was shown to have different regulators, Msn1, Msn2, Msn4, or Hot1, depending on the stressor (31). Through all of these transcription factors, and many more not mentioned, the ESR can quickly react to cellular stressors by changing the expression of ~900 genes.
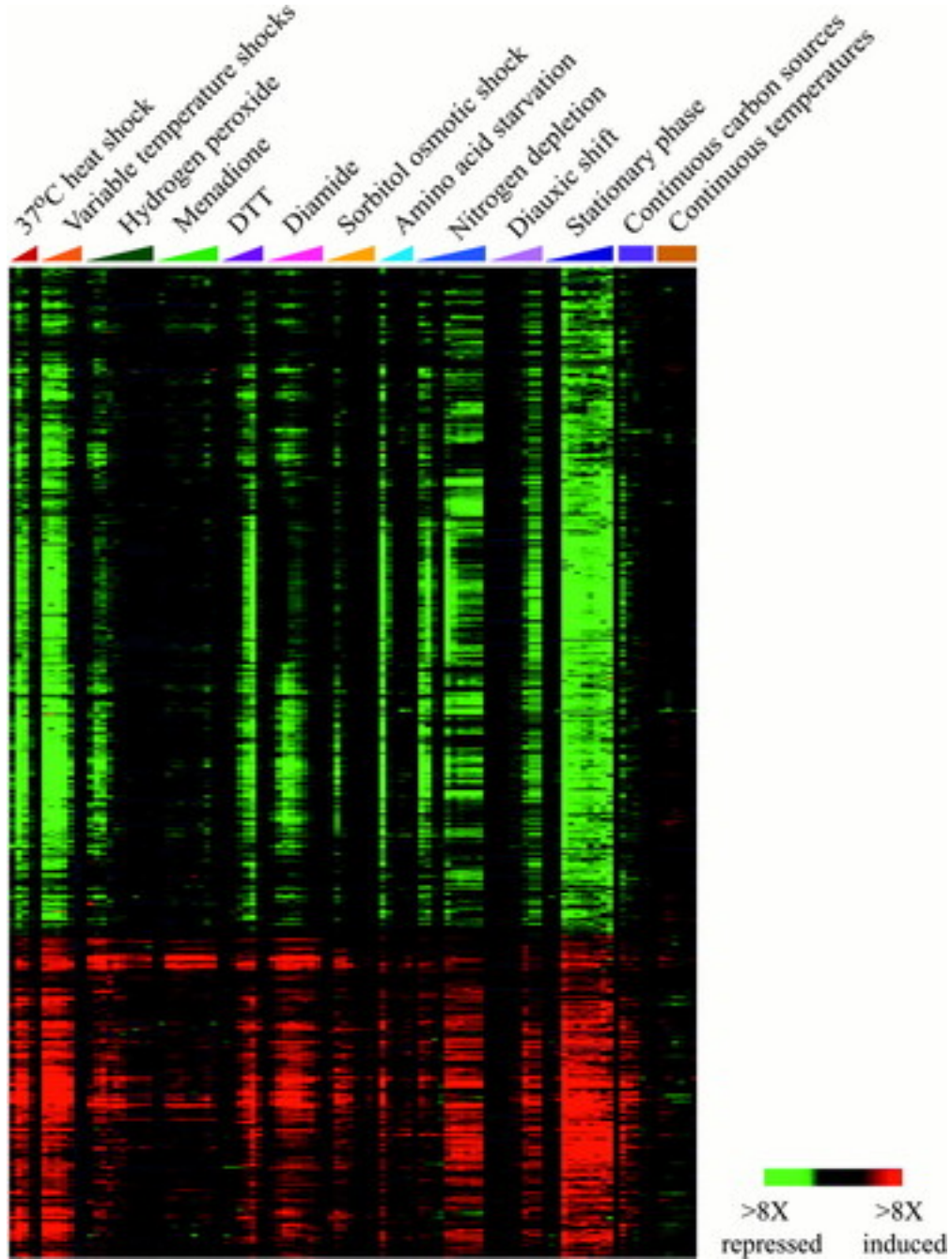
Figure 5. DNA microarray experiments revealed the environmental stress response. Adapted from Gasch et al. (2000; 28). *S. cerevisiae* cells were grown under different

environmental conditions, and their transcriptomes were studied using DNA microarrays. In 11

extracellular stresses, including heat shocks, hydrogen peroxide, menadione, DTT, diamide, hyperosmotic shock, amino acid starvation, nitrogen depletion, diauxic shift, and stationary phase, approximately 900 genes responded similarly. Gasch et al. (2000; 28) termed this the environmental stress response (ESR). Within the ~900 genes, ~300 were upregulated (iESR), and ~600 were downregulated (rESR).


Cell division

Along with biomass accumulation, the other key process that constitutes cell size regulation is cell division. The presence of nutrient signals, growth factors, and mitogens promotes cells to enter a cyclic process, known as the cell cycle, during which cells grow and divide. Numerous mechanisms are present to ensure production of a viable daughter cells (32, 33, 34). Many of these mechanisms have similarities throughout eukaryotic species, from unicellular yeast to humans. One main similarity is the sequence of events in the cell cycle. After the previous division, cells have a phase of growth, known as G1. When cells have accumulated enough biomass, their DNA is replicated in S phase, and cells then experience a second growth phase, known as G2. Finally, cells package and segregate their DNA into two daughter cells during mitosis, or M phase (1). Before committing to S phase, cells can exit G1 and enter a quiescent non-proliferating state known as G0 or stationary phase (33, 34).

In all eukaryotes, progression of the cell cycle is dictated by the activity of cyclin-dependent kinases (CDKs), serine/threonine protein kinases that can be activated during different phases of the cell cycle to regulate checkpoints and progress. CDKs are activated by transient cyclin proteins and CDK activating kinases (CAKs) and can be inhibited by CDK inhibitors (CKIs) (32, 33). While the amount of CDK in a cell remains constant throughout the cell cycle,

the levels of cyclins change and are controlled by the transcription, translation, and degradation. In all eukaryotes, different cyclins are required at different points, and this is what causes CDKs to be active and inactive at specific/periodic points throughout the cell cycle (32, 33, 34).

The cell cycle in *S. cerevisiae*

The eukaryotic cell cycle was initially studied in *S. cerevisiae* due to the ease of genetic manipulation, clear similarities to mammalian cells, and short cell cycle duration of 90 minutes at 25ºC (34). However, there are some unique features of mitosis in budding yeast that differ from those in mammalian cells. First, budding yeast cell division is asymmetric in terms of cell mass, and, therefore, produces a small daughter cell and a larger mother cell. In contrast, mammalian cells divide symmetrically to create two identical daughter cells (2). Second, the nucleus remains intact throughout cell division, in contrast to the breakdown of the nucleus in mammalian cells (33, 35). Finally, although budding yeast has five CDKs (Cdc28, Pho85, Kin28, Ssn3, and Ctk1), only Cdc28 is the main regulator of cell cycle progression, in contrast to the variety of essential CDKs in mammalian cells. There are nine cyclins that regulate Cdc28: three G1 cyclins (Cln1-3), which are important during G1 and Start, and six B-type cyclins (Clb1-6), which are required for progression from Start to M phase (36). The activity of Cdc28 and its association with different cyclins throughout the cell cycle is described in Figure 4 (37). These key differences are apparent and important throughout the cell cycle and will be further discussed.
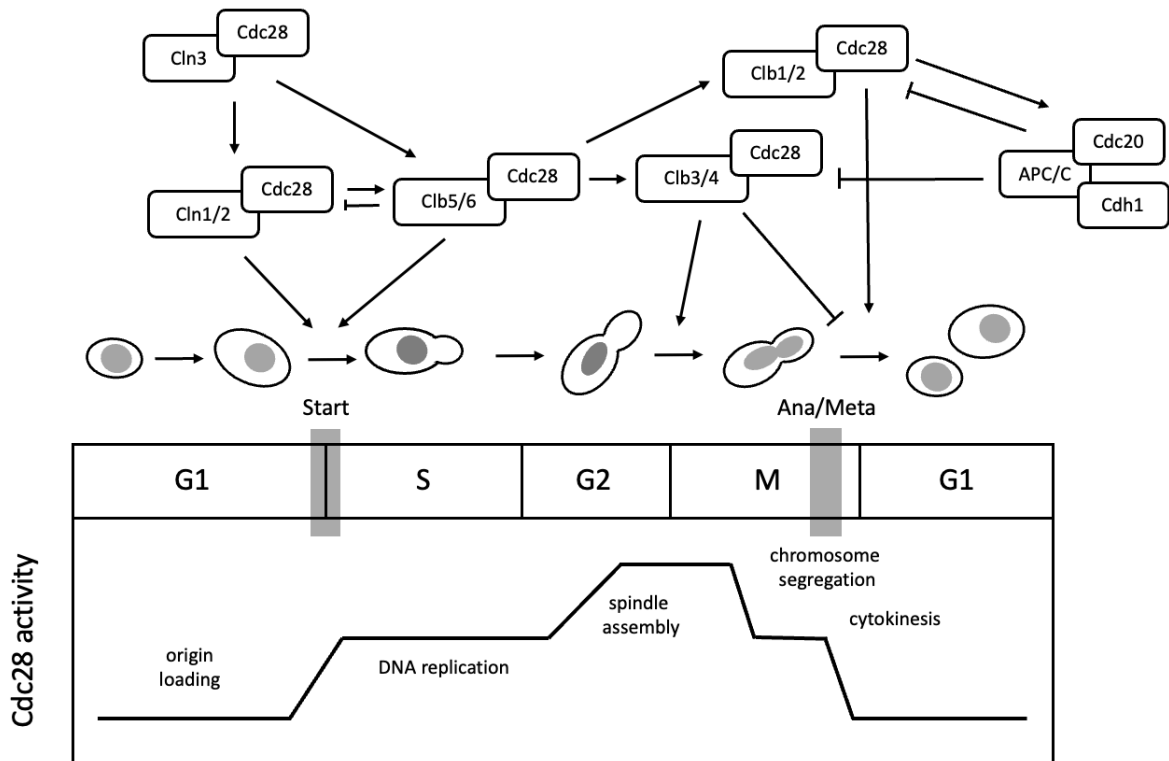
Figure 6. Cyclin and Cdc28 activity throughout the *S. cerevisiae* cell cycle. Adapted from Campbell (2019; 37). In early G1, Cdc28 is bound to CKIs, and its activity is low, allowing ORCs to load onto origins of replication. As G1 progresses, *CLN3* is transcribed, and the active Cln3-Cdc28 complex is formed. Cln3-Cdc28 then indirectly promotes transcription of *CLN1*, *CLN2*, *CLB5*, and *CLB6*. The Cln1/2-Cdc28 complexes cause the daughter bud to form and inactivate CKIs bound to Clb5/6-Cdc28, allowing activation of Clb5/6-Cdc28 complexes. Clb5/6-Cdc28 complexes initiate DNA replication, degrade Cln1/2–Cdc28, and promote transcription of *CLB1-4*. *CLB3* and *CLB4* are transcribed first, and Clb3/4-Cdc28 complexes initiate entrance into mitosis and formation of the mitotic spindle. While the nuclear envelope remains intact, the mitotic spindle attaches to sister chromatids in a bi-oriented manner via kinetochore protein structures. When equal and opposing tension is applied to each sister

chromatid, Clb1/2-Cdc28 activity causes spindle elongation, driving the sister chromatids to opposite sides of the cell. Clb1/2-Cdc28 complexes also activate the APC/C through the protein Cdc20. The APC/C inhibits Cdc28 and partially degrades Clb1-4, causing activation of Cdc14, the MEN, and cytokinesis. APC/C is further activated by Cdh1 and decreases Cdc28 activity to basal levels as cells enter G1 again.

G1 and Start

G1 is the first growth stage of the cell cycle and is regulated by three G1 cyclins: Cln1, Cln2, and Cln3, which each differ in their functions, properties, and regulation (2, 36). The most important goal of G1 is to gain biomass. As previously described, this is done by synthesis of proteins, lipids, and organelles. Cells must have enough biomass to commit to forming a daughter cell, and once this occurs, cells can progress through Start. Start is the period of transition between G1 and S phases. After Start occurs, cells will continue through the cell cycle until the next G1 phase despite external factors regulating growth, such as nutrient availability or mating pheromones, highlighting the importance of the G1/S-phase transition via Start (2, 34).

In the early stages of G1, the activity of Cdc28 is low due to association with CKIs. As G1 progresses, the amount of the cyclin Cln3 increases, which is highly unstable and ultimately activates Start (2). Cln3 associates with and activates Cdc28, forming the Cln3-Cdc28 complex, Cln3-Cdc28 then phosphorylates and relocalizes Whi5, a formerly DNA-bound inhibitor of the SBF (Swi4/Swi6) and MBF (Mbp1/Swi6) complexes that activate transcription of approximately 200 genes (2). Among the transcripts produced are those of G1 cyclins *CLN1* and *CLN2*, B-type cyclins *CLB5* and *CLB6*, which drive DNA synthesis, and genes responsible for accurate replication of DNA. Cln1 and Cln2 bind to and activate Cdc28, and the Cln1/2–Cdc28

complexes cause formation of the daughter bud and inactivate CKIs that inhibit Clb5/6-Cdc28 activity (2, 36). This allows activation of the Clb5/6-Cdc28 complexes, which subsequently promote DNA replication in S phase (2).

Cells can only pass Start once they have reached their "critical size," or size required for division set by nutrient availability in the surrounding environment. The ability of cells to set this size threshold is an important mechanism of coordinating biomass accumulation and cell division and ensures that the mother cell has enough resources to replicate and divide to create a viable daughter cell (2). The "critical size" threshold also helps cells maintain their average cell size despite asymmetrical divisions. Larger mother cells are often in G1 phase for a minimal amount of time, while smaller daughter cells must spend longer in G1 phase to grow to "critical size" (2). How cells set and subsequently know they have reached "critical size" is still unknown but appears to involve measurement of a cell's biosynthetic capacity, or rate of protein synthesis (2). Although the mechanism size sensing is a topic of ongoing research, one or more of the proteins involved in SBF/MBF transcription, such as Cln3, Whi5, or Swi4/6, appear to be involved (1, 2, 38).

DNA synthesis in S phase

S phase in budding yeast is characterized by bud formation and DNA and spindle pole body (SPB) duplication (36). Cell must replicate their DNA accurately and only once per cell division (32, 39). During Start, Cln2/3-Cdc28 complexes degrade CKIS that bind and inhibit Clb5/6-Cdc28 complexes. Active Clb5/6-Cdc28 complexes initiate replication at origins of replication (39). Origins of replication are DNA sequences of 100-150 base pairs that identify where DNA replication can begin (39). In early G1, Cdc28 activity is low, and the origin of

replication complex (ORC), a six-protein complex of Orc1-6, binds to origin of replications in an ATP-dependent manner (39). Next, more proteins, including the core components of DNA helicase, Mcm2-7, are loaded onto the ORC in a process called replicative origin licensing (34, 39). The remaining components of DNA helicase bind to the ORC-Mcm complex as well as a second DNA helicase complex. Together, the two DNA helicase unwind the doubled strands of DNA bidirectionally to allow for replication. When Cdc28 activity increases at Start, a series of proteins are recruited to select licensed origins, and Clb5/6-Cdc28 complexes can initiate DNA replication (37, 39, 40).

After helicase unwinds the double stranded DNA, DNA polymerase replicates DNA semi-conservatively, meaning that each chromosome contains one strand of DNA from the mother cell and one newly synthesized DNA strand (39, 40). Pairs of identical chromosomes formed from DNA replication are known as sister chromatids (39, 40). DNA polymerase proofreads the newly synthesized nucleotides, and a variety of editing mechanisms exist to remedy mistakes undetected by DNA polymerase, decreasing the mutation rate to 1 in every 10^{-7}-10^{-8} nucleotides synthesized (41). DNA damage or errors in replication causes most eukaryotes to arrest in S phase or G2 by inhibiting Cdk activity until the damage or error is fixed (32, 33, 34 42). The DNA damage response functions slightly differently in budding yeast and occurs at the metaphase-to-anaphase transition during mitosis (32, 33, 34 42).

Clb5/6-Cdc28 complexes act in multiple mechanisms to ensure that DNA replication only occurs once and that the cell cycle progresses unidirectionally. Re-firing of origins of replication is prevented through Clb5/6-Cdc28 activity, and ORCs and Mcm proteins can only load onto origin or replications when Cdc28 activity is low in G1 (34, 39). To guarantee the sequence of the cell cycle occurs in the correct order, active Clb5/6-Cdc28 complexes degrade

G1 cyclins and promote the transcription of the M phase cyclins (36, 39). Through these

mechanisms, cells are able to properly replicate their DNA only once and continue onto mitosis.

G2 and M phase

G2 is the second growth phase of the cell cycle, following S phase and preceding M

phase. In many eukaryotes, an important checkpoint for damaged or unreplicated DNA occurs in

G2, guaranteeing proper DNA replication before mitosis (32, 33, 34 42). In budding yeast, this

checkpoint instead functions at the metaphase-to-anaphase transition, prior to chromosome

segregation, and G2 is brief (32, 33, 34, 42).

Mitosis is the process of DNA segregation between mother and daughter cells and

requires precise mechanisms and checkpoints. The four M-phase cyclins that promote mitosis are

Clb1-4. *CLB3* and *CLB4* are transcribed in S phase, further increasing Cdc28 activity, and are

important in the formation of the mitotic spindle. The mitotic spindle is composed of

microtubules, regulatory proteins, motors, and two spindle pole bodies (SPBs), which are

homologs of the mammalian centrosomes and organize microtubules used in chromosome

segregation. Ultimately, this wave of Cdc28 activity leads to entry into mitosis (36, 42, 43, 44).

In the early mitosis stages of prophase, prometaphase, and metaphase, SPBs move to

opposite sides of the nuclear envelope, and chromosomes condense and attach to SPBs across the

nuclear membrane in *S. cerevisiae*. In mammalian cells, the nuclear envelope must first break

down for microtubules to attach properly to chromosomes (33). One end of the microtubules is

attached to the SPB while the other is attached to the chromosome through the kinetochore

protein complex (35, 43, 44). For correct attachment of sister chromatids to the mitotic spindle,

sister chromatids must be attached to different SBPs to create equal and opposite tension on each

chromosome. This alignment is termed bi-orientation and ensures that both the mother cell and the daughter cell receive an entire set of the genome (45). Sister chromatids are held together by a ring-shaped protein complex, cohesin, until bi-orientation is achieved. High Cdc28 activity prevents cleavage of cohesin through activation of the inhibitor securin, which sequesters the cohesin protease, separase (46). Held together and properly aligned, the sister chromatids are prepared to separate.

CLB1 and *CLB2* transcription occurs during G2 and M phase, prior to anaphase, and Clb1/2-Cdc28 activity initiates spindle elongation, separating sister chromatids and driving a portion of the dividing nucleus into the bud (35, 36). At the core of the metaphase-to-anaphase transition is the E3 ubiquitin ligase anaphase-promoting complex (APC/C). Clb1/2-Cdc28 complexes activate Cdc20, which in turn activates APC/C. APC/C promotes the metaphase-to-anaphase transition unidirectionally by inhibiting Cdc28 and degrading Clb1-4. Initially, APC/C-Cdc20 is partially active and only moderately decreases Cdc28 activity, which is sufficient to inhibit securin, activate separase, and cleave cohesin (36, 43). The spatial and temporal regulation of the phosphatase Cdc14 prevents exit from mitosis until sister chromatids are properly segregated between the mother and daughter cells, after which Cdc14 activates CKIs and the APC/C activator Cdh1, resulting in complete Cdc28 inhibition (47, 48, 49). Finally, through the mitotic exit network, a highly regulated pathway involving Cdc14 and the kinase Cdc15, cells exit mitosis, and the cytoplasm divides, a process known as cytokinesis. Both the mother and daughter cells enter G1 with low Cdc28 activity (36, 47, 48, 49).

The DNA-damage checkpoint and spindle-assembly checkpoint (SAC) act at the metaphase-to-anaphase transition in *S. cerevisiae.* Both checkpoints cause arrest in metaphase by inhibiting Cdc20, preventing activation of APC/C-Cdc20. Instead, Cdc28 activity does not

decrease, and cells cannot proceed through the cell cycle, providing sufficient time for DNA repair or reattachment of the mitotic spindle (33, 36). Damage or errors in DNA can be recognized and processed to single-stranded DNA, the presence of which initiates the DNA-damage checkpoint. Once activated, the DNA-damage checkpoint inhibits cohesin cleavage, preventing chromosome segregation and arresting cells in metaphase (50). When the mitotic spindle is not appropriately attached to sister chromatids, the SAC arrests cells at the metaphase-to-anaphase transition through inhibition of Cdc20, preventing APC/C activation (51). These checkpoints are a cell's main safeguard against erroneous propagation of genetic material, and failure of either checkpoint can result in loss of fitness in the mother cell and/or daughter cell (33, 36, 50, 51).

Errors in cell division

The cell cycle is prone to errors, and cell cycle regulators and checkpoints are tasked with sensing mistakes in replication or division and arresting the cell cycle until the issue can be resolved. The two main checkpoints of the yeast cell cycle are Start, which is the transition from G1 to S phase, and the metaphase-to-anaphase transition (34). When the checkpoints at Start or the metaphase-to-anaphase transition fail, cells can enter the cell cycle without accumulating sufficient biomass or erroneously segregate their DNA, respectively (2, 52, 53). Subsequent cell cycles will inherit these issues and have difficultly proceeding as well, leading to decreased proliferation capacity (34, 54, 55). Mutations in key cell cycle regulators also prevent cell cycle progression, but cell growth is not immediately attenuated (56, 57). By understanding how specific errors in cell division lead to changes in biomass accumulation, we can further understand how the two are coordinated in cell size control mechanisms.

Aneuploidy

An important objective of mitosis is for both the mother cell and the daughter cell to receive a complete set of the genome during cell division. A euploid karyotype, or a genome with the correct number of chromosomes, is essential for proper growth and fitness of a cell (55). In contrast, a cell with an aberrant karyotype that is not a multiple of the haploid genome, termed an aneuploid cell, has defects in many basic and essential cellular functions (55). Aneuploidy is caused by missegregation of chromosomes during mitosis or meiosis (52-55). Errors in mitosis that lead to chromosome missgregation are described in Figure 7 and include SAC mutations, chromatid cohesion loss, aberrant kinetochore attachments, and excess SPBs (55). Aneuploidy can occur in any proliferating cell, but the ability for a cell to tolerate aneuploidy varies in different contexts. Trisomy 21, or Down Syndrome, is the most notable occurrence of aneuploidy in humans and can be characterized by decreased development of key physiological systems. Although proliferation defects are seen in many aneuploid cells, the majority of fast-growing cancers accumulate aneuploidies of varying degrees (52-55, 61). Aneuploidy is a paradoxical phenomenon and reveals the sensitivity of the eukaryotic genome.
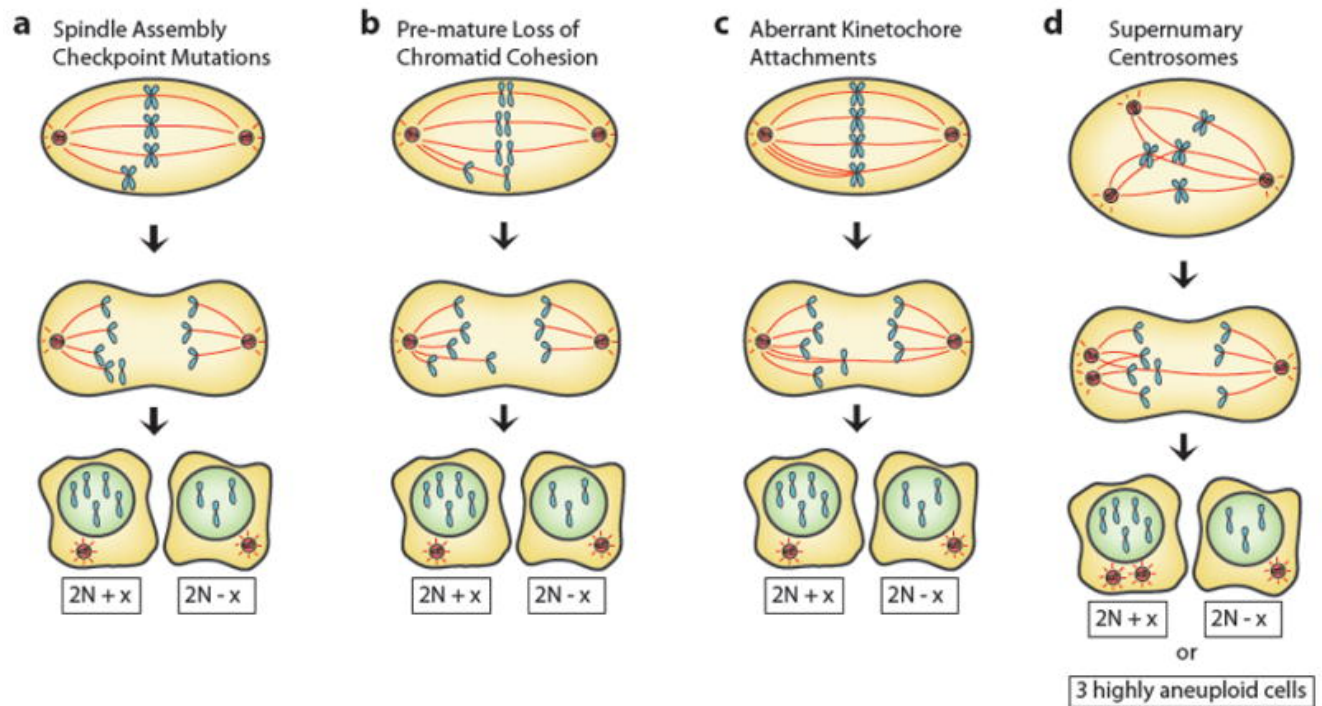
Figure 7. Errors in chromosome segregation cause aneuploidy. Adapted from Siegel & Amon (2012; 55).

(a) Mutations and subsequent failures of the SAC cause cells to segregate their chromosomes without proper bi-orientation, leading to chromosomes gains or losses.

(b) Sister chromatids that lose their cohesion prematurely can segregate erroneously.

(c) The attachment of too many or too few microtubules to a kinetochore can disrupt proper chromosome segregation. A merotelic attachment is shown above and is characterized by the attachment of a kinetochore to both SPBs.

(d) An incorrect number of SPBs, or mammalian centrosomes, prevents bi-orientation of chromosomes and leads to chromosome missegregation.

For the most part, cells do not tolerate aneuploidy (52, 53, 55). Many chromosome-specific effects as well as global effects can occur in aneuploid cells. It has been shown that an

increase or decrease in gene copy number usually results in a correlated change of mRNA and protein levels, meaning that aneuploid cells synthesize too many or too few proteins from the missegregated chromosomes (55, 58). Cells are particularly sensitive to changes in expression of genes that encode subunits of macromolecular complexes. As a dosage compensation mechanism, subunits of macromolecular complexes encoded in excess aggregate or are degraded, leading to proteotoxic stress and further burden on protein quality control machinery (53, 59, 60). Global effects of aneuploidy are independent of karyotype and cause general proliferation defects in aneuploid cells, and the causes and consequences of the slowed cell cycle in aneuploid cells are still debated and further discussed in this thesis (54, 55, 58).

Temperature-sensitive *cdc* mutants

To understand the molecular mechanisms of the cell cycle, early *S. cerevisiae* screens revealed temperature-sensitive mutations in genes responsible for essential cell division cycle proteins, termed *cdc-ts* mutations. At the permissive temperature, *cdc-ts* mutant cells can proliferate although often slower than wild-type cells (53, 54). At the restrictive temperature, cells continue to accumulate biomass but cannot divide due to mutations causing misfolding in essential cell cycle proteins (53). Cells arrest in the stage of the cell cycle that requires their mutant protein, and images of *cdc-ts* cell morphology and budding state at the restrictive temperature are shown in Figure 8. These mutants have been crucial in understanding both the budding yeast cell cycle as well as the mammalian cell cycle.

cdc gene number	prototype phenotype
1,19,25,29	
22,28,32	
24	
4	
2,6,7,8,9,13,16,17,20,21,23,26,30	
14,15,27,31	
5,18	
3,10,11,12	

Figure 8. Morphology of *cdc-ts* mutants at the restrictive temperature. Adapted from Hartwell et al. (1973; 56). At the restrictive temperature, *cdc-ts* mutants arrest at different phases of the cell cycle, depending on how a mutant protein is preventing cell cycle progression. Hartwell et al. (1973; 56) first characterized *cdc-ts* mutants by their cell morphology.

Previous work from our lab, shown in Figure 9, determined that at the restrictive temperature, the growth of many *cdc-ts* mutants eventually slows, suggesting the presence cell size regulation. Cells can reach a final volume of up to 800 fL, which is approximately 16-fold larger than the cell volume of proliferating wild-type cells (57). Protein concentration does not

scale with the increase in cell volume, resulting in cytoplasmic dilution and decrease of cell density (5). However, some *cdc-ts* cells are able to survive cell cycle arrests and eventually continue to proliferate, and the efficiency of which *cdc-ts* cells can re-enter the cell cycle is dependent on cell size, suggesting a possible mechanism for coordinating cell growth and division to ensure viability throughout arrest in the cell cycle (5, 57).
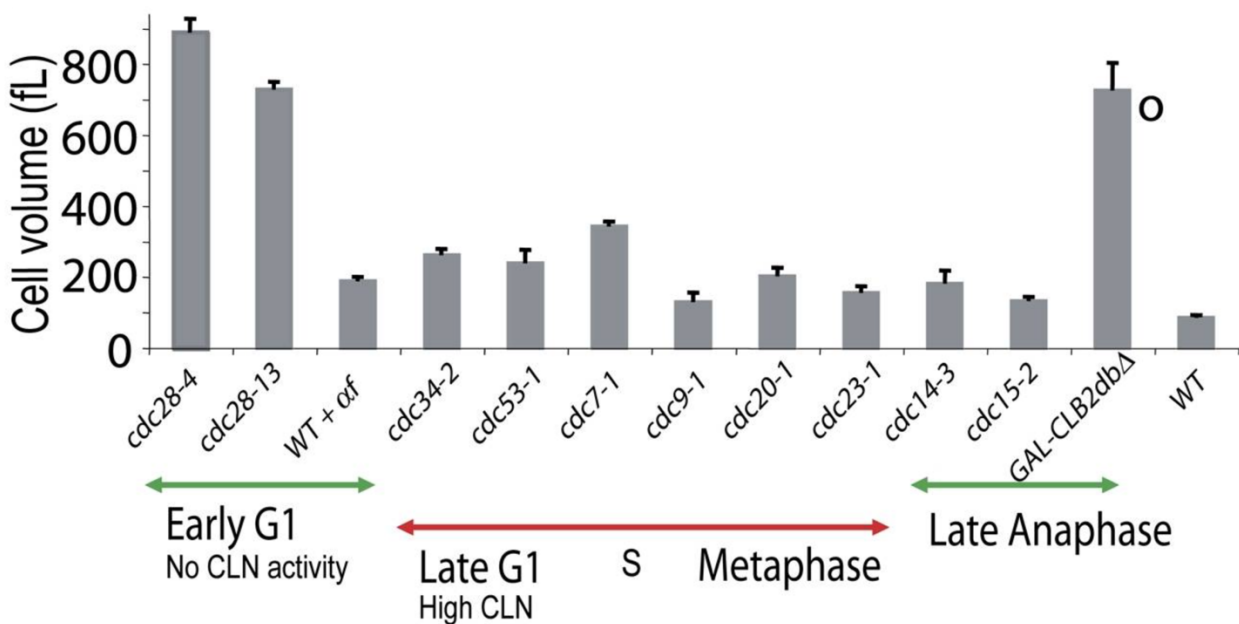
Figure 9. Arrested *cdc-ts* mutants increase in size. Adapted from Goranov et al. (2009; 57). Temperature-sensitive *cdc* mutants arrest in the cell cycle at different stages, determined by the role of the mutant protein. After being arrested in the cell cycle by growth at 37°C for 10 hours, *cdc-ts* mutants increase their cell volume to a maximum limit, which differs between strains and can be up to 16-fold larger than proliferating wild-type cells. Upon arrest, cell growth rate is highest in cells arrested in G1.

Concluding remarks

Homeostasis of cell size is essential to the survival and proliferation of eukaryotic cells and is regulated by the tight coordination of biomass accumulation and cell division (1, 2). Cells accumulate biomass by transcribing genes into mRNA and subsequently translating mRNA into proteins, the latter relying on a macromolecular machine composed of RNA and proteins, known as the ribosome (11, 13, 14). The portion of ribosomal proteins in the cell's proteome can represent the capacity for ribosomes to produce proteins and correlates to growth rate (17, 21, 22). Nutrients sensing pathways, specifically the Ras/PKA and TORC1 pathways, are able to regulate ribosome biosynthesis to ensure that growth rate matches nutrient availability through the ESR (2, 22, 23).

The ability of cells to accumulate biomass is known to affect cell cycle progression. In G1, the first stage of the cell cycle, cells must grow to a size threshold set by nutrient availability, termed "critical size," in order to commit to replicating and segregating their genome. When cells have mutations in essential cell cycle progression genes or missegregate their chromosomes, cell cycle progression slows or halts, often leading to increases in cell volume (52-57). A key question remains: how do changes in progression of the cell cycle affect a cell's ability to accumulate biomass?

Here, I investigate how cells alter their translational capacity in response to a slowed or arrested cell cycle in aneuploid and *cdc-ts* budding yeast, respectively. In both, the ESR is activated, and ribosomes are subsequently downregulated. Similar ESR activation and ribosome downregulation occurs under conditions known to inhibit the TORC1 or Ras/PKA pathway. Finally, I show that in *cdc-ts* mutants, hyperactivation of the Ras/PKA pathway suppresses ESR activation and decreases cell viability, while cells no longer attenuate their volume growth

through ribosomal downregulation, revealing a potentially essential role of the ESR in

coordination of cell size and cell cycle progression.

References

1. Amodeo, A. A., & Skotheim, J. M. (2016). Cell-Size Control. *Cold Spring Harbor perspectives in biology*, *8*(4), a019083. https://doi.org/10.1101/cshperspect.a019083

2. Jorgensen, P., & Tyers, M. (2004). How cells coordinate growth and division. *Current biology: CB*, *14*(23), R1014–R1027. https://doi.org/10.1016/j.cub.2004.11.027

3. Koonin E. V. (2010). The origin and early evolution of eukaryotes in the light of phylogenomics. *Genome biology*, *11*(5), 209. https://doi.org/10.1186/gb-2010-11-5-209

4. Björklund, M., & Marguerat, S. (2017). Editorial: Determinants of Cell Size. *Frontiers in cell and developmental biology*, *5*, 115. https://doi.org/10.3389/fcell.2017.00115

5. Neurohr, G. E., Terry, R. L., Lengefeld, J., Bonney, M., Brittingham, G. P., Moretto, F., Miettinen, T. P., Vaites, L. P., Soares, L. M., Paulo, J. A., Harper, J. W., Buratowski, S., Manalis, S., van Werven, F. J., Holt, L. J., & Amon, A. (2019). Excessive Cell Growth Causes Cytoplasm Dilution and Contributes to Senescence. *Cell*, *176*(5), 1083–1097.e18. https://doi.org/10.1016/j.cell.2019.01.018

6. Onofre, S. B., Bertoldo, I. C., Abatti, D., Refosco, P. D. (2017). Chemical Composition of the Biomass of Saccharomyces cerevisiae - (Meyen ex E. C. Hansen, 1883) Yeast obtained from the Beer Manufacturing Process. International Journal of Environment Agriculture and Biotechnology (ISSN: 2456-1878).2(2), 0558-0562.10.22161/ijeab/2.2.2

7. Lange, H. C., & Heijnen, J. J. (2001). Statistical reconciliation of the elemental and molecular biomass composition of Saccharomyces cerevisiae. *Biotechnology and bioengineering*, *75*(3), 334–344. https://doi.org/10.1002/bit.10054

8. Futcher, B., Latter, G. I., Monardo, P., McLaughlin, C. S., & Garrels, J. I. (1999). A sampling of the yeast proteome. *Molecular and cellular biology*, *19*(11), 7357–7368. https://doi.org/10.1128/mcb.19.11.7357

9. Björkeroth, J., Campbell, K., Malina, C., Yu, R., Di Bartolomeo, F., & Nielsen, J. (2020). Proteome reallocation from amino acid biosynthesis to ribosomes enables yeast to grow faster in rich media. *Proceedings of the National Academy of Sciences of the United States of America*, *117*(35), 21804–21812. https://doi.org/10.1073/pnas.1921890117

10. Goffeau, A., Barrell, B. G., Bussey, H., Davis, R. W., Dujon, B., Feldmann, H., Galibert, F., Hoheisel, J. D., Jacq, C., Johnston, M., Louis, E. J., Mewes, H. W., Murakami, Y., Philippsen, P., Tettelin, H., & Oliver, S. G. (1996). Life with 6000 genes. *Science (New York, N.Y.)*, *274*(5287), 546–567.

11. Hahn, S., & Young, E. T. (2011). Transcriptional regulation in Saccharomyces cerevisiae: transcription factor regulation and function, mechanisms of initiation, and roles of activators and coactivators. *Genetics*, *189*(3), 705–736. https://doi.org/10.1534/genetics.111.127019

12. Bernstein, J., & Toth, E. A. (2012). Yeast nuclear RNA processing. *World journal of biological chemistry*, *3*(1), 7–26. https://doi.org/10.4331/wjbc.v3.i1.7

13. Müller, P. P., & Trachsel, H. (1990). Translation and regulation of translation in the yeast Saccharomyces cerevisiae. *European journal of biochemistry*, *191*(2), 257–261. https://doi.org/10.1111/j.1432-1033.1990.tb19118.x

14. Warner J. R. (1999). The economics of ribosome biosynthesis in yeast. *Trends in biochemical sciences*, *24*(11), 437–440. https://doi.org/10.1016/s0968-0004(99)01460-7

15. Metzl-Raz, E., Kafri, M., Yaakov, G., Soifer, I., Gurvich, Y., & Barkai, N. (2017). Principles of cellular resource allocation revealed by condition-dependent proteome profiling. *eLife*, *6*, e28034. https://doi.org/10.7554/eLife.28034

16. Verschoor, A., Warner, J. R., Srivastava, S., Grassucci, R. A., & Frank, J. (1998). Three-dimensional structure of the yeast ribosome. *Nucleic acids research*, *26*(2), 655–661. https://doi.org/10.1093/nar/26.2.655

17. Woolford, J. L., Jr, & Baserga, S. J. (2013). Ribosome biogenesis in the yeast Saccharomyces cerevisiae. *Genetics*, *195*(3), 643–681. https://doi.org/10.1534/genetics.113.153197

18. Greber B. J. (2016). Mechanistic insight into eukaryotic 60S ribosomal subunit biogenesis by cryo-electron microscopy. *RNA (New York, N.Y.)*, *22*(11), 1643–1662. https://doi.org/10.1261/rna.057927.116

19. Bosio, M. C., Fermi, B., & Dieci, G. (2017). Transcriptional control of yeast ribosome biogenesis: A multifaceted role for general regulatory factors. *Transcription*, *8*(4), 254–260. https://doi.org/10.1080/21541264.2017.1317378

20. Bosio, M. C., Fermi, B., Spagnoli, G., Levati, E., Rubbi, L., Ferrari, R., Pellegrini, M., & Dieci, G. (2017). Abf1 and other general regulatory factors control ribosome biogenesis gene expression in budding yeast. *Nucleic acids research*, *45*(8), 4493–4506. https://doi.org/10.1093/nar/gkx058

21. Mager, W. H., & Planta, R. J. (1991). Coordinate expression of ribosomal protein genes in yeast as a function of cellular growth rate. *Molecular and cellular biochemistry*, *104*(1-2), 181–187. https://doi.org/10.1007/BF00229818

22. Broach, J. R. (2012). Nutritional Control of Growth and Development in Yeast. *Genetics, 192*(1), 73-105. htts://doi.org/10.1534/genetics.111.135731

23. Conrad, M., Schothorst, J., Kankipati, H. N., Van Zeebroeck, G., Rubio-Texeira, M., & Thevelein, J. M. (2014). Nutrient sensing and signaling in the yeast *Saccharomyces cerevisiae*. *Fems Microbiology Reviews*, *38*(2), 254–299. http://doi.org/10.1111/1574-6976.12065

24. González, A., & Hall, M. N. (2017). Nutrient sensing and TOR signaling in yeast and mammals. *The EMBO journal*, *36*(4), 397–408. https://doi.org/10.15252/embj.201696010

25. Jorgensen, P., Rupes, I., Sharom, J. R., Schneper, L., Broach, J. R., & Tyers, M. (2004). A dynamic transcriptional network communicates growth potential to ribosome synthesis and critical cell size. *Genes & development*, *18*(20), 2491–2505. https://doi.org/10.1101/gad.1228804

26. Kunkel J, Luo X, Capaldi AP. Integrated TORC1 and PKA signaling control the temporal activation of glucose-induced gene expression in yeast. Nat Commun. 2019 Aug 8;10(1):3558. doi: 10.1038/s41467-019-11540-y. PMID: 31395866; PMCID: PMC6687784.

27. Smith, A., Ward, M. P., & Garrett, S. (1998). Yeast PKA represses Msn2p/Msn4p-dependent gene expression to regulate growth, stress response and glycogen accumulation. *The EMBO journal*, *17*(13), 3556–3564. https://doi.org/10.1093/emboj/17.13.3556

28. Gasch, A. P., Spellman, P. T., Kao, C. M., Carmel-Harel, O., Eisen, M. B., Storz, G., Botstein, D., & Brown, P. O. (2000). Genomic expression programs in the response of

yeast cells to environmental changes. *Molecular biology of the cell*, *11*(12), 4241–4257. https://doi.org/10.1091/mbc.11.12.4241

29. Ho, Y. H., & Gasch, A. P. (2015). Exploiting the yeast stress-activated signaling network to inform on stress biology and disease signaling. *Current genetics*, *61*(4), 503–511. https://doi.org/10.1007/s00294-015-0491-0

30. Brauer, M. J., Huttenhower, C., Airoldi, E. M., Rosenstein, R., Matese, J. C., Gresham, D., Boer, V. M., Troyanskaya, O. G., & Botstein, D. (2008). Coordination of growth rate, cell cycle, stress response, and metabolic activity in yeast. *Molecular biology of the cell*, *19*(1), 352–367. https://doi.org/10.1091/mbc.e07-08-0779

31. Rep, M., Reiser, V., Gartner, U., Thevelein, J. M., Hohmann, S., Ammerer, G., & Ruis, H. (1999). Osmotic stress-induced gene expression in Saccharomyces cerevisiae requires Msn1p and the novel nuclear factor Hot1p. *Molecular and cellular biology*, *19*(8), 5474–5485. https://doi.org/10.1128/mcb.19.8.5474

32. Hunt, T., Nasmyth, K., & Novák, B. (2011). The cell cycle. *Philosophical transactions of the Royal Society of London. Series B, Biological sciences*, *366*(1584), 3494–3497. https://doi.org/10.1098/rstb.2011.0274

33. Vermeulen, K., Van Bockstaele, D. R., & Berneman, Z. N. (2003). The cell cycle: a review of regulation, deregulation and therapeutic targets in cancer. *Cell proliferation*, *36*(3), 131–149. https://doi.org/10.1046/j.1365-2184.2003.00266.x

34. Cooper GM. The Cell: A Molecular Approach. 2nd edition. Sunderland (MA): Sinauer Associates; 2000. The Eukaryotic Cell Cycle. Available from: https://www.ncbi.nlm.nih.gov/books/NBK9876/

35. Boettcher, B., & Barral, Y. (2013). The cell biology of open and closed mitosis. *Nucleus (Austin, Tex.)*, *4*(3), 160–165. https://doi.org/10.4161/nucl.24676

36. Mendenhall, M. D., & Hodge, A. E. (1998). Regulation of Cdc28 cyclin-dependent protein kinase activity during the cell cycle of the yeast Saccharomyces cerevisiae. *Microbiology and molecular biology reviews: MMBR*, *62*(4), 1191–1243.

37. Campbell, I. C. (2019). *The Mitotic Exit Network detects spindle position and anaphase entry* (Doctoral dissertation). Retrieved from DSpace (1117709695).

38. Dorsey, S., Tollis, S., Cheng, J., Black, L., Notley, S., Tyers, M., & Royer, C. A. (2018). G1/S Transcription Factor Copy Number Is a Growth-Dependent Determinant of Cell Cycle Commitment in Yeast. *Cell systems*, *6*(5), 539–554.e11. https://doi.org/10.1016/j.cels.2018.04.012

39. Bell, S. P., & Labib, K. (2016). Chromosome Duplication in Saccharomyces cerevisiae. *Genetics*, *203*(3), 1027–1067. https://doi.org/10.1534/genetics.115.186452

40. Stillman B. (1996). Cell cycle control of DNA replication. *Science (New York, N.Y.)*, *274*(5293), 1659–1664. https://doi.org/10.1126/science.274.5293.1659

41. Williams, J. S., Clausen, A. R., Nick McElhinny, S. A., Watts, B. E., Johansson, E., & Kunkel, T. A. (2012). Proofreading of ribonucleotides inserted into DNA by yeast DNA polymerase ε. *DNA repair*, *11*(8), 649–656. https://doi.org/10.1016/j.dnarep.2012.05.004

42. Weinert, T. A., Kiser, G. L., & Hartwell, L. H. (1994). Mitotic checkpoint genes in budding yeast and the dependence of mitosis on DNA replication and repair. *Genes & development*, *8*(6), 652–665. https://doi.org/10.1101/gad.8.6.652

43. King, S. M. & Hyams, J. S. (1982). The mitotic spindle of Saccharomyces cerevisiae: Assembly, structure and function. *Micron*, *13*(2), 93-117. https://doi.org/10.1016/0047-7206(82)90078-4

44. Carminati, J. L., & Stearns, T. (1997). Microtubules orient the mitotic spindle in yeast through dynein-dependent interactions with the cell cortex. *The Journal of cell biology*, *138*(3), 629–641. https://doi.org/10.1083/jcb.138.3.629

45. Tanaka T. U. (2005). Chromosome bi-orientation on the mitotic spindle. *Philosophical transactions of the Royal Society of London. Series B, Biological sciences*, *360*(1455), 581–589. https://doi.org/10.1098/rstb.2004.1612

46. Nasmyth, K., & Haering, C. H. (2009). Cohesin: its roles and mechanisms. *Annual review of genetics*, *43*, 525–558. https://doi.org/10.1146/annurev-genet-102108-134233

47. Amon A. (2008). A decade of Cdc14--a personal perspective. Delivered on 9 July 2007 at the 32nd FEBS Congress in Vienna, Austria. *The FEBS journal*, *275*(23), 5774–5784. https://doi.org/10.1111/j.1742-4658.2008.06693.x

48. Campbell, I. W., Zhou, X., & Amon, A. (2019). The Mitotic Exit Network integrates temporal and spatial signals by distributing regulation across multiple components. *eLife*, *8*, e41139. https://doi.org/10.7554/eLife.41139

49. Bardin, A. J., Visintin, R., & Amon, A. (2000). A mechanism for coupling exit from mitosis to partitioning of the nucleus. *Cell*, *102*(1), 21–31. https://doi.org/10.1016/s0092-8674(00)00007-6

50. Cagney, G., Alvaro, D., Reid, R. J., Thorpe, P. H., Rothstein, R., & Krogan, N. J. (2006). Functional genomics of the yeast DNA-damage response. *Genome biology*, *7*(9), 233. https://doi.org/10.1186/gb-2006-7-9-233

51. Pan, J., & Chen, R. H. (2004). Spindle checkpoint regulates Cdc20p stability in Saccharomyces cerevisiae. *Genes & development*, *18*(12), 1439–1451. https://doi.org/10.1101/gad.1184204

52. Torres, E. M., Williams, B. R., Tang, Y. C., & Amon, A. (2010). Thoughts on aneuploidy. *Cold Spring Harbor symposia on quantitative biology*, *75*, 445–451. https://doi.org/10.1101/sqb.2010.75.025

53. Santaguida, S., & Amon, A. (2015). Short- and long-term effects of chromosome mis-segregation and aneuploidy. *Nature reviews. Molecular cell biology*, *16*(8), 473–485. https://doi.org/10.1038/nrm4025

54. Sheltzer, J. M., Torres, E. M., Dunham, M. J., & Amon, A. (2012). Transcriptional consequences of aneuploidy. *Proceedings of the National Academy of Sciences of the United States of America*, *109*(31), 12644–12649. https://doi.org/10.1073/pnas.1209227109

55. Siegel, J. J., & Amon, A. (2012). New insights into the troubles of aneuploidy. *Annual review of cell and developmental biology*, *28*, 189–214. https://doi.org/10.1146/annurev-cellbio-101011-155807

56. Hartwell, L. H., Mortimer, R. K., Culotti, J., & Culotti, M. (1973). Genetic Control of the Cell Division Cycle in Yeast: V. Genetic Analysis of cdc Mutants. *Genetics*, *74*(2), 267–286.

57. Goranov, A. I., Cook, M., Ricicova, M., Ben-Ari, G., Gonzalez, C., Hansen, C., Tyers, M., & Amon, A. (2009). The rate of cell growth is governed by cell cycle stage. *Genes & development*, *23*(12), 1408–1422. https://doi.org/10.1101/gad.1777309

58. Torres, E. M., Sokolsky, T., Tucker, C. M., Chan, L. Y., Boselli, M., Dunham, M. J., & Amon, A. (2007). Effects of aneuploidy on cellular physiology and cell division in haploid yeast. *Science (New York, N.Y.)*, *317*(5840), 916–924. https://doi.org/10.1126/science.1142210

59. Morrill, S. A., & Amon, A. (2019). Why haploinsufficiency persists. *Proceedings of the National Academy of Sciences of the United States of America*, *116*(24), 11866–11871. https://doi.org/10.1073/pnas.1900437116

60. Brennan, C. M., Vaites, L. P., Wells, J. N., Santaguida, S., Paulo, J. A., Storchova, Z., Harper, J. W., Marsh, J. A., & Amon, A. (2019). Protein aggregation mediates stoichiometry of protein complexes in aneuploid cells. *Genes & development*, *33*(15-16), 1031–1047. https://doi.org/10.1101/gad.327494.119

61. Pfau, S. J., & Amon, A. (2012). Chromosomal instability and aneuploidy in cancer: from yeast to man. *EMBO reports*, *13*(6), 515–527. https://doi.org/10.1038/embor.2012.65

62. Goranov, A. I., & Amon, A. (2010). Growth and division--not a one-way road. *Current opinion in cell biology*, *22*(6), 795–800. https://doi.org/10.1016/j.ceb.2010.06.004

63. Goranov, A. I., Gulati, A., Dephoure, N., Takahara, T., Maeda, T., Gygi, S. P., Manalis, S., & Amon, A. (2013). Changes in cell morphology are coordinated with cell growth through the TORC1 pathway. *Current biology: CB*, *23*(14), 1269–1279. https://doi.org/10.1016/j.cub.2013.05.035

Chapter 2: The environmental stress response causes ribosome loss in aneuploid yeast cells

The experiments in Figures 3A-C; 4D; S5A; S6C-E were performed by AS and AT.
The experiments in Figure 3D; 4E; S5B were performed by AS, AK, MJD, and AT.
All RNASeq processing and ssGSEA projection value generation was performed by CAW.
All other experiments and analyses were performed by AT.

Significance statement

Aneuploid cells experience significant cellular stress, however, the transcriptional consequences of aneuploidy remain highly debated. In aneuploid budding yeast, two opposing gene expression patterns have been reported: the "environmental stress response" (ESR) and the "common aneuploidy gene-expression" (CAGE) signature, in which many ESR genes are oppositely regulated. Here we resolve this controversy. We show that the ESR represents a common response to aneuploidy and explain why the CAGE signature does not. Our data further suggest that activation of the ESR has profound consequences on the cellular physiology of aneuploid cells, leading to ribosome loss. Thus, our work provides critical insights into the coordination between cell division and macromolecule biosynthesis and a potential explanation for why aneuploid cells are less dense.

Abstract

Aneuploidy, a condition characterized by whole chromosome gains and losses, is often associated with significant cellular stress and decreased fitness. However, how cells respond to the aneuploid state has remained controversial. In aneuploid budding yeast, two opposing gene expression patterns have been reported: the "environmental stress response" (ESR) and the "common aneuploidy gene-expression" (CAGE) signature, in which many ESR genes are oppositely regulated. Here, we investigate this controversy. We show that the CAGE signature is not an aneuploidy-specific gene expression signature but the result of normalizing the gene expression profile of actively proliferating aneuploid cells to that of euploid cells grown into stationary phase. Because growth into stationary phase is amongst the strongest inducers of the ESR, the ESR in aneuploid cells was masked when stationary phase euploid cells were used for

normalization in transcriptomic studies. When exponentially growing euploid cells are used in gene expression comparisons with aneuploid cells, the CAGE signature is no longer evident in aneuploid cells. Instead, aneuploid cells exhibit the ESR. We further show that the ESR causes selective ribosome loss in aneuploid cells, providing an explanation for the decreased cellular density of aneuploid cells. We conclude that aneuploid budding yeast cells mount the ESR, rather than the CAGE signature, in response to aneuploidy-induced cellular stresses, resulting in selective ribosome loss. We propose that the ESR serves two purposes in aneuploid cells: protecting cells from aneuploidy-induced cellular stresses and preventing excessive cellular enlargement during slowed cell cycles by downregulating translation capacity.

Introduction

Dividing cells rely on multiple complex mechanisms to correctly segregate their chromosomes and create euploid progeny. When chromosome missegregation occurs, daughter cells can acquire an incorrect number of chromosomes that is not a complete multiple of the haploid genome, a condition termed aneuploidy. Aneuploidy can occur naturally; for example, 17% of wild budding yeast isolates harbor aneuploidies and are thought to have evolved mechanisms to tolerate these aneuploid karyotypes (1, 2). In most cases, however, aneuploidy is highly detrimental, especially in multicellular animals (3).

Various models have been developed to study aneuploidy in *S. cerevisiae*. Their analyses led to the conclusions that aneuploidy affects a wide range of cellular processes, such as protein homeostasis, metabolism, and cell wall integrity, and results in an overall decrease in cellular fitness (3, 4). However, how aneuploidy affects gene expression has remained controversial. While it is clear that gene expression scales with gene copy number in aneuploid cells, there is

not yet a consensus on whether aneuploidy elicits a global transcriptional response in yeast and what this response may be.

We previously described that haploid aneuploid yeast cells harboring only one additional chromosome (henceforth disomic yeast strains) experience an environmental stress response (ESR) (5). The ESR is a transcriptional signature observed in response to nearly every type of exogenous stress, including hyper-osmotic, heat shock, oxidative and reductive stress, and nutrient limitation. These conditions cause the coordinated upregulation of approximately 300 genes, also known as the "induced (i)ESR" and downregulation of approximately 600 genes, also known as the "repressed (r)ESR" (6, 7). Genes that are upregulated compensate for various stressors and encode chaperones, amino acid transporters, and proteins involved in increasing endocytosis and proteasome activity. Downregulated genes encode factors critical for transcription and translation, among them are genes encoding ribosomal proteins and proteins involved in ribosome biogenesis (5, 6). The ESR is not only observed in response to stress but also in cells that grow slowly or cells that are cell cycle-arrested (4, 5, 8). Indeed, the strength of the ESR, that is the degree to which iESR genes are upregulated and rESR genes are downregulated, correlates remarkably well with growth rate, suggesting that this transcriptional signature is primarily determined by proliferation rate (4).

A recent study by Tsai et al. (2019; 9) reported that yeast cell populations harboring heterogenous aneuploidies do not exhibit the ESR. Instead, these aneuploid populations were described to exhibit a transcriptional response, termed the "common aneuploidy gene-expression" (CAGE) response. In the CAGE response, the genes that are upregulated in the ESR are downregulated, and those that are downregulated in the ESR are upregulated. The authors further found that the CAGE response bears similarity to a hypo-osmotic shock gene expression
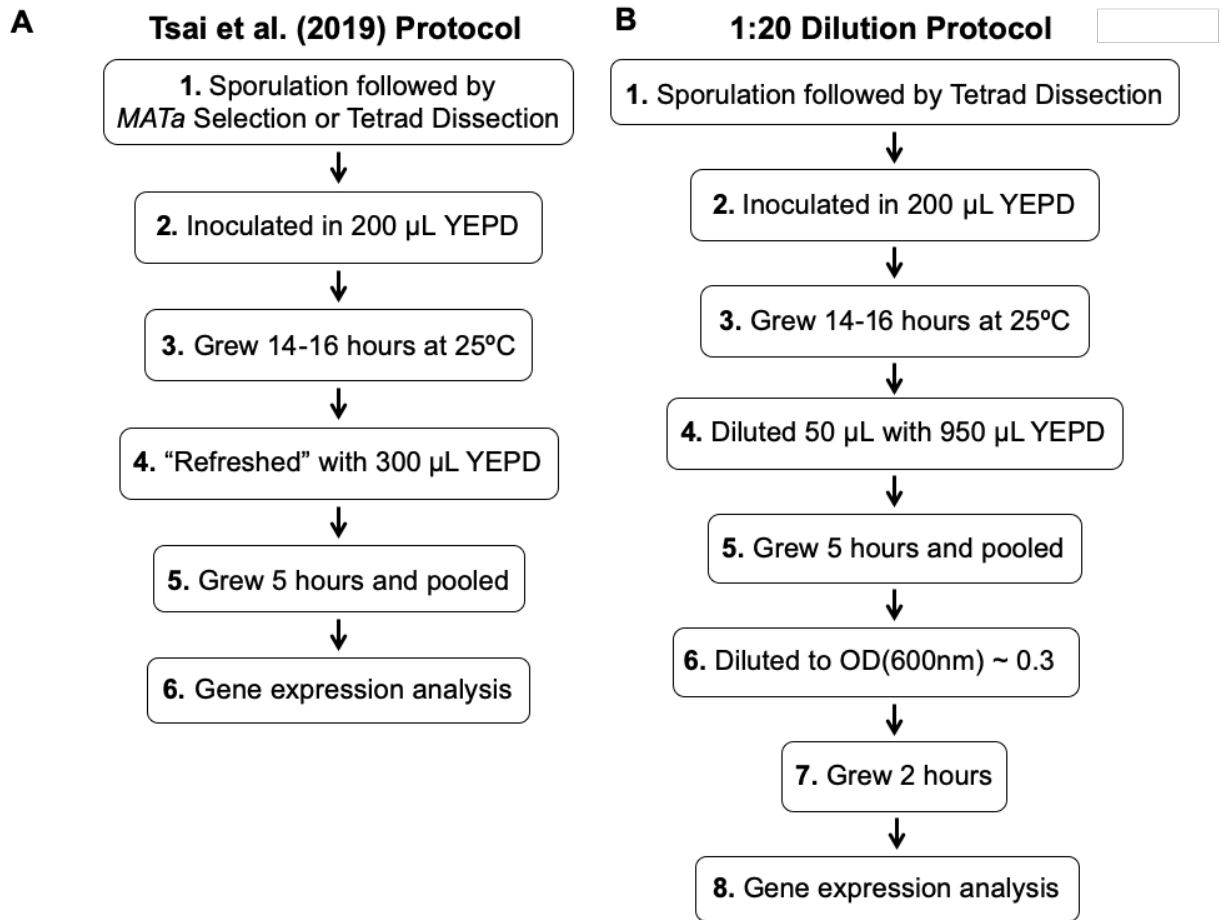
pattern, which was proposed to counter a decrease in cytoplasmic density observed in aneuploid cells (9, 10).

We report here the reanalysis of the gene expression data generated by Tsai et al. (2019; 9) as well as replication of their experimental approach. These analyses showed that the CAGE gene expression signature described by Tsai et al. (2019; 9) is an artifact caused by normalizing the gene expression of actively dividing aneuploid cells to that of euploid control cells that had grown to stationary phase. Growth into stationary phase is amongst the strongest inducers of the ESR (6). Thus, when Tsai et al. (2019; 9) compared the gene expression pattern of euploid stationary phase cells to that of aneuploid cells that, due to their poor proliferation, had not yet reached stationary phase, the ESR caused by aneuploidy was obscured. We find that when exponentially growing euploid cells were used in gene expression comparisons with aneuploid cells, the CAGE signature of aneuploid cells is no longer evident. Instead, aneuploid cell populations are found to exhibit the ESR, confirming previous reports (5). Using strains harboring multiple aneuploidies, we further show that the ESR causes a selective loss of ribosomes in aneuploid cells, providing a potential explanation for decreased cellular density previously reported to occur in response to chromosome gains and losses. We conclude that aneuploid budding yeast cells mount the ESR in response to aneuploidy-induced cellular stresses that results in ribosome loss.

Results

Exponentially growing haploid cells exhibit a transcriptional response, previously described to be unique to aneuploid cells.

A recent study (9) reported the absence of the "environmental stress response" (ESR) in populations of yeast cells harboring different, random aneuploid karyotypes. Instead, it was reported that these heterogeneous aneuploid yeast populations exhibit the "common aneuploidy gene-expression" (CAGE) signature. In this study, Tsai et al. (2019; 9) developed two protocols to generate heterogeneous populations of aneuploid cells, taking advantage of the fact that sporulation of triploid cells results in high levels of aneuploid progeny. In the first method, Tsai et al. (2019; 9) dissected spores obtained from triploid cells, grew individual aneuploid spores into colonies, pooled these colonies and analyzed the gene expression pattern of these cells (Fig. S1*A*). We will refer to these aneuploid populations as "aneuploid populations obtained from tetrads." Euploid haploid cells obtained from sporulating diploid cells and handled in the same manner as aneuploid cells served as the control (henceforth "euploid populations obtained from tetrads"). In the second protocol, Tsai et al. (2019; 9) sporulated triploid cells, and then selected viable *MATa* aneuploid colonies by selecting for histidine prototrophy brought about by *HIS5* expressed from the *MATa*-specific *STE2* promoter (Fig. S1*A*). We will refer to these aneuploid populations as "aneuploid populations obtained from *MATa* selection." Again, euploid haploid cells obtained by sporulating diploid cells and *MATa* selected served as the euploid control (henceforth "euploid populations obtained from *MATa* selection"). Gene expression analysis of these cell populations led to the identification of an expression signature Tsai et al. (2019; 9) termed "common aneuploidy gene-expression" (CAGE) response. This gene expression signature resembles a hypo-osmotic stress response and is essentially oppositely regulated to the ESR; 59.8% of genes upregulated in the CAGE response are downregulated in the ESR, while 13.2% of CAGE downregulated genes are upregulated in the ESR (9).

A   Tsai et al. (2019) Protocol

1. Sporulation followed by *MATa* Selection or Tetrad Dissection
↓
2. Inoculated in 200 μL YEPD
↓
3. Grew 14-16 hours at 25ºC
↓
4. "Refreshed" with 300 μL YEPD
↓
5. Grew 5 hours and pooled
↓
6. Gene expression analysis

B   1:20 Dilution Protocol

1. Sporulation followed by Tetrad Dissection
↓
2. Inoculated in 200 μL YEPD
↓
3. Grew 14-16 hours at 25ºC
↓
4. Diluted 50 μL with 950 μL YEPD
↓
5. Grew 5 hours and pooled
↓
6. Diluted to OD(600nm) ~ 0.3
↓
7. Grew 2 hours
↓
8. Gene expression analysis

Figure S1. Generation of heterogeneous aneuploid populations.

(*A*) Protocol developed by Tsai et al. (2019; 9) to generate aneuploid cell populations. Cells harboring random aneuploidies were generated by sporulation of *pRS315-STE2pr-spHIS5* S288C triploids (A40878) and subsequent tetrad dissection or *MATa* selection through histidine prototrophy. Individual colonies were grown for 14-16 hours in 200 μL of YEPD in a 96 deep-well plate. 300 μL of YEPD were then added to cultures. The cultures were grown for 5 additional hours, pooled, and analyzed.

(*B*) Protocol to avoid growth of cell populations into stationary phase (1:20 dilution protocol). Cells harboring random aneuploidies were generated by sporulation of *pRS315-STE2pr-spHIS5* S288C triploids (A40878) and subsequent tetrad dissection. Individual colonies were grown for
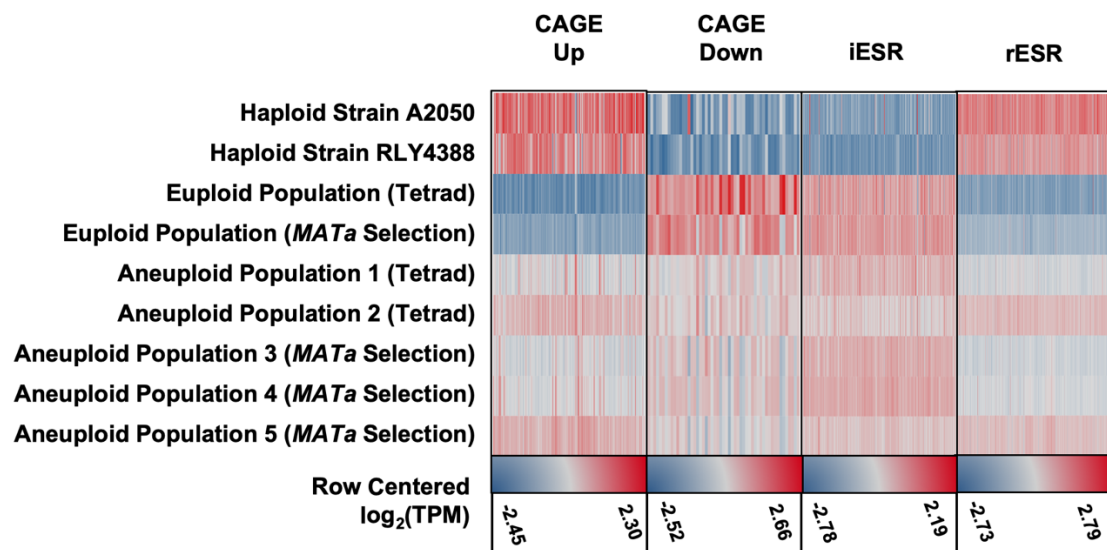
14-16 hours in 200 μL of YEPD in a 96 deep-well plate. Cultures were then diluted 1:20 in YEPD, grown for another 5 hours, then pooled, and diluted to approximately OD(600nm) = 0.3. The pooled aneuploid populations were grown for an additional 2 hours, and samples were taken.
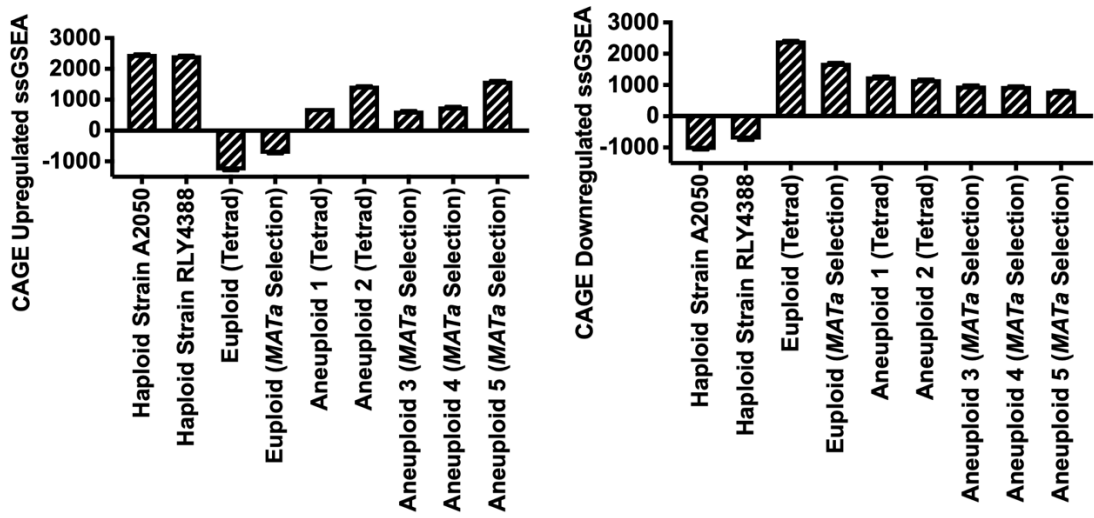

Having previously identified the ESR in yeast strains harboring defined aneuploidies (4, 5), we wished to determine why pooled aneuploid populations did not exhibit the ESR but instead the CAGE gene expression signature. To this end, we reanalyzed the gene expression data reported by Tsai et al. (2019; 9) by individually processing the samples rather than normalizing the aneuploid cell populations to the euploid control populations.

Among the RNA-Seq data sets deposited by Tsai et al. (2019; 9) was one termed "haploid control" that was obtained from a haploid strain RLY4388 grown in test tubes on roller drums (accession number: GSM2886452 and GSM2886453) that the authors did not analyze. Using the RNA-Seq by Expectation Maximization (RSEM) processing method, we calculated the raw transcripts per million (TPM) values for the aneuploid and euploid cell populations as well as strain RLY4388, then $\log_2$ transformed these values with a +1 offset to avoid negative expression values, and created row-centered heatmaps for genes upregulated and downregulated in both the CAGE and ESR gene expression signature (Fig. 1*A*). As previously reported, we observed the CAGE gene expression signature in the pooled aneuploid populations. Unexpectedly, however, strain RLY4388 exhibited the strongest CAGE gene expression signature, and the pooled euploid populations, used as normalization controls by Tsai et al. (2019; 9), exhibited the strongest ESR gene expression signature (Fig. 1*A*).

A

	CAGE Up	CAGE Down	iESR	rESR

Haploid Strain A2050
Haploid Strain RLY4388
Euploid Population (Tetrad)
Euploid Population (*MATa* Selection)
Aneuploid Population 1 (Tetrad)
Aneuploid Population 2 (Tetrad)
Aneuploid Population 3 (*MATa* Selection)
Aneuploid Population 4 (*MATa* Selection)
Aneuploid Population 5 (*MATa* Selection)

Row Centered log$_2$(TPM)

-2.45 2.30   -2.52 2.66   -2.78 2.19   -2.73 2.79

B

C

+500mM NaCl 40 minutes
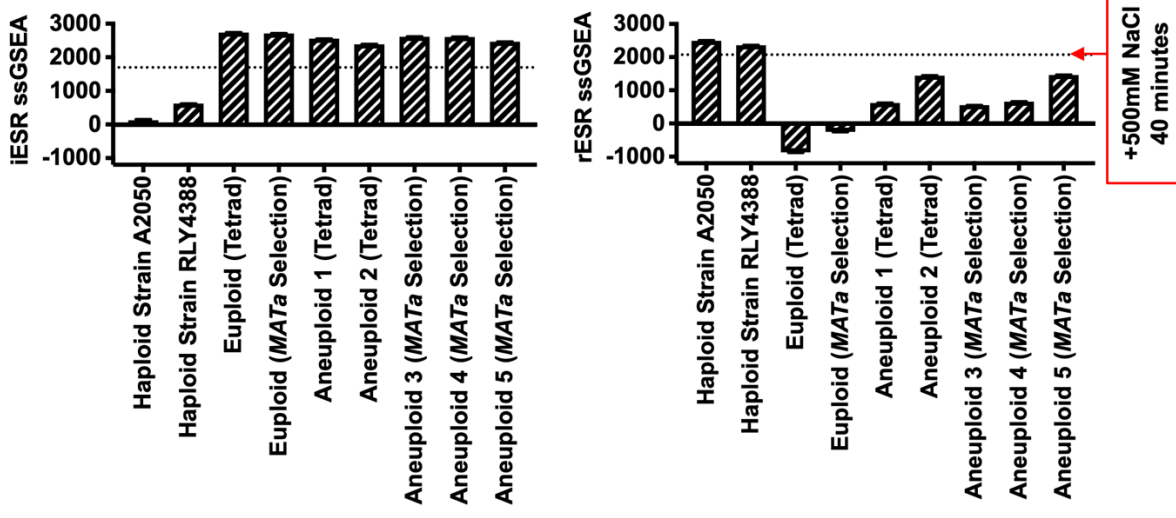
Figure 1. Reanalysis of published aneuploid transcription data from Tsai et al. (2019; 9).

Transcription data of haploid strain RLY4388 and euploid and aneuploid cell populations obtained from tetrad dissection (Tetrad) or *MATa* selection (*MATa* Selection) were reanalyzed with the RNA-Seq by Expectation Maximization (RSEM) processing method (Tsai et al. (2019; 9), accession number: GSE107997). Raw transcript per million (TPM) values were calculated for euploid cell populations, aneuploid cell populations, the haploid strain RLY4388 and exponentially growing haploid strain A2050.

(*A*) Row centered $\log_2$(TPM) values for each gene expression set (CAGE upregulated, CAGE downregulated, iESR, and rESR). Each gene set was row centered individually and has a separate maximum (red) and minimum (blue) values, noted underneath.

(*B*) CAGE upregulated and downregulated ssGSEA projection values for the haploid strains A2050 and RLY4388, and euploid and aneuploid cell populations (Tetrad and *MATa* Selection).

(*C*) iESR and rESR ssGSEA projection values for the haploid strains A2050 and RLY4388, and euploid and aneuploid cell populations (Tetrad and *MATa* Selection). The horizontal lines represent the iESR and rESR ssGSEA projection values for W303 wild-type cells (A2587) treated with 500 mM NaCl for 40 minutes, a positive control for the ESR induction. Error bars represent standard deviation from the mean of technical replicates.

Given that the haploid strain RLY4388 exhibited the strongest CAGE gene expression signature it was of interest to determine the growth state of these cells. According to Tsai et al. (2019; 9), this strain was grown in regular test tubes, but the OD(600nm) at which it was harvested was not recorded. To determine in which growth phase haploid strain RLY4388 was when harvested, we compared its gene expression profile to that of an exponentially growing

haploid strain of the same genetic background (S288C) from our lab (A2050; Strain Table S1). We observed a strong correlation between the genes expressed in both strains, indicating that haploid strain RLY4388 was in exponential phase when harvested (Fig. S2; Pearson, $R^2 = 0.91$, $P < 0.001$).
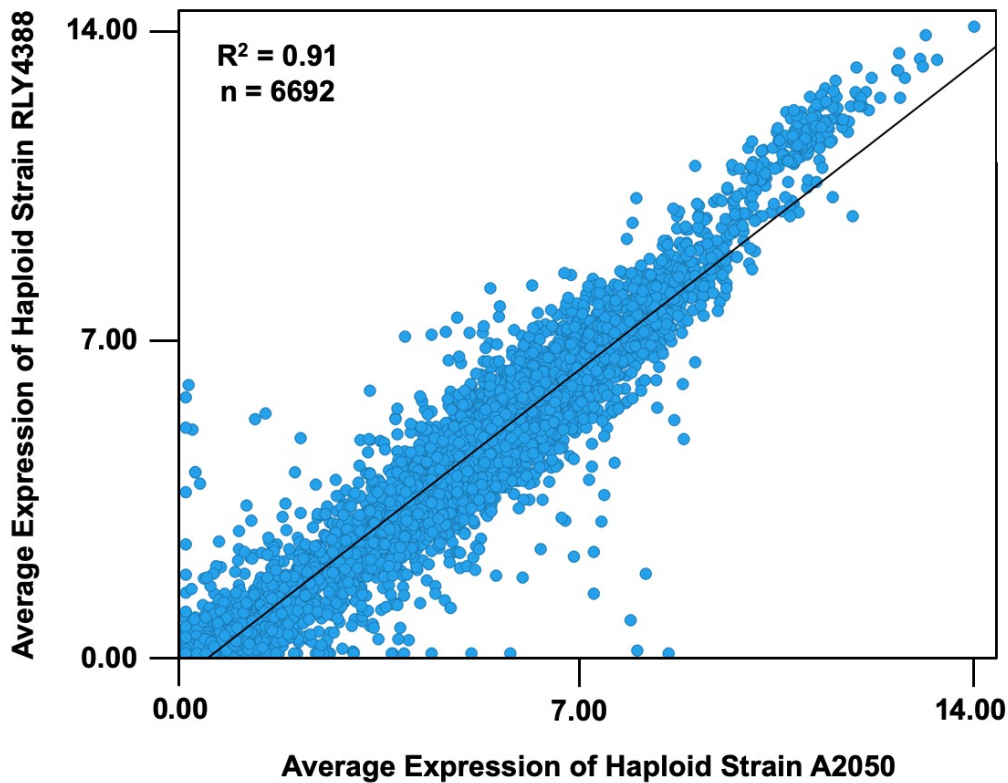
Figure S2. Correlation between average gene expression of haploid strain RLY4388 and average gene expression of haploid strain A2050.
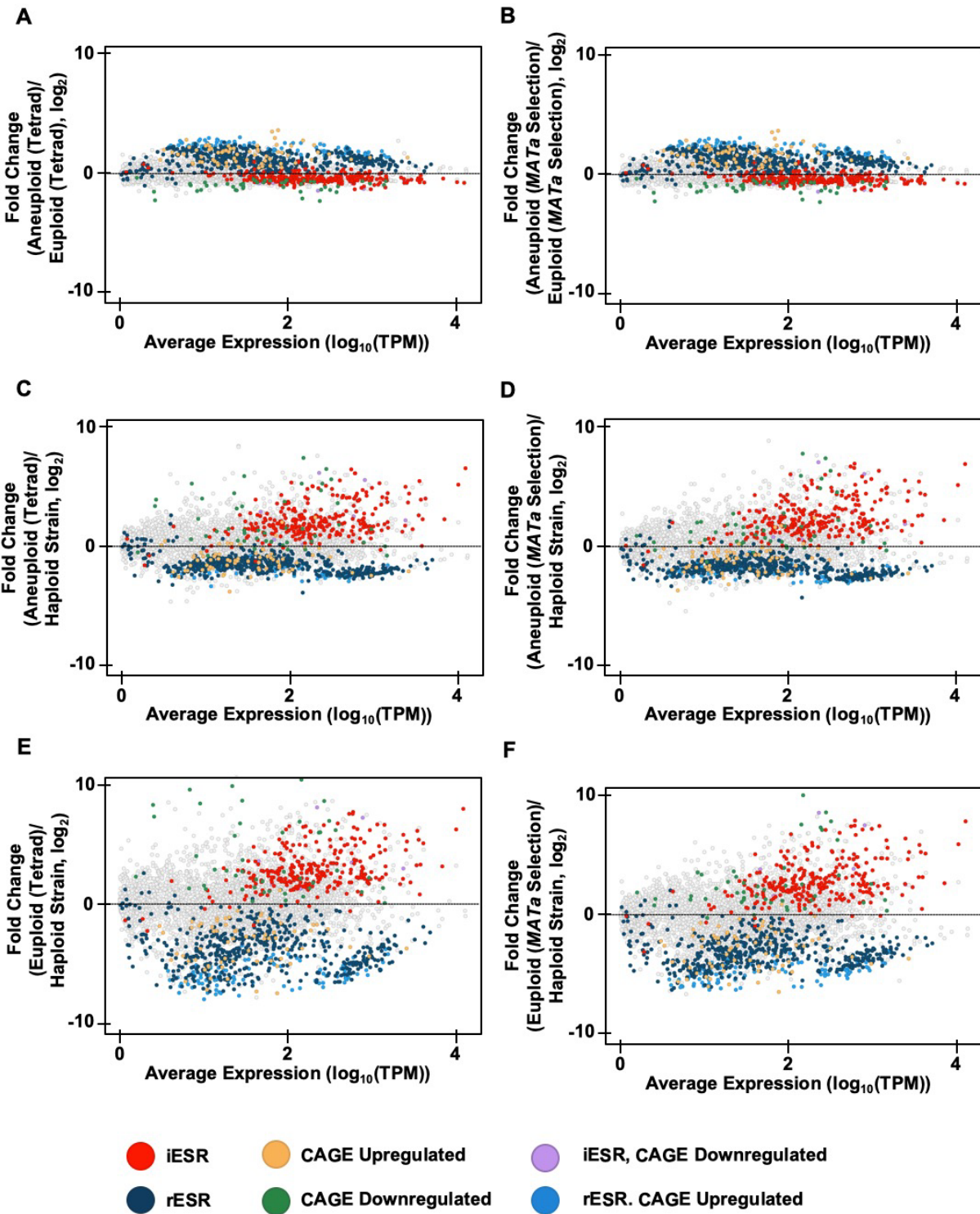
RNA-Seq data from strain RLY4388 (Tsai et al. (2019; 9)) and from exponentially growing haploid strain A2050 were processed using the Expectation Maximization (RSEM) method. Transcript per million (TPM) values were calculated and log_2 transformed with a +1 offset to

65

avoid negative expression values. Two techincal replicates from haploid strain RLY4388 and three technical replicates from haploid strain A2050 were averaged, and average gene expression between the two strains was compared (Pearson, $R^2 = 0.91$, $P < 0.001$).

Tsai et al. (2019; 9) discovered the CAGE response and the absence of the ESR in aneuploid cell populations by normalizing the gene expression of aneuploid cell populations to euploid control cell populations (9; Fig. S3*A* and *B*). Given that our analysis of their raw data showed that the euploid control populations exhibited a strong ESR, we used the gene expression data set obtained from the haploid strain RLY4388 to normalize the gene expression data from aneuploid populations instead of normalizing the data to that of euploid control populations. When compared to the gene expression data generated from strain RLY4388, aneuploid populations obtained from tetrad dissection and *MATa* selection exhibited the ESR, and the CAGE signature was no longer evident (Fig. S3*C* and *D*). When we measured the differential gene expression between euploid populations and strain RLY4388, it was also apparent that the euploid populations (Tetrad and *MATa* Selection) were experiencing the ESR (Fig. S3*E* and *F*).

Figure S3. Comparison of aneuploid and euploid gene expression patterns from Tsai et al. (2019; 9) to haploid strain RLY4388.

RNA-Seq data from Tsai et al. (2019; 9) were processed using the Expectation Maximization (RSEM) method. Transcript per million (TPM) values were calculated and $\log_2$ transformed. Expression data from aneuploid cell populations generated by tetrad dissection were pooled to create "aneuploid populations (Tetrad)". Expression data from aneuploid populations obtained from *MATa* selection were pooled to create "aneuploid populations (*MATa* Selection)". The x axis shows $\log_{10}$(average basal expression), and the y axis shows differential expression between euploid or aneuploid populations (Tetrad and *MATa* Selection) and two separate euploid controls: euploid cell populations and haploid strain RLY4388 (Tsai et al. (2019; 9), accession number: GSE107997). Colors specified refer to iESR, rESR, CAGE upregulated, CAGE downregulated, and those iESR genes downregulated in the CAGE signature and rESR genes upregulated in the CAGE signature. Differential expression graphs are shown for aneuploid cell populations (Tetrad) compared to euploid cell population (Tetrad) **(A)**, aneuploid cell populations (*MATa* Selection) compared to euploid cell population (*MATa* Selection) **(B)**, aneuploid cell populations (Tetrad) compared to haploid strain RLY4388 **(C)**, aneuploid cell populations (*MATa* Selection) compared to haploid strain RLY4388 **(D)**, euploid cell population (Tetrad) compared to haploid strain RLY4388 **(E)**, and euploid cell population (*MATa* Selection) compared to haploid strain RLY4388 **(F)**.

Given that the choice of euploid control (euploid populations versus a haploid wild-type strain RLY4388) made such a large difference in the experimental outcome, we decided to employ a data analysis method that does not depend on normalization. Single-sample gene set

enrichment analysis (ssGSEA) generates a single projection value for a set of genes within a sample. These values can then be compared between samples in order to measure how the gene expression distribution of that gene set changes across an experiment, i.e. overall increased or decreased expression of gene sets across samples (11). Using this approach, we confirmed that aneuploid cell populations exhibited the CAGE signature, while the euploid control cell populations did not (Fig. 1*B*). However, the samples with the strongest CAGE signature, thought to be a characteristic of aneuploidy, were obtained from exponentially growing haploid strain A2050 and strain RLY4388 (Fig. 1*B*).
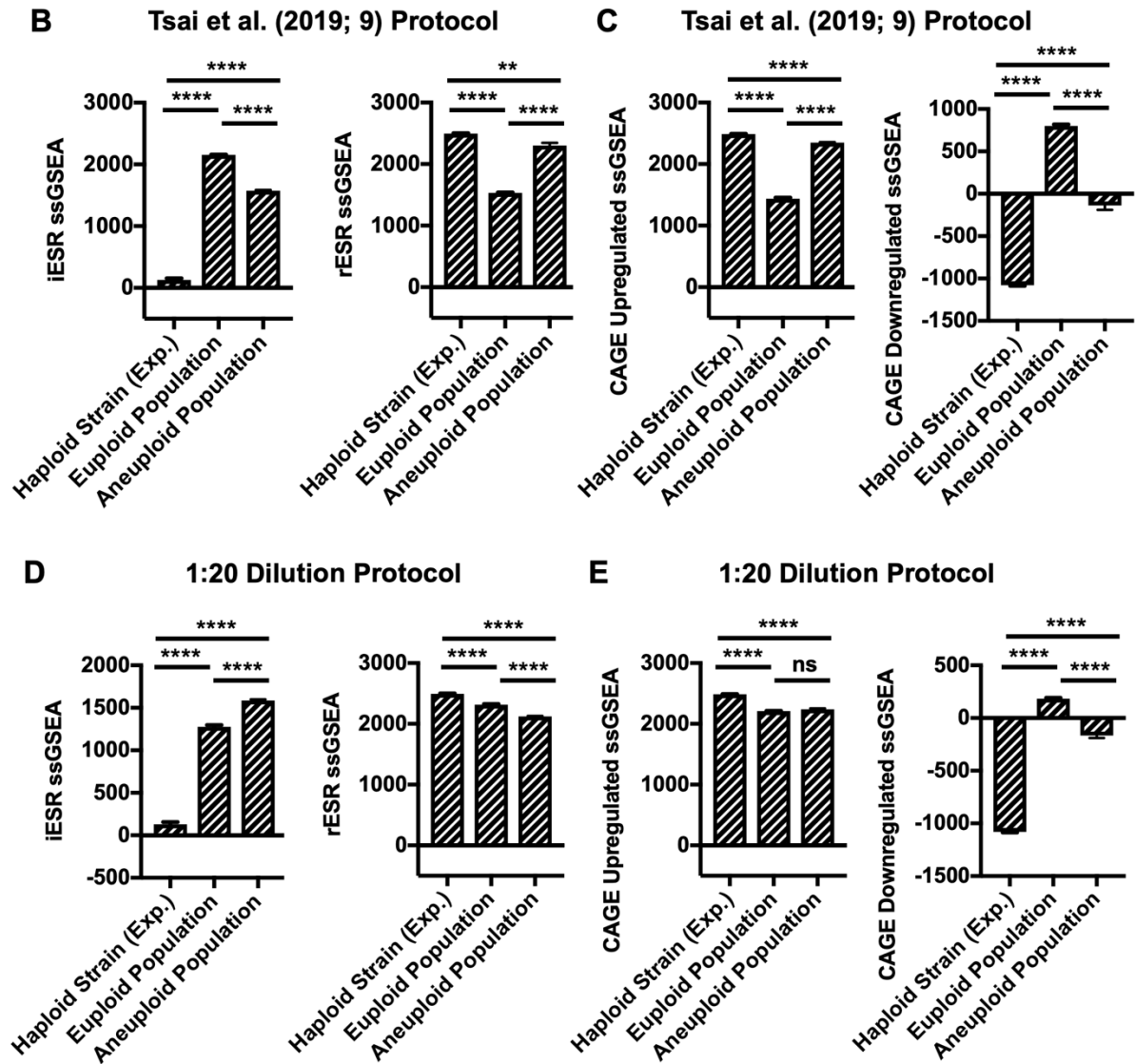
ssGSEA analysis of the ESR in aneuploid and euploid cell populations revealed equally unanticipated results. As expected, the exponentially growing haploid strain A2050 and RLY4388 did not exhibit the ESR (Fig. 1*C*). Consistent with our previous observations in disomic yeast strains (5), aneuploid cell populations showed the ESR, but the euploid control populations exhibited the ESR even more strongly (Fig. 1*C*). The degree to which the ESR was induced in these euploid control populations was greater than in exponentially growing wild-type cells (A2587) treated with 500 mM NaCl for 40 minutes. We conclude that the euploid control populations analyzed by Tsai et al. (2019; 9) exhibit the strongest ESR signature, indicating that they experienced significant exogenous stress.

Stationary phase cells exhibit the environmental stress response.

It was curious that the euploid control populations generated by Tsai et al. (2019; 9) strongly exhibited the ESR. To determine the cause of this robust ESR, we repeated their tetrad dissection protocol to obtain euploid and aneuploid cell populations, employing the strains used by Tsai et al. (2019; 9) after detailed consultation with the authors. We dissected 200 and 770

tetrads obtained from diploid and triploid cells, respectively. Spore viability for the euploid strain was 97.3% and, as expected, significantly lower for triploid strains (40.2%) because many aneuploid strains are inviable. We then followed the protocol developed by Tsai et al. (2019; 9) and grew colonies obtained from viable spores in individual wells of a 96-well deep well plate for 14-16 hours in 200 μL YEPD medium at 25 ºC (Fig. S1*A*) Thereafter, we added 300 μL YEPD medium to cultures and grew them for an additional 5 hours at 25 ºC. The euploid and aneuploid cultures were then separately pooled to create heterogeneous euploid and aneuploid cell populations. Using this growth protocol, pooled euploid populations had reached an OD(600nm) of 8.54. As expected, owing to aneuploid cells having significant proliferation defects, pooled aneuploid populations reached an OD(600nm) of only 2.62.

The high OD(600nm) values reached by the euploid population provided a potential explanation for why they exhibited a strong ESR. As cultures approach stationary phase, cells experience starvation, which is among the strongest inducers of the ESR (6). To test this hypothesis, we determined at which OD(600nm) S288C wild-type haploid cells activate the ESR. We grew cells into stationary phase in YEPD medium and measured rESR and iESR gene expression over time (Fig. 2*A*). iESR gene induction was observed at around an OD(600nm) of 3.5, determined by an increase in iESR ssGSEA projection values; rESR gene expression began to decline dramatically at an OD(600nm) of 5.5. These results provided a potential explanation for why euploid control populations analyzed by Tsai et al. (2019; 9) exhibited such a strong ESR but aneuploid populations did not. The aneuploid cells had not yet reached an OD(600nm) value where starvation-induced ESR induction occurs.

A

B Tsai et al. (2019; 9) Protocol

C Tsai et al. (2019; 9) Protocol

D 1:20 Dilution Protocol

E 1:20 Dilution Protocol
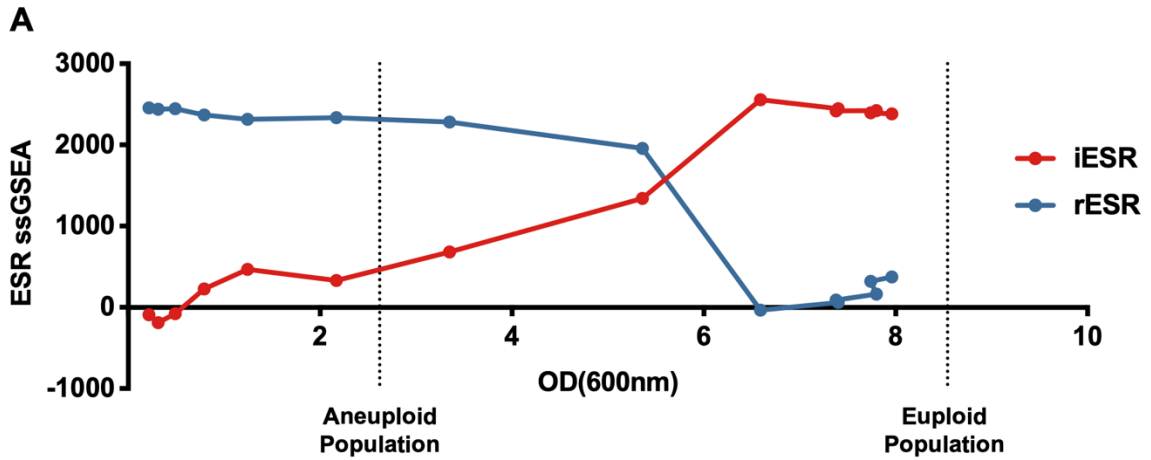
Figure 2. Effects of culture density on ESR strength in aneuploid cell populations.

(***A***) iESR (red) and rESR (blue) ssGSEA projection values were determined at the indicated OD(600nm) for S288C wild-type haploid cells (A2050) grown in YEPD over 28 hours. Vertical lines represent the OD(600nm) values of pooled euploid and aneuploid cell populations generated by tetrad dissection. Error bars represent standard deviation from the mean of technical replicates.

(***B*** and ***C***) Tetrads of sporulated S288C diploid and triploid cells (A40877, A40878) were dissected to produce heterogeneous haploid and aneuploid cell populations, respectively. 144 individual haploid colonies and 432 aneuploid colonies were inoculated and grown overnight in 200 μL YEPD. The next morning 300 μL YEPD were added to cultures and grown for an additional 5 hours. Individual euploid and aneuploid cultures were then pooled and their transcriptomes analyzed. An exponentially growing haploid strain (A2050) was included as a control. Gene expression data were analyzed by calculating ssGSEA projection values for the (***B***) iESR and rESR and (***C***) CAGE upregulated and downregulated genes. Error bars represent standard deviation from the mean of technical replicates; one-way two-tailed ANOVA test with multiple comparisons and Bonferroni correction, $P < 0.0001$ (****), $P = 0.0021$ (**). For additional statistical analysis see Figure S4.

(***D*** and ***E***) Tetrads of sporulated S288C diploid and triploid cells (A40877, A40878) were dissected to produce heterogeneous haploid and aneuploid cell populations, respectively. 144 individual haploid colonies and 432 aneuploid colonies were inoculated and grown overnight in 200 μL YEPD. The next morning cultures were diluted 1:20 and grown for an additional 5 hours. Colonies were then pooled, further diluted to approximately OD(600nm) = 0.3, and grown for 2 additional hours. Transcriptomes of pooled euploid and aneuploid populations and an

exponentially growing haploid strain (A2050) were analyzed with RNA-Seq, and ssGSEA

projection values were calculated for **(D)** iESR and rESR and **(E)** CAGE upregulated and

downregulated genes. Error bars represent standard deviation from the mean of technical

replicates; one-way two-tailed ANOVA test with multiple comparisons and Bonferroni

correction, $P < 0.0001$ (****), $P = 0.1234$ (ns). For additional statistical analysis see Figure S4.

To confirm this conclusion, we analyzed the gene expression profile in our euploid and

aneuploid cell populations grown using the protocol employed by Tsai et al. (2019; 9). Euploid

control populations exhibited a stronger ESR than aneuploid cell populations (Fig. 2*B*; Fig. S4).

Consistent with the idea that the CAGE signature is essentially the opposite of the ESR,

aneuploid strains exhibited a stronger CAGE signature than euploid strains (Fig. 2*C*; Fig. S4).
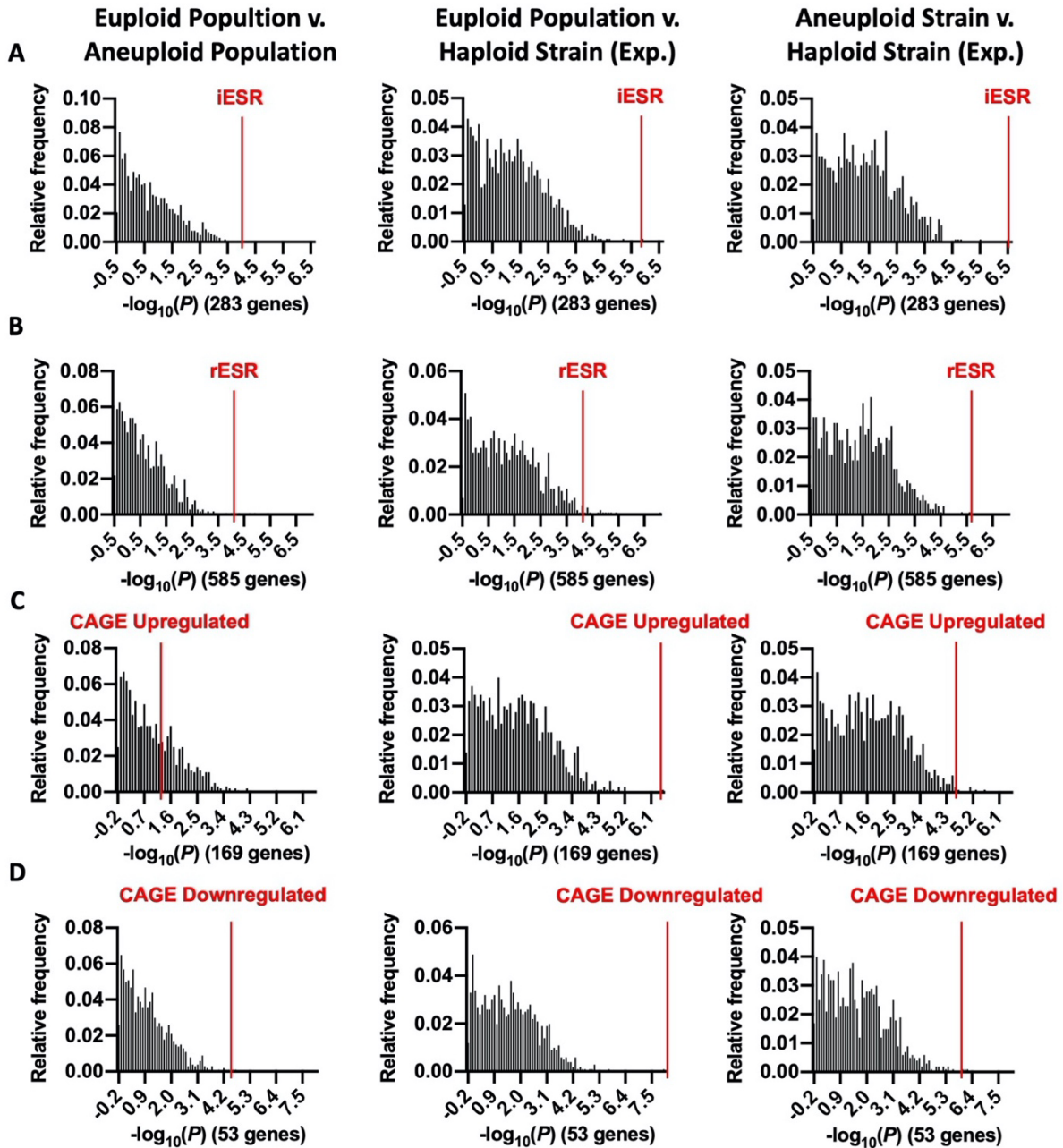
	Euploid Population v. Aneuploid Population	Euploid Population v. Haploid Strain (Exp.)	Aneuploid Population v. Haploid Strain (Exp.)
iESR	= 0.003	< 0.001	< 0.001
rESR	= 0.004	= 0.014	< 0.001
CAGE Upregulated	= 0.354	< 0.001	= 0.006
CAGE Downregulated	= 0.004	< 0.001	= 0.002

74

Figure S4. ssGSEA bootstrapping of ANOVA tests between randomized gene sets.

To further validate the significance of the differences in gene expression between aneuploid and euploid cell populations shown in Figure 2*B-E*, a bootstrapping analysis was performed on four separate groups of gene sets of the same sizes of the iESR gene set (283 genes), rESR gene set (585 genes), CAGE Upregulated gene set (169 genes), and CAGE Downregulated gene set (53 genes). 1000 random gene sets of each size were generated, and ssGSEA projection values for the exponentially growing haploid strain A2050 and the euploid and aneuploid populations (1:20 Dilution Protocol) were calculated. For each randomly generated gene set, the significance of the differences between the euploid population and the aneuploid population (Euploid Population v. Aneuploid Population), the euploid population and the exponentially growing haploid strain A2050 (Euploid Population v. Haploid Strain (Exp.)), and the aneuploid population and the exponentially growing haploid strain A2050 (Aneuploid Population v. Haploid Strain (Exp.)) were calculated as *P* values. *P* values from the randomly generated gene sets were then compared to the *P* value of the corresponding gene set and samples used. For all comparisons where a significant difference was observed, the experimentally obtained *P* value was significantly different from the *P* values from the randomly generated gene sets.

(*A-D*) 1000 gene sets of four different sizes were randomly generated, and ssGSEA projection values were calculated for the exponentially growing haploid strain A2050 and euploid and aneuploid populations (1:20 Dilution Protocol). With a one-way two-tailed ANOVA test with multiple comparisons and Bonferroni correction (*P* value multiplied by 3), $-\log_{10}(P)$ values were calculated for 1000 gene sets of sizes 283 genes (iESR) (*A*), 585 genes (rESR) (*B*), 169 genes (CAGE Upregulated) (*C*), and 53 genes (CAGE Downregulated) (*D*) comparing differences between Euploid Population v. Aneuploid Population, Euploid Population v. Haploid Strain

(Exp.), and Aneuploid Population v. Haploid Strain (Exp.). Vertical red lines represent transformed *P* values generated by each comparison for the indicated gene set (iESR, rESR, CAGE Upregulated, and CAGE Downregulated).

(*E*) *P* values generated by the bootstrapping analysis for each gene set and comparison. The bootstrapping *P* values were not multiple-test corrected.

We also included an exponentially growing haploid wild-type strain (A2050) in our analysis. As expected, this strain did not exhibit the ESR (Fig. 2*B*, S4) but instead showed the strongest CAGE response among all the cultures analyzed (Fig. 2*C*; Fig. S4). Together, these data indicate that the CAGE response is not an aneuploidy-specific gene expression signature but the result of differences in proliferation rates between aneuploid and euploid cell populations. In the growth protocol employed by Tsai et al. (2019; 9), euploid cells had reached stationary phase, which causes a very strong ESR. In contrast, aneuploid cells had not. Because the ESR of aneuploid cells is weaker than that of stationary phase euploid cells, normalization of the aneuploid gene expression profile to that of stationary euploid cells led to the incorrect conclusion that aneuploid cells exhibited a transcriptional signature opposite of the ESR. This conclusion predicts that when growth into stationary phase is avoided, aneuploid cell populations ought to exhibit the ESR stronger than euploid control populations.

Aneuploid cell populations exhibit the ESR.

To determine whether growth of the control euploid population into stationary phase precluded the identification of the ESR in aneuploid cell populations, we repeated the protocol developed by Tsai et al. (2019; 9) to generate euploid and aneuploid cell populations. However,

76

instead of diluting cultures 1:2 fold after 14–16 hours of growth in 200 uL of YEPD, we diluted cultures 1:20 fold (Fig. S1*B*; henceforth 1:20 dilution protocol). This prevented either culture from reaching stationary phase, and the final OD(600nm) of pooled euploid and aneuploid populations was 0.29 and 0.3, respectively.

Gene expression analysis of these cultures resulted in a strikingly different outcome compared to that obtained from cells where euploid control populations had reached stationary phase. Aneuploid populations exhibited a stronger ESR than euploid control populations (Fig. 2*D*; Fig. S4; iESR $P < 0.0001$, rESR $P < 0.0001$). It is, however, noteworthy that euploid control populations also exhibited the ESR, although not as strong as aneuploid populations, when compared to an exponentially growing haploid strain (Fig. 2*D*; Fig. S4). This is likely due to the fact that euploid cell populations grown in deep wells experience nutrient limitation. Aeration is poorer and proliferation rate slower in deep well plates compared to in a vigorously shaking flask.

Analysis of the CAGE signature revealed that the exponentially growing haploid strain A2050 expressed CAGE genes much more strongly than either the euploid (CAGE Upregulated $P < 0.0001$, CAGE Downregulated $P < 0.0001$) or aneuploid cell populations (Fig. 2*E*; Fig. S4; CAGE Upregulated $P < 0.0001$, CAGE Downregulated $P < 0.0001$). We note that the aneuploid population showed a slightly greater decrease in expression of the downregulated CAGE response than euploid control populations (Fig 2*E*). While this difference is statistically significant ($P < 0.0001$), it is likely biologically irrelevant given the dramatically higher downregulation of CAGE genes in the exponentially growing haploid strain. We conclude that aneuploid cell populations exhibit the ESR and that the previously reported aneuploidy specific CAGE signature is most prominent in an exponentially growing haploid strain.

Degree of aneuploidy correlates with ESR strength in complex aneuploid strains.

Previous results from our lab indicated that yeast strains harboring an additional chromosome (disomes) activate the ESR, and our results shown here demonstrate that heterogeneous aneuploid populations do too (5). We next wished to determine whether this gene expression signature is also present in yeast strains harboring multiple specific aneuploidies. Pavelka et al. (2010; 12) created a large number of yeast strains carrying multiple aneuploidies by sporulating a pentaploid strain (12). Strains obtained from such spores harbor multiple aneuploidies ranging in genome content between 2N and 3N (Strain Table S2; 12). Because the strength of the ESR is largely defined by proliferation rate (4, 8), we first measured doubling times of these complex aneuploid strains to ask whether proliferation rate was correlated with degree of aneuploidy also in strains harboring multiple aneuploidies. We calculated degree of aneuploidy as the fraction of base pairs in the aneuploid strain vis-à-vis a haploid euploid control strain. We found that the proliferation defect of aneuploid strains correlated remarkably well with their degree of aneuploidy (Fig. 3*A*; Spearman, $\rho^2 = 0.7620$, $P < 0.0001$).
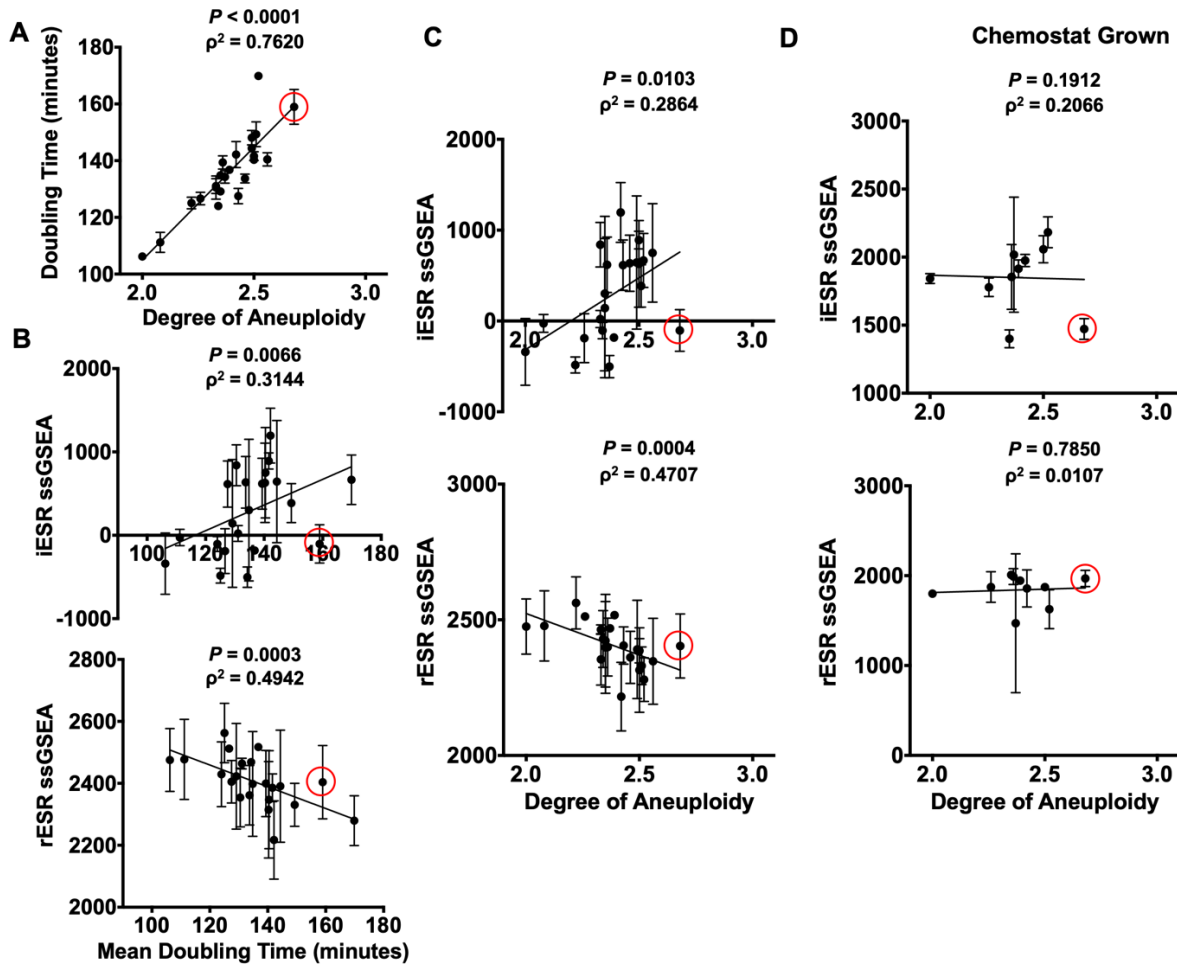
Figure 3. Complex aneuploid yeast strains exhibit the ESR.

(***A-C***) Aneuploid yeast strains harboring aneuploidies ranging from 2N to 3N were grown to log

phase in YEPD. For each strain, degree of aneuploidy was calculated as the fraction of base pairs

in the aneuploid strain/base pairs in a haploid control strain. Doubling times were calculated

from growth curves generated by measuring OD(600nm) in 20 minute intervals over 5 hours in a

plate reader. (***A***) Correlation between doubling time and degree of aneuploidy (Spearman, $\rho^2 =$

0.7620, *P* < 0.0001). Transcriptomes of the complex aneuploid strains were analyzed by RNA-

Seq, and ssGSEA projection values were calculated for iESR and rESR genes. Correlations

between iESR ssGSEA projections and mean doubling time (Spearman, $\rho^2 = 0.3144$, *P* = 0.0066)

and rESR ssGSEA projections and mean doubling time (Spearman, $\rho^2 = 0.4942$, $P = 0.0003$) are shown in (**B**). Correlations between iESR ssGSEA projections and degree of aneuploidy (Spearman, $\rho^2 = 0.2864$, $P = 0.0103$) and rESR ssGSEA projections and degree of aneuploidy (Spearman, $\rho^2 = 0.4707$, $P = 0.0004$) are shown in (**C**). Error bars represent standard deviation from the mean.

(**D**) Select complex aneuploid strains were grown in a phosphate-limiting chemostat until steady state was reached. Transcriptomes of harvested cells were analyzed by RNA-Seq. ssGSEA projection values were calculated for iESR and rESR genes. Correlations between iESR ssGSEA projections and degree of aneuploidy (Spearman, $\rho^2 = 0.1912$, $P = 0.2066$) and rESR ssGSEA projections and degree of aneuploidy (Spearman, $\rho^2 = 0.0107$, $P = 0.7850$) are shown. Error bars represent standard deviation from the mean of experimental replicates. The data point circled in red represents a complex aneuploid strain that does not mount the ESR.

Gene expression analysis of these complex aneuploid strains further revealed a strong correlation between mean doubling time and ESR strength (Fig. 3*B*; Spearman, iESR $\rho^2 = 0.3144$, $P = 0.0066$; Spearman, rESR $\rho^2 = 0.4942$, $P = 0.0003$) as well as between degree of aneuploidy and ESR strength (Fig. 3*C*; Spearman, iESR $\rho^2 = 0.2864$, $P = 0.0103$; Spearman, rESR $\rho^2 = 0.4707$, $P = 0.0004$). It is worth noting that a few aneuploid strains were not able to mount the ESR, despite their slowed proliferation (i.e. strain A22 from Pavelka et al. (2010; 12); circled in red in Fig. 3). The strains that were unable to activate the ESR all harbored gains of chromosomes 2, 7, 11, 15, and 16. This observation suggests that some specific gene combinations prevent activation of the ESR despite slow proliferation. It will be interesting to determine the mechanism of this ESR suppression.

Finally, we probed for the existence of the CAGE signature in these complex aneuploid strains. The upregulated CAGE signature did not correlate with degree of aneuploidy (Fig. S5A; Spearman, Upregulated CAGE $\rho^2 = 0.0679$, $P = 0.2416$). We observed a correlation between the downregulated CAGE signature and degree of aneuploidy, but it was opposite to what would be expected if it were determined by degree of aneuploidy. Increased degree of aneuploidy correlated with increased expression of CAGE downregulated genes (Fig. S5A; Spearman, Downregulated CAGE $\rho^2 = 0.2368$, $P = 0.0217$). We conclude that the CAGE signature is not a common aneuploidy gene expression signature among complex aneuploid strains, but the ESR is.

Proliferation rate determines ESR strength.

The strong correlation between ESR strength and doubling times in complex aneuploid strains suggested that proliferation rate was the primary determinant of ESR strength. To directly test this possibility, we examined whether equalizing proliferation rate among complex aneuploid strains and euploid control strains affected the correlation between ESR strength and degree of aneuploidy by culturing cells in a phosphate-limited chemostat (4, 13). When proliferation rate was equalized in this manner, the ESR gene expression signature was no longer evident in aneuploid strains (Fig. 3D; Spearman, iESR $\rho^2 = 0.1912$, $P = 0.2066$; Spearman, rESR $\rho^2 = 0.0107$, $P = 0.7850$). We also probed for the existence of the CAGE signature in complex aneuploid strains grown under phosphate-limiting conditions. We observed no correlation between degree of aneuploidy and genes upregulated in the CAGE response and the opposite correlation as would have been expected for the downregulated genes of the CAGE signature (Fig. S5B; Spearman, Upregulated CAGE $\rho^2 = 0.0030$, $P = 0.8916$; Spearman,

Downregulated CAGE $\rho^2 = 0.4364$, $P = 0.0.0438$). We conclude that when proliferation is equally slow in euploid and aneuploid cells, the ESR caused by aneuploidy is no longer evident. This suggests that in both euploid and aneuploid cells, proliferation rate is the primary determinant of ESR strength.
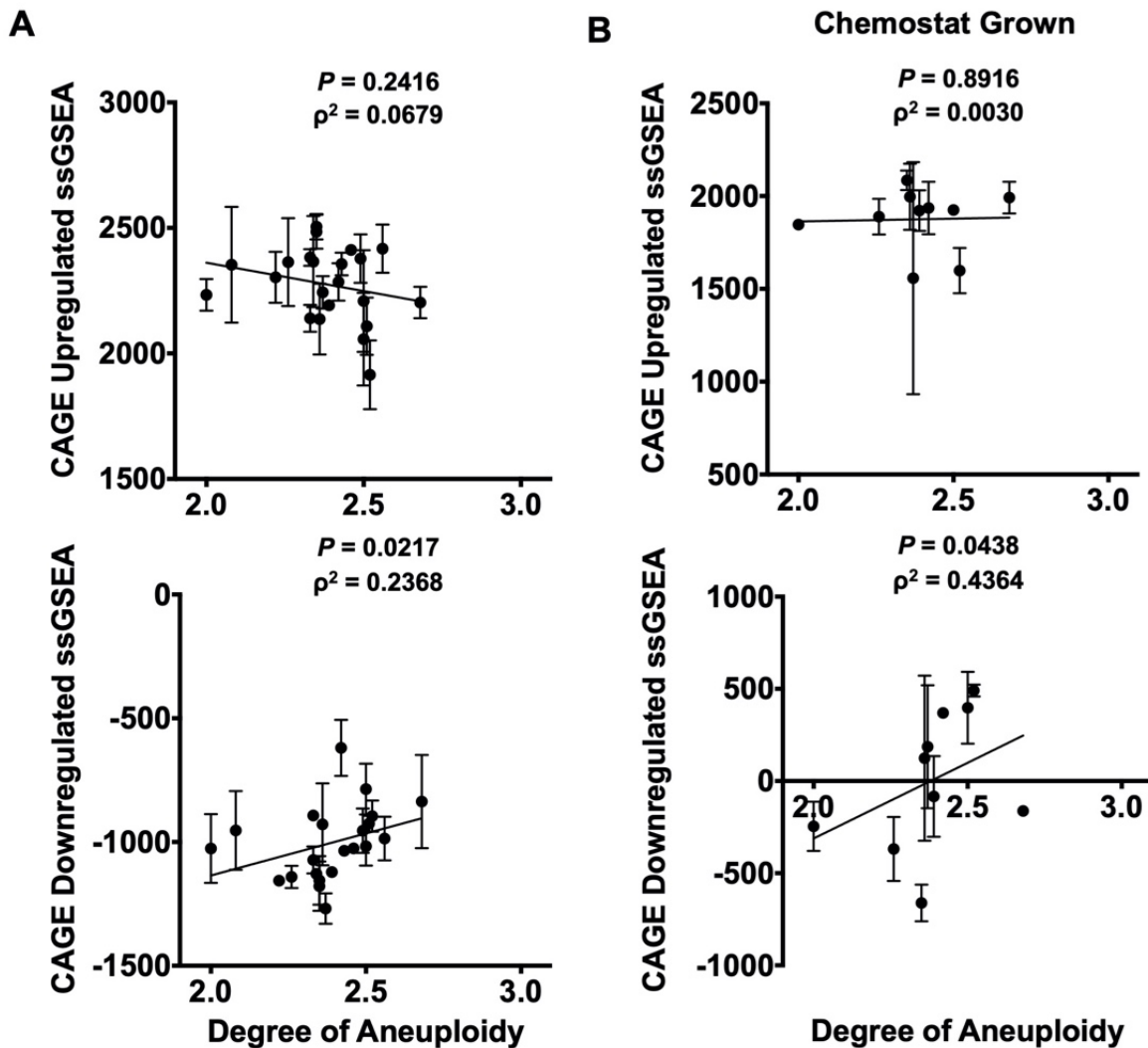
Figure S5. Correlation between growth rate and the CAGE gene expression signature in complex aneuploid strains.

Transcriptomes of the complex aneuploid strains were analyzed by RNA-Seq, and ssGSEA projection values were calculated for CAGE upregulated and CAGE downregulated genes.

(*A*) Correlation between CAGE upregulated ssGSEA projections and degree of aneuploidy (Spearman, $\rho^2 = 0.0679$, $P = 0.2416$) and CAGE downregulated ssGSEA projections and degree of aneuploidy (Spearman, $\rho^2 = 0.2368$, $P = 0.0217$) in complex aneuploid strains grown in YEPD.

(*B*) Correlations between CAGE upregulated ssGSEA projections and degree of aneuploidy (Spearman, $\rho^2 = 0.0030$, $P = 0.8916$) and CAGE downregulated ssGSEA projections and degree of aneuploidy (Spearman, $\rho^2 = 0.4364$, $P = 0.0438$) grown in a phosphate-limited chemostat. Error bars represent standard deviation from the mean of experimental replicates.
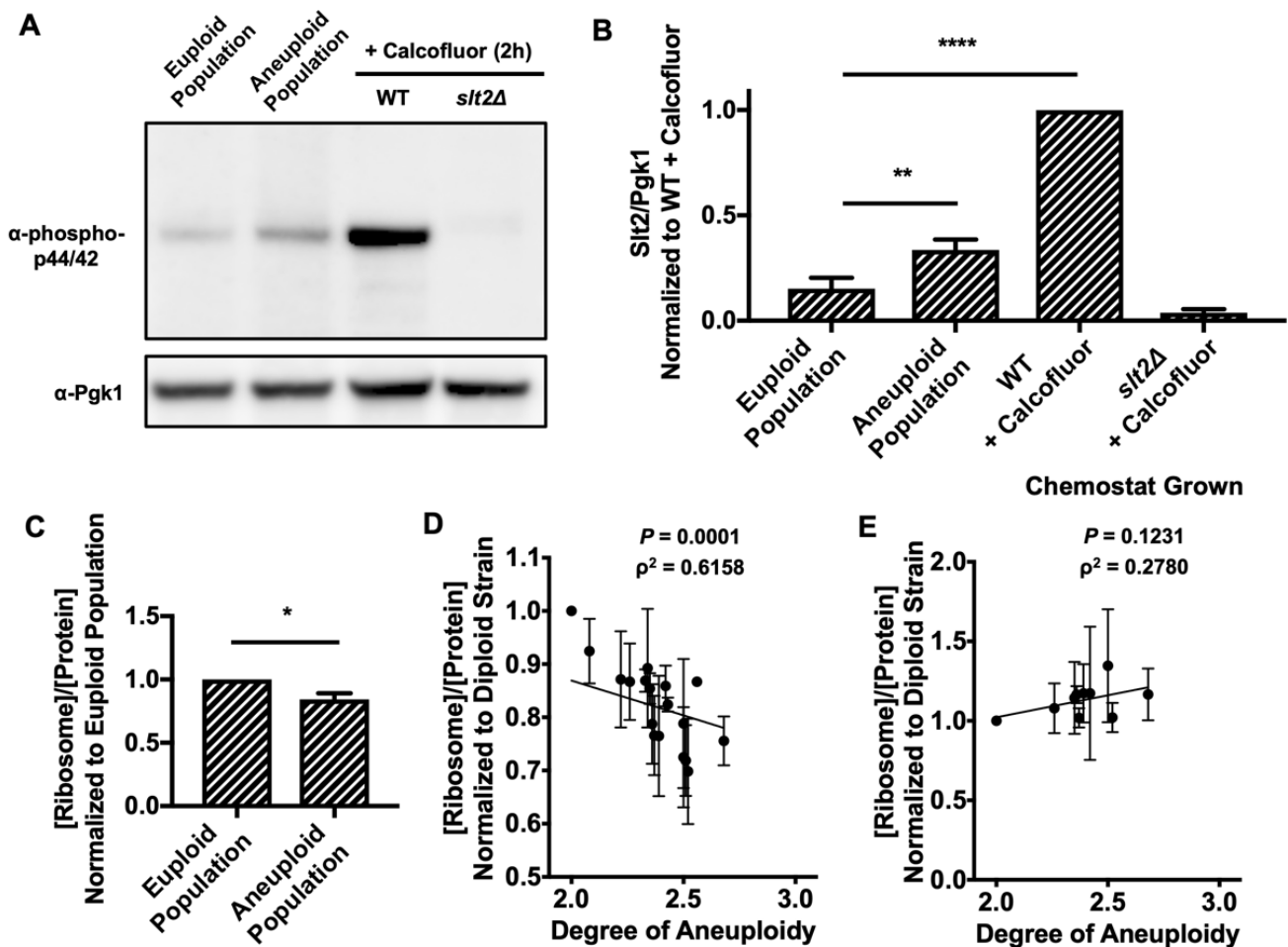

ESR induction in aneuploid cells causes ribosome loss.

Tsai et al. (2019; 9) reported the CAGE gene expression signature as aneuploidy-specific and most similar to the hypo-osmotic stress response. This similarity is not surprising given that both the CAGE signature and the hypo-osmotic stress response are essentially oppositely regulated to the ESR. Given our findings that heterogeneous aneuploid populations do not exhibit a CAGE signature, we next determined whether aneuploid cells indeed experience hypo-osmotic stress that was proposed to occur in response to a decrease in cytoplasmic density in aneuploid cells (9).

To assess induction of the hypo-osmolarity stress pathway, we probed activation of the hypo-osmolarity pathway MAP kinase Slt2 using a phospho-specific antibody that recognizes active phospho-Slt2 (14). Aneuploid cell populations showed a 2.22-fold increase in mean Slt2-phosphorylation compared to euploid control populations (Fig. 4*A* and *B*). The activation in the aneuploid cell populations was subtle compared to cell wall stress induced by prolonged Calcofluor White treatment (6.59-fold increase over euploid cell population). This difference in

induction was not due to acute versus chronic induction of the hypo-osmolarity pathway because we treated cells with Calcofluor White for two hours before analyzing the phosphorylation state of Slt2. The subtle activation of the hypo-osmolarity pathway in aneuploid strains suggested that either all aneuploidies cause weak activation of this stress pathway or that only a subset of aneuploid cells activates the pathway. We favor the latter possibility because we previously showed that not all disomies cause cell wall defects in yeast (15).

Figure 4. ESR induction causes ribosome loss in aneuploid strains.

(*A and B*) Euploid and aneuploid cell populations were grown in YEPD with the 1:20 dilution

protocol, and Slt2 Thr202/Tyr204 phosphorylation was determined. Wild-type euploid (A2050) and *slt2Δ* cells (A41265) treated with 5 μg/mL Calcofluor White for two hours served as positive and negative controls, respectively, in immunoblots (**A**). Pgk1 served as a loading control. Quantifications of Slt2 Thr202/Tyr204 phosphorylation are shown in (**B**). Slt2/Pgk1 values were normalized to the wild-type cells treated with Calcofluor White. Error bars represent standard deviation from the mean of experimental replicates.; one-way ANOVA test with multiple comparisons and Bonferroni correction, $P < 0.0001$ (****), $P = 0.0021$ (**). All other comparisons between samples had a significant difference of $P < 0.0001$ (****) with the exception of the euploid populations and *slt2Δ* + Calcofluor, which had a significant difference of $P = 0.0288$.

(**C**) The fraction of ribosome in total protein extracts ([Ribosome]/[Protein]) was determined in euploid and aneuploid cell populations grown with the 1:20 dilution protocol. [Ribosome]/[Protein] in aneuploid cell populations was normalized to that in euploid cell populations. Error bars represent standard deviation from the mean of technical replicates; unpaired two-tailed t-test test, $P = 0.0332$ (*).

(**D**) Aneuploid yeast strains harboring aneuploidies ranging from 2N to 3N were grown to log phase in YEPD and the fraction of ribosomes in total protein extracts ([Ribosome]/[Protein]) was determined. Correlation between [Ribosome]/[Protein] and degree of aneuploidy ($\rho^2 = 0.6158$, $P = 0.0001$, Spearman) is shown. The calculated values were normalized to the [Ribosome]/[Protein] of a diploid control.

(**E**) Aneuploid yeast strains harboring aneuploidies ranging from 2N to 3N were grown in a phosphate-limited chemostat and the fraction of ribosome in total protein extracts ([Ribosome]/[Protein]) was determined. Correlation between [Ribosome]/[Protein] and degree of

aneuploidy ($\rho^2 = 0.2780$, $P = 0.1231$, Spearman) is shown. The calculated values were normalized to the [Ribosome]/[Protein] of a diploid control. Error bars represent standard deviation from the mean of experimental replicates.


The subtle activation of the hypo-osmolarity pathway in aneuploid cell populations was hard to reconcile with the comparatively dramatic effects on cytoplasmic density reported to occur in aneuploid cell populations (9). Our observation that aneuploid cell populations exhibit the ESR provided an alternative hypothesis. A recent study by Delarue et al. (2018; 16) showed that the major determinant of cytoplasm density is the ribosomal fraction within a cell's proteome. Given that aneuploid cell populations exhibit the ESR, which is characterized by the downregulation of ribosomal protein and ribosome biogenesis gene expression, we asked whether aneuploid cell populations harbor fewer ribosomes than euploid control populations.

To address this question, we isolated ribosomes from aneuploid and euploid populations grown using the 1:20 dilution protocol (Fig. S1*B*). For this, we used a protocol that was adapted from methods developed to purify 80S assembled ribosomes (17, 18, 19). We previously examined the purity of this ribosome preparation in (20). To ensure that this preparation consisted largely of 80S assembled ribosomes, we quantified the Coomassie staining pattern of our ribosome preparation published in Brennan et al. (2019; 20) and compared it with that obtained by Munoz et al. (2017; 18), who published the SDS PAGE banding pattern of purified 40S and 60S subunits (Fig. S6*A-B*). This analysis confirmed that the method we employed to isolate ribosomes enriches for assembled ribosomes. Ribosome preparations were then subjected to absorbance meassurements at 260nm to determine ribosome content. To assess the sensitivity of this quantification method, we compared protein and ribosome content between a wild-type

haploid strain (A2587) and a wild-type diploid strain (A33821) (Strain Table S1). Diploid cells are twice as large as haploid cells and are thus expected to have twice as many proteins and ribosomes. Our measurements showed this to be the case (Fig. S6*C-D*), indicating that our method was highly sensitive.
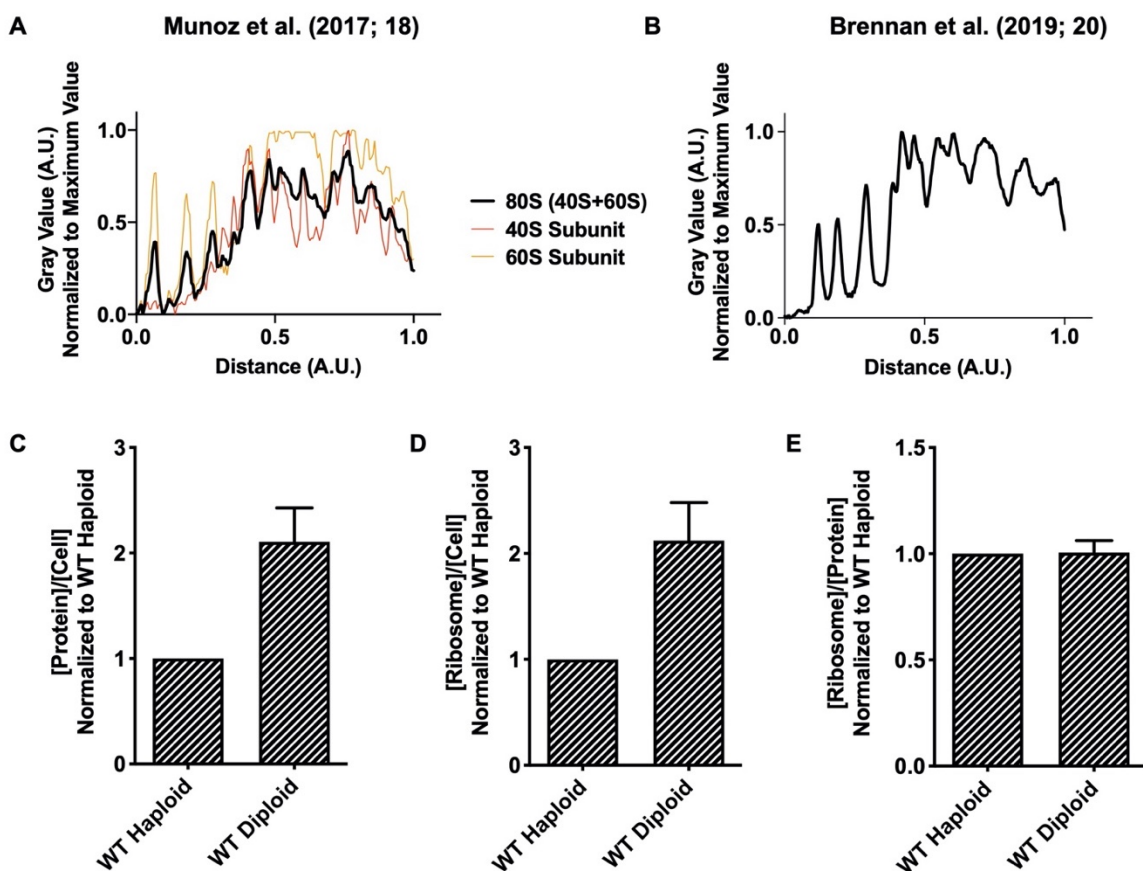
Figure S6. Ribosome purification method

(*A*) Quantification of Coomassie-stained gels of 40S and 60S ribosomal subunits purified by sucrose cushion in Munoz et al. (2017; 18). A line was drawn in the middle of the lane of the Coomassie-stained gels. Gray values, defined as pixel intensities, were then determined for the

gel lanes containing 40S and 60S ribosomal subunits and normalized to the maximum gray value. To infer the banding pattern of 80S ribosomes, averaged the traces obtained from 40S and 60S particles (40S+60S) were averaged prior to normalization.

(**B**) Coomassie-stained gel electrophoresis quantification of ribosomes purified by sucrose cushion in Brennan et al. (2019; 20). Gray values were determined as in (*A*) for the lane containing purified ribosomes and normalized to the maximum gray value.

(***C-E***) Ribosomes were purified from wild-type haploid (A2587) and wild-type diploid (A33821) cultures to determine [Protein]/[Cell] (***C***), [Ribosome]/[Cell] (***D***), and [Ribosome]/[Protein] (***E***). All values were normalized to the wild-type haploid strain A2587. Error bars represent standard deviation from the mean of experimental replicates.

Having established a method to determine a cell's ribosome content, we next compared the ribosome content between aneuploid and euploid populations. This analysis revealed that ribosomes made up a significantly smaller fraction of total protein in aneuploid cell populations than in euploid cell populations (Fig. 4*C*). Our analysis of complex aneuploid strains confirmed these results. Ribosome content inversely correlated with degree of aneuploidy (Fig. 4*D*; Spearman, $\rho^2 = 0.6158$, $P = 0.0001$), which is consistent with ESR strength correlating with degree of aneuploidy. This correlation suggested that the ESR triggered ribosome loss and hence loss of cytoplasmic density in aneuploid cells. If true, we would predict that equalizing proliferation rates among aneuploid and euploid cells should eliminate this correlation. This is what we observed. When we grew euploid and complex aneuploid strains in continuous culture under phosphate-limiting conditions, all strains not only exhibited similar ESR strengths, but ribosome content was no longer inversely correlated with degree of aneuploidy (Fig. 4*E*;

Spearman, $\rho^2 = 0.2780$, $P = 0.1231$). We propose that the decrease in cytoplasmic density observed in aneuploid cells is caused by an ESR-induced loss of ribosomes.

Discussion

Whether aneuploidy elicits a stereotypic transcriptional response in yeast and what this response may be has been controversial. The analysis of a series of disomic yeast strains harboring an additional copy of one of yeast's 16 chromosomes showed that these strains exhibit the generic environmental stress response (ESR). However, other reports found this not to be the case. The analysis of five complex aneuploid yeast strains showed that only three out of these five strains exhibited the ESR (12). Most recently, Tsai et al. (2019; 9) reported that heterogeneous aneuploid cell populations also lack the ESR. We re-evaluated these reports to find that when a large number of complex aneuploid strains is analyzed and when gene expression profiles of mixed aneuploid cell populations are normalized to euploid populations that are in the same proliferation state as aneuploid populations, the ESR is evident. Together, these results indicate that aneuploid yeast strains exhibit the ESR. We consider this result not surprising given that the ESR is largely a consequence of slowed cell division (4, 8) and that aneuploidy causes proliferation defects (5). We further note that the ESR-like transcriptional signature is also observed in aneuploid mammalian cells (4). Together, these results indicate that the ESR and relatives of this signature are a pervasive response to aneuploidy.

In wild isolates of yeast that are naturally aneuploid, the ESR is less prevalent (1, 2). This observation indicates that under selective pressure, aneuploidies evolve and adaptation to aneuploidy-induced cellular stresses occurs such that proliferation rate is less affected by a particular chromosome gain or loss. Indeed, an aneuploidy tolerating natural gene variant has

recently been described (2). Based on the analysis of two wild yeast isolates disomic for either chromosome 8 or 12, Hose et al. (2020; 2) proposed that the ESR in aneuploid cells is strongly influenced by the type of *SSD1* allele that a strain carries. Specifically, the ESR observed in aneuploid strains of the W303 background was attributed to the fact that W303 harbors a truncation allele of *SSD1*. The complex aneuploid strains and the aneuploid cell populations employed in our study are derivatives of the S288C strain background, which harbors a full-length *SSD1* allele. The finding that ESR strength correlates with degree of aneuploidy in these aneuploid S288C derivatives indicates that the ESR is not defined by *SSD1* allele identity but degree of aneuploidy. It is nevertheless possible that specific *SSD1* alleles and other genomic alterations exist that suppress the ESR gene signature. We found that strains harboring a gain of chromosomes 2, 7, 11, 15, and 16 do not exhibit the ESR despite proliferating slowly. Understanding why these chromosome combinations suppress the ESR will be interesting. We speculate that growth-promoting pathways known to negatively regulate the ESR, such as the PKA and TOR pathways, are hyperactive in these strains.

Our data indicate that the previously described aneuploidy-specific CAGE gene expression signature is an artifact caused by normalizing the gene expression of actively dividing aneuploid cells to that of euploid control cells that had grown to stationary phase. We show that the ESR in the euploid control populations that had grown into stationary phase was stronger than the ESR observed in aneuploid cell populations that, due to their poor proliferation, were still actively proliferating. Thus, when euploid stationary phase cells were used for normalization, aneuploid cells exhibited the CAGE signature in which many ESR genes are oppositely regulated. As such, it is not surprising that the CAGE signature is most similar to the previously described hypo-osmolarity gene expression signature. Gasch et al. (2000; 6) identified

two stresses that do not result in activation of the ESR: cold shock and hypo-osmotic shock. Under these stresses, the ESR is oppositely regulated. In particular the rESR, which encompasses genes encoding transcription and translation factors and ribosomal proteins are upregulated rather than downregulated (6). While it is not clear why ribosome production must be upregulated during cold shock, we understand why this occurs during hypo-osmotic shock. During hypo-osmotic shock, water uptake increases (10). To avoid cytoplasm dilution during this water influx, production of ribosomes, which are the main determinants of cytoplasm density (16), must be upregulated or at least prevented from being downregulated. Further analysis of these exceptional stress conditions, during which the rESR is not downregulated will provide key insights into regulation of this central stress and slow proliferation response.

Under most, if not all stress conditions, cell proliferation is slowed or halted, and the ESR signature is evident with the exceptions noted above. Downregulation of the rESR generally correlates much better with degree of slow proliferation than induction of the iESR. This is not surprising. The vast majority of the genes that are part of the rESR are involved in transcription and translation. Cell growth, or cellular enlargement, needs to be attenuated during any stress that causes a slowing or halting of cell division to prevent cells from growing too large. When growth continues unabated during cell cycle arrest, DNA becomes limiting, causing numerous defects including impaired cell proliferation, cell signaling, and gene expression (21, 22). We speculate that a role of the rESR is to attenuate macromolecule biosynthesis and hence cell growth during cell cycle arrest. In contrast, the iESR may be aimed at alleviating cellular stress, which requires expression of genes unique to specific stresses rather than control of biomass production.

91

Our results suggest that repression of rESR genes in response to aneuploidy has profound consequences on cellular proteome composition. It leads to a significant drop in the contribution of ribosomes to the cell's total protein. This not only leads to downregulation of translational capacity but, because ribosomes are the key determinant of cytoplasmic density (16), is likely the major cause of loss in cellular density previously reported to occur in aneuploid cells (9). We propose that activation of the ESR in aneuploid cells serves two purposes. It protects cells from cellular stresses caused by an unbalanced genome and prevents excessive cellular enlargement during their slowed cell cycles. Understanding how slowed proliferation leads to activation of the ESR will provide critical insights into the coordination between cell division and macromolecule biosynthesis.

Materials and Methods

Dataset Processing and Single-Sample Gene Set Enrichment Analysis

Raw RNA-Seq data was obtained as described below or through download from Tsai et al. (2019; 9) with gene accession number GSE107997. Reads were aligned to a *S. cerevisiae* transcriptome with STAR version 2.5.3a (23) and gene expression was quantified with RSEM version 1.3.0 (24). Transcript per million (TPM) values were offset by +1, $\log_2$ transformed, and used to prepare GCT files for single-sample Gene Set Enrichment Analysis (ssGSEA, version 7.7; 25, 26) obtained from the Indian University public GenePattern server (27). ssGSEA projections were prepared for the Environmental Stress Response (ESR) originally described by Gasch et al. (2000; 6) "common aneuploidy gene-expression" (CAGE) signatures identified in Tsai et al. (2019; 9). Sort order has a subtle effect on ssGSEA.

Differential Gene Expression Analysis

Raw RNA-Seq data was obtained through download from Tsai et al. (2019; 9) with gene accession number GSE107997. Integer count values derived from RSEM processing were used as input to differential expression analysis with DESeq2 (version 1.24.0; 28) using normal log fold change shrinkage. Expression data from aneuploid cell populations generated by tetrad dissection were pooled to create "aneuploid populations (Tetrad)". Expression data from aneuploid populations obtained from *MATa* selection were pooled to create "aneuploid populations (*MATa* Selection)". These populations, as well as both the euploid populations obtained from tetrad dissection and *MATa* selection, were compared to the exponentially growing haploid control. Differential expression data was visualized using TIBCO Spotfire Analyst version 7.11.1.

Stationary-Phase Growth Timecourse

S288C wild-type cells (A2050) were inoculated into 25 mL YEPD and grown overnight at 25 ºC. After approximately 12-14 hours of growth, cells were diluted to OD(600nm) = 0.1 with YEPD + 2% glucose and grown for an additional 4 hours at 25 ºC. Once the (OD600nm) reached approximately OD(600nm) = 0.3, samples for transcriptomics were taken and OD(600nm) was measured every 2 hours for 28 hours. Optical Density was measured at 600 nm (OD(600nm)) with a spectrophotometer.

Heterogeneous Euploid and Aneuploid Population Generation Using the Tsai et al. (2019; 9) Protocol

pRS315-STE2pr-spHIS5 S288C diploids (A40877) and triploids (A40878) (Strain Table S1) were grown overnight in SD - LEU medium and subsequently sporulated in "Super Sporulation Medium" (1% potassium acetate and 0.02% raffinose) from Tsai et al. (2019; 9). Sporulated tetrads were then dissected. (Note in the publication by Tsai et al. (2019; 9), sporulated tetrads were also *MATa* selected through histidine prototrophy. We did not generate cell populations in this manner). Individual colonies were grown for 14-16 hours in 200 μL of YEPD + 2% glucose in a 96 deep-well plate. 300 μL of YEPD were then added to cultures. The cultures were grown for 5 additional hours, pooled, and samples for RNA-Seq and [Ribosome]/[Protein] content measurements were taken.

Heterogeneous Euploid and Aneuploid Population Generation Using the 1:20 Dilution Protocol

pRS315-STE2pr-spHIS5 S288C diploids (A40877) and triploids (A40878) (Strain Table S1) were grown overnight in SD - LEU medium and subsequently sporulated in the "Super Sporulation Media" mentioned above. Sporulated tetrads were then tetrad dissected. Individual colonies obtained from spores were grown for 14-16 hours in 200 μL of YEPD in a 96 deep-well plate. Cultures were then diluted 1:20 in YEPD + 2% glucose, grown for another 5 hours, then pooled, and diluted to approximately OD(600nm) = 0.3. The pooled aneuploid populations were grown for an additional 2 hours, and samples for RNA-Seq, [Ribosome]/[Protein] content measurements, and Slt2 phosphorylation state analysis were taken.

ssGSEA Bootstrapping Analysis

Four groups of 1000 random gene sets were generated. Each group was the same size as one of the following gene sets: iESR (283 genes), rESR (585 genes), CAGE Upregulated (169 genes), and CAGE Downregulated (53 genes). For the exponentially growing haploid strain A2050 and euploid and aneuploid populations (grown using the 1:20 dilution protocol), ssGSEA projections were prepared for the 4000 total gene sets. For each gene set, a one-way two-tailed ANOVA test with multiple comparisons and Bonferroni correction (P value multiplied by 3) was computed for ssGSEA values of euploid population v. aneuploid population, euploid population v. haploid strain, and aneuploid population v. haploid strain. In the end, 1000 P values were generated for each of the 3 comparisons, for each of the 4 differently-sized groups of 1000 random gene sets. P values from the randomly generated gene sets were then compared to the P value of the corresponding gene set and samples used. The overall significance of this bootstrapping analysis was determined by dividing the number of randomly generated comparisons which had a P value smaller than the original P value by 1000. For example, of the 1000 randomly generated gene sets of 283 genes comparing euploid v. aneuploid populations, three comparisons had a P value smaller than the P value generated for iESR gene set (which contains 283 genes) in these strains. The bootstrapping P values were not multiple-test corrected.

Growth Conditions for Complex Aneuploid Strains

Complex aneuploid strains were generated by Pavelka et al. (2010; 12) (Strain Table S2). Complex aneuploid strains were grown on YEPD + 2% glucose plates for 2 days at 25 ºC. Colonies were inoculated overnight in 25 mL YEPD + 2% glucose and grown at 25 ºC. After 12-14 hours of growth at 25 ºC, cells were diluted to approximately OD(600nm) = 0.1 and grown

for an additional 4 hours at 25 ºC. Cells were then harvested for RNA-Seq and [Ribosome]/[Protein] content measurements.

Doubling Time Measurements

Doubling time of complex aneuploid strains were measured in a 96 well format in YEPD + 2% glucose at 25 ºC. OD(600nm) values were taken in 20 minute intervals over 5 hours, and doubling time was calculated from the growth curves generated.

Growth in Phosphate-Limiting Chemostats

Selected complex aneuploid strains were grown on YEPD + 2% glucose plate for 2 days at 30 ºC. Strains were inoculated in phosphate-limited media (29) and grown overnight. Once chemostats were set up and filled, phosphate-limited media in the chemostat was inoculated with 2 mL of overnight culture, and cells were allowed to grow for 30-36 hours although some strains required 48+ hours of growth. The dilution pumps were then turned on at a dilution rate of 0.11 +/- 0.01 chemostat volumes per hour. The chemostat was sampled daily to measure effluent volume, hemocytometer counts, and OD(600nm) measurements. When growth in the chemostat had reached a steady-state, defined by less than 5% change from the previous day's measurements, samples were harvested for RNA-Seq and [Ribosome]/[Protein] content.

RNA-Seq

3-5 mL samples of culture were taken, spun down at 3000rpm for 5 minutes, washed with 1 mL DEPC water, and transferred to a 2 mL RNase-free screw-cap tube. Samples were spun again at 8000rpm for 3 minutes, and supernatant was aspirated. Cells were snap frozen with

liquid nitrogen and stored at -80 ºC. RNA samples were prepared with RNeasy mini kit from Qiagen and treated with DNase on-column treatment (RNase-free) from Qiagen. Purified RNA was used in two different library preparation methods. In experiments with complex aneuploid strains, total RNA was sequenced using Illumina Truseq followed by Nextera or Roche KAPA. In all other experiments, total RNA was sequenced using Illumina Truseq followed by Roche KAPA. All sequencing was done using an Illumina HiSeq2000.

[Ribosome]/[Protein] Content Measurements

1 mL of 1:100 diluted samples of culture were used to determine cell number in the culture using a Beckman Multisizer 3 Coulter Counter ([Cell]). Concurrently, 50 mL samples of culture were taken, spun down at 3000rpm for 5 minutes, frozen with liquid nitrogen, and stored at -80 ºC. Cells were resuspended in 30 mL lysis buffer (20mM HEPES pH 7.4, 100mM potassium acetate, 2mM magnesium acetate, 3mM DTT, and EDTA-free protease inhibitor (Roche, 11836170001)), and 0.5 mg/mL zymolyase was added. Resuspended cells were lysed twice with a French Press. Lysed samples were then spun at 19,000rpm for 20 minutes at 4 ºC to remove cell debris. Protein concentration of the cell lysate ([Protein]) was measured in triplicate by Bradford Assay.

10 mL cell lysate was overlaid onto 15 mL pre-chilled (4 ºC) sucrose solution (30% sucrose, 20mM HEPES pH 7.4, 500mM potassium acetate, 2mM magnesium acetate, and 3mM DTT), which was then spun at 50,000 rpm for 4 hours at 4 ºC to purify 80S ribosomes (17, 18, 19). Solution above assembled ribosome pellet was poured from the tube after spin, and the tubes were dried upside-down for 10 minutes to remove excess liquid. Pellets were resuspended with 1 mL lysis buffer, and absorbance at 260nm was measured with a Nanodrop to obtain concentration of purified assembled ribosomes ([Ribosome]).

Calcofluor Treatment

S288C wild-type (A2050) and *slt2Δ* (A41265) cells were inoculated into 25 mL YEPD + 2% glucose, and grown at 25 ºC for 12-14 hours. Cells were diluted to approximately OD(600nm) = 0.1, grown for an additional 4 hours, and treated with 5 μg/mL Calcofluor White for 2 hours. Samples were harvested for Western Blot analysis.

Western Blot and Quantification

1 OD(600nm) unit of sample was Trichloroacetic acid (TCA) precipitated. 20 μL of each sample was run on a NuPAGE 4-12% Bis-This protein gel from Invitrogen and then transferred to PVDF membrane from EMD Millipore. Phospho-p44/42 MAPK (Thr202/Tyr204) antibody (1:1000; Cell Signaling Technology, #9101) was used to detect phosphorylated Slt2. Pgk1 (Pgk1 antibody, 1:4000; ThermoFisher, 22C5D8) was used as a loading control. Immunoblots were incubated with HRP-conjugated secondary antibodies and ECL Western Blotting Detection Reagents from Amersham and then scanned on an ImageQuant LAS4000.

Signals were quantified on an ImageQuant LAS4000 and integrated densities of bands quantified using ImageJ. Three separate immunoblots were quantified and normalized to wild-type cells treated with Calcofluor. To quantify ribosomal proteins (Fig. S6) we mimicked a densitometer measurement. A line was drawn in the middle of the lane of the Coomassie-stained gels from Munoz et al. (2017; 18) and Brennan et al. (2019; 20). The pixel intensity, measured as gray values, along this line was then quantified using ImageJ and normalized to the maximum pixel intensity value. For the 40S+60S measurements, pixel intensity measurements of the 40S subunit and the 60S subunit were averaged prior to normalization. Quantifications were recorded

starting directly above the slowest migrating ribosomal band and ending below the fastest

migrating band. This distance was set to 1 arbitrary unit.

Data Availability

RNA-Seq data has been deposited in the Gene Expression Omnibus (GEO) database

(accession no. GSE146791).

Strain Tables

Strain Table S1. Euploid strains.

Description of the strain names, genotypes, and source used in this paper.

Strain Name	Genotype	Source
A2587	W303, *MATa ade*2-1, *leu*2-3, *ura*3, *trp*1-1, *his*3-11,15, *can*1-100, *GAL, psi+*	Kim Nasmyth
A33821	W303, *MATa/α ade*2-1, *leu*2-3, *ura*3, *trp*1-1, *his*3-11,15, *can*1-100, *GAL, psi+*	Kim Nasmyth
A2050	S288C, *MATa ura*3-52 *his*3Δ *leu*2-3 112 *trp*1Δ	Frank Luca
A41265	BY4741, *MATa his*3Δ *leu*2Δ *met*15Δ *ura*3Δ *slt*2Δ*::KanMX*	BY4741 Deletion Collection
A40877	BY4743, *MATa/α his*3Δ*/his*3Δ *leu*2Δ*/leu*2Δ *met*15Δ*/MET*15 *ura*3Δ*/ura*3Δ *lys*2Δ*/LYS*2 *pRS315-STE2pr-spHIS5*	Tsai et al. (2019; 9) RLY9593
A40878	WT Triploid, *MATa/a/α his*3Δ*/his*3Δ*/his*3Δ *leu*2Δ*/leu*2Δ*/leu*2Δ *met*15Δ*/met*15Δ*/MET*15 *ura*3Δ*/ura*3Δ*/ura*3Δ *lys*2Δ*/LYS*2*/LYS*2 *pRS315-STE2pr-spHIS5*	Tsai et al. (2019; 9) RLY9596

Description of the strain names, aliases, karyotypes and mean doubling times of complex aneuploid strains generated by Pavelka et al. (2010; 12).

Strain Name	Alias	Chromosome copy number																Degree of Aneuploidy (Normalized to Haploid)	Mean Doubling Time (Minutes)
		I	II	III	IV	V	VI	VII	VIII	IX	X	XI	XII	XIII	XIV	XV	XVI		
RLY4737	U2	2	2	2	2	2	2	2	2	2	2	2	2	2	2	2	2	2.00	106.2
RLY4888	A1	2	2	2	2	2	2	2	2	2	2	2	2	3	2	2	2	2.08	111.2
RLY4946	A18	2	2	2	2	3	2	3	2	3	3	3	2	2	2	2	3	2.37	134.25
RLY4947	A19	3	3	2	2	2	2	3	2	3	3	2	3	3	3	2	2	2.51	149.3
RLY4948	A20	2	2	2	2	2	2	3	2	3	2	2	2	3	3	3	2	2.36	139.35
RLY4949	A21	2	3	2	3	2	2	3	2	2	2	2	2	3	3	3	2	2.52	169.85
RLY4950	A22	2	3	2	3	2	2	3	3	2	3	3	2	2	3	3	3	2.68	158.95
RLY4951	A23	3	3	2	2	2	2	2	2	3	2	3	3	3	3	3	2	2.50	140.3
RLY4952	A24	2	3	2	2	2	2	3	2	3	2	2	2	2	3	2	2	2.26	126.65
RLY4953	A25	2	3	2	2	2	2	3	2	2	2	2	2	2	3	2	2	2.22	125.05
RLY4954	A26	2	3	2	2	2	2	2	2	2	3	3	2	3	3	2	2	2.33	130.5
RLY4955	A27	2	3	2	2	2	2	2	2	2	3	3	2	3	3	2	2	2.33	131.1
RLY4956	A28	2	3	2	2	2	3	3	3	3	3	3	2	3	2	2	2	2.46	133.7
RLY4957	A29	2	3	2	2	2	3	3	2	3	3	2	2	3	2	2	3	2.43	127.5
RLY4958	A30	3	3	2	2	2	3	3	3	3	2	3	2	3	3	2	3	2.56	140.45
RLY4959	A31	2	3	2	2	2	3	3	2	2	2	2	2	3	3	3	3	2.49	148.1
RLY4960	A32	3	2	2	3	2	2	2	3	3	3	3	2	2	2	2	2	2.35	134.8
RLY4961	A33	2	3	2	2	2	3	3	2	2	2	2	2	3	3	3	3	2.49	144.35
RLY4962	A34	3	2	2	3	2	2	2	3	3	3	3	2	2	2	2	2	2.35	129.15
RLY4963	A35	3	2	2	2	3	2	3	2	3	2	3	3	2	2	2	2	2.34	124
RLY4964	A36	2	2	2	2	2	2	3	3	2	3	3	2	3	2	3	3	2.50	141.6
RLY4965	A37	2	3	2	2	2	2	3	2	2	2	2	2	2	3	3	3	2.39	136.75
RLY4966	A38	2	3	2	3	2	2	2	3	3	2	3	2	2	2	3	2	2.42	142.15

102

References

1. J. Peter, *et al.*, Genome evolution across 1,011 Saccharomyces cerevisiae isolates. *Nature* **556**, 339–344 (2018).

2. J. Hose, *et al.*, The genetic basis of aneuploidy tolerance in wild yeast. *Elife* **9**, e52063 (2020).

3. N. K. Chunduri, Z. Storchová, The diverse consequences of aneuploidy. *Nat Cell Biol* **21**, 54–62 (2019).

4. J. M. Sheltzer, E. M. Torres, M. J. Dunham, A. Amon, Transcriptional consequences of aneuploidy. *P Natl Acad Sci Usa* **109**, 12644–12649 (2012).

5. E. M. Torres, *et al.*, Effects of Aneuploidy on Cellular Physiology and Cell Division in Haploid Yeast. *Science* **317**, 916–924 (2007).

6. A. P. Gasch, *et al.*, Genomic Expression Programs in the Response of Yeast Cells to Environmental Changes. *Mol Biol Cell* **11**, 4241–4257 (2000).

7. Y. H. Ho, E. Shishkova, J. Hose, J. J. Coon, A. P. Gasch, Decoupling Yeast Cell Division and Stress Defense Implicates mRNA Repression in Translational Reallocation during Stress. *Curr Biology Cb* **28**, 2673-2680.e4 (2018).

8. M. J. Brauer, *et al.*, Coordination of Growth Rate, Cell Cycle, Stress Response, and Metabolic Activity in Yeast. *Mol Biol Cell* **19**, 352–367 (2008).

9. H. J. Tsai, *et al.*, Hypo-osmotic-like stress underlies general cellular defects of aneuploidy. *Nature* **570**, 117–121 (2019).

10. T. Altenburg, B. Goldenbogen, J. Uhlendorf, E. Klipp, Osmolyte homeostasis controls single-cell growth rate and maximum cell size of Saccharomyces cerevisiae. *Npj Syst Biology Appl* **5**, 34 (2019).

11. A. L. Tarca, G. Bhatti, R. Romero, A comparison of gene set analysis methods in terms of sensitivity, prioritization and specificity. *Plos One* **8**, e79217 (2013).

12. N. Pavelka, *et al.*, Aneuploidy confers quantitative proteome changes and phenotypic variation in budding yeast. *Nature* **468**, 321–325 (2010).

13. M. J. Dunham, E. O. Kerr, A. W. Miller, C. Payen, Chemostat Culture for Yeast Physiology and Experimental Evolution. *Cold Spring Harb Protoc* **2017**, pdb.top077610 (2017).

14. J. S. Hahn, D. J. Thiele, Regulation of the Saccharomyces cerevisiae Slt2 Kinase Pathway by the Stress-inducible Sdp1 Dual Specificity Phosphatase. *J Biol Chem* **277**, 21278–21284 (2002).

15. S. E. Dodgson, *et al.*, Chromosome-Specific and Global Effects of Aneuploidy in Saccharomyces cerevisiae. *Genetics* **202**, 1395–1409 (2016).

16. M. Delarue, *et al.*, mTORC1 Controls Phase Separation and the Biophysical Properties of the Cytoplasm by Tuning Crowding. *Cell* **174**, 338-349.e20 (2018).

17. M. C. Rivera, B. Maguire, J. A. Lake, Isolation of ribosomes and polysomes. *Cold Spring Harb Protoc* **2015**, 293-299 (2015).

18. A. M. Munoz, P. Yourik, V. Rajagopal, J. S. Nanda, J. R. Lorsch, S. E. Walker, Active yeast ribosome preparation using monolithic anion exchange chromatography. *RNA Biol* **14**, 188-196 (2017).

19. M. A. Algire, *et al.*, Development and characterization of a reconstituted yeast translation initiation system. *RNA* **8**, 382-397 (2002).

20. C. M. Brennan, *et al.*, Protein aggregation mediates stoichiometry of protein complexes in aneuploid cells. *Genes Dev* **33**, 15-16 (2019).

21. G. E. Neurohr, *et al.*, Excessive Cell Growth Causes Cytoplasm Dilution And Contributes to Senescence. *Cell* **176**, 1083-1097.e18 (2019).

22. G. E. Neurohr, A. Amon, Relevance and Regulation of Cell Density. *Trends Cell Biol* **30**, 213-225 (2020).

23. A. Dobin, *et al.*, STAR: ultrafast universal RNA-seq aligner. *Bioinformatics* **29,** 15-21 (2013).

24. B. Li, C. N. Dewey, RSEM: accurate transcript quantification from RNA-Seq data with or without a reference genome. *BMC Bioinformatics* **12**, 323 (2011).

25. A. Subramanian, *et al.*, Gene set enrichment analysis: A knowledge-based approach for interpreting genome-wide expression profiles. *P Natl Acad Sci Usa* **102**,15545-15550 (2005).

26. D. A. Barbie, *et al.*, Systematic RNA interference reveals that oncogenic KRAS-driven cancers require TBK1. *Nature* **462**, 108-112 (2009).

27. M. Reich, *et al.*, GenePattern 2.0, *Nature Genetics* **38**, 500-501 (2006).

28. M. I. Love, W. Huber, S. Anders, Moderated estimation of fold change and dispersion for RNA-seq data with DESeq2. *Genome Biology* **15**, 550 (2014).

29. M. Dunham, E. Mitchell, Dunham Lab Chemostat Manual. *Dunham Lab, University of Washington* (2010) (March 25, 2020).

Chapter 3: The environmental stress response regulates ribosome content in cell cycle-arrested *S. cerevisiae*

The experiments in Figure S1 were performed by TS and LJH.
The experiments in Figure 1; 2; S2; 3 were performed by AS and AT.
The experiments in Figure S3 were performed by GN.
All RNASeq processing and ssGSEA projection value generation was performed by CAW.
All other experiments and analyses were performed by AT.

Significance Statement

Throughout eukaryotes, the coordination between cell growth and division regulates cell size homeostasis. Here, we show that cell growth and division are no longer coupled in cell cycle arrested *cdc-ts* mutants, but, in response, the ESR downregulates ribosomes to attenuate volume growth. We further show that hyperactivation of the Ras/PKA pathway leads to suppression of the ESR, causing arrested cells lose viability and no longer downregulate their ribosomes. Our work suggests that when cell growth and cell cycle progression are uncoupled, the ESR is a mechanism for regaining control of cell size homeostasis.

Abstract

Temperature sensitive cell division cycle (*cdc-ts*) cells are unable to progress through the cell cycle at the restrictive temperature due to mutations in genes essential to cell cycle progress. Cells harboring *cdc-ts* mutations increase in cell volume upon arrest but eventually stop growing. We found that this attenuation in growth was due to selective downregulation of ribosome concentration. We saw similar ribosome downregulation in cells arrested in the cell cycle through alpha factor addition, rapamycin addition, and entrance into stationary phase. In all cell cycle arrests studied, cells activated the Environmental Stress Response (ESR), a key transcriptional response to many stressors in *S. cerevisiae*. When we combined cell cycle arrest with hyperactivation of the Ras/PKA pathway, ESR activation was prevented, cells were unable to downregulate their ribosomes, and cell viability was decreased. Our work uncovers a key role for the environmental stress response in coupling cell cycle progression to biomass accumulation.

Introduction

For organisms to maintain both their fitness as well as their organismal and cellular homeostasis, biomass accumulation and cell division must be tightly coordinated (1, 2). Throughout the G1 phase, the presence of growth signals, amino acids, and glucose stimulates the rate of macromolecule biosynthesis, increasing the cell's volume. Entry into the cell cycle relies on sufficient biosynthetic capacity to reach a cell's "critical size," or minimum size threshold dependent on nutrient availability (3, 4). While cell size control mechanisms seem to prevent cells from entering cell division while too small, there are also issues associated with cells being too large, such as decreased surface area to volume and DNA to cytoplasm ratios. Because alterations of these key cellular parameters can detrimentally affect cell viability, it is likely that cells have evolved to maintain homeostatic size and biomass production (3, 5, 6, 7).

Saccharomyces cerevisiae, or budding yeast, has proven to be critical in the study of the relationship between cell growth and progression through the cell cycle. In order to understand this relationship, cell growth and division can be uncoupled using temperature-sensitive cell division cycle (*cdc-ts*) mutants, which have mutations in genes required for cell cycle progression. At the restrictive temperature, the *cdc-ts* mutants are unable to progress through the cell cycle but continue to accumulate biomass and thus increase in size, in some mutant strains up to 16 times the size of a wild-type cell (8, 9). Previous work from our lab determined that, at the restrictive temperature, the size of many *cdc-ts* mutants eventually plateaus (9). In one of these *cdc-ts* mutants, attenuation of cell growth in oversized cells correlated with an unusual dilution of the cytoplasm, suggesting that reduced overall biomass production might cause attenuation of growth during prolonged cell cycle arrests (6).

The ability or inability to produce ribosomes has been shown to cause dramatic changes in cell size (4). A significant portion of a cells' energy is involved in accumulating biomass through protein synthesis by ribosomes. Ribosomes, which are composed of ribosomal proteins and rRNA, translate mRNA into proteins. The biogenesis of ribosomes is highly regulated within the cell, to prevent cells from unnecessarily expending energy (10). When energy is abundant, cells rapidly make ribosomes, and the ribosomal fraction of the proteome correlates with growth rate (11). We hypothesized that cell cycle arrested cells would shift energy expenditure from growth to maintenance of viability. Using different *cdc-ts* mutants as a model system, we here describe our studies determining how ribosome content regulates cell size in arrested cells.

In this report, we determined how cells regulate growth and biomass production during prolonged cell cycle arrests in budding yeast. Using ribosome purification and Tandem Mass Tag (TMT) Proteomics, we found that ribosomes were specifically downregulated during cell cycle arrests in *cdc-ts* mutants. We saw a similar ability to attenuate size through downregulation of ribosome biogenesis in physiological cell cycle arrests. All investigated cell cycle arrests led to activation of the Environmental Stress Response (ESR), a transcriptional response to stress in *S. cerevisiae* that decreases translational capacity (12, 13). Preventing ESR activation through hyperactivation of the Ras/PKA pathway interfered with downregulation of ribosome content and reduced cell survival during the cell cycle arrest. We conclude that activation of the ESR, potentially through attenuation of ribosome biogenesis, is required for survival of cell-cycle arrested cells.

Results

Cell volume is regulated in *cdc-ts* arrested cells.

In order to determine how cells attenuate their biomass accumulation during cell cycle arrests, we studied three independent *cdc-ts* mutants: *cdc28-13*, *cdc20-1*, and *cdc15-2*. We decided to examine these three separate *cdc-ts* mutants because they arrest in three distinct phases of the cell cycle and grow to different maximum cell volumes. This allowed us to distinguish between global, size-specific, and cell cycle phase-specific observations. Cdc28 is the main cyclin-dependent kinase that coordinates the yeast cell cycle, and *cdc28-13* cells arrest in G1 (9, 14). Previous work from our lab has shown that in *cdc28-13* cells, the mean cell volume growth is driven by growth of the whole cell, including the cytoplasm, rather than solely vacuole enlargement (6). Cdc20 is the activator subunit of the anaphase promoting complex that drives the metaphase-anaphase transition, therefore *cdc20-1* mutants arrest in metaphase at the restrictive temperature (9, 15). Cdc15 is a critical kinase required for mitotic exit, and *cdc15-2* mutants at the restrictive temperature arrest in late anaphase (9, 16).

We measured the mean cell volume of all three *cdc-ts* strains was measured using a Coulter Counter to confirm the previous findings of Goranov et al. (2009; 9). In agreement with previous cell size data (9), the mean cell volume of all three *cdc-ts* strains increased over 9 hours and eventually plateaued (Fig. 1*A*). As a control, a *WT* strain (Fig. 1*A*, gray) was grown concurrently and was kept in log phase, termed "cycling," to avoid confounding factors caused by growth into stationary phase, which is a response to glucose depletion and known to cause many physiological changes including changes in cell size (17, 18). The cell volume of *cdc28-13* mutant cells grew exponentially for the first two hours of arrest, grew linearly until 6 hours, and eventually plateaued to the largest of the strains, at 800 fL (Fig. 1*A*, pink). The mean cell volume of *cdc20-1* cells initially was the largest of the strains and appeared to have two distinct plateaus, one at 300 fL after being arrested for five hours and the other at 450 fL after 9 hours of cell cycle

arrest (Fig. 1*A*, purple). Cell harboring the *cdc15-2* mutation had linear growth and plateaued to approximately 500 fL (Fig. 1*A*, blue). We note that both *cdc20-1* and *cdc15-2* strains have final sizes that differ from those previously reported in Goranov et al. (2009; 9), likely due to the slightly differing methods used to measure cell size.
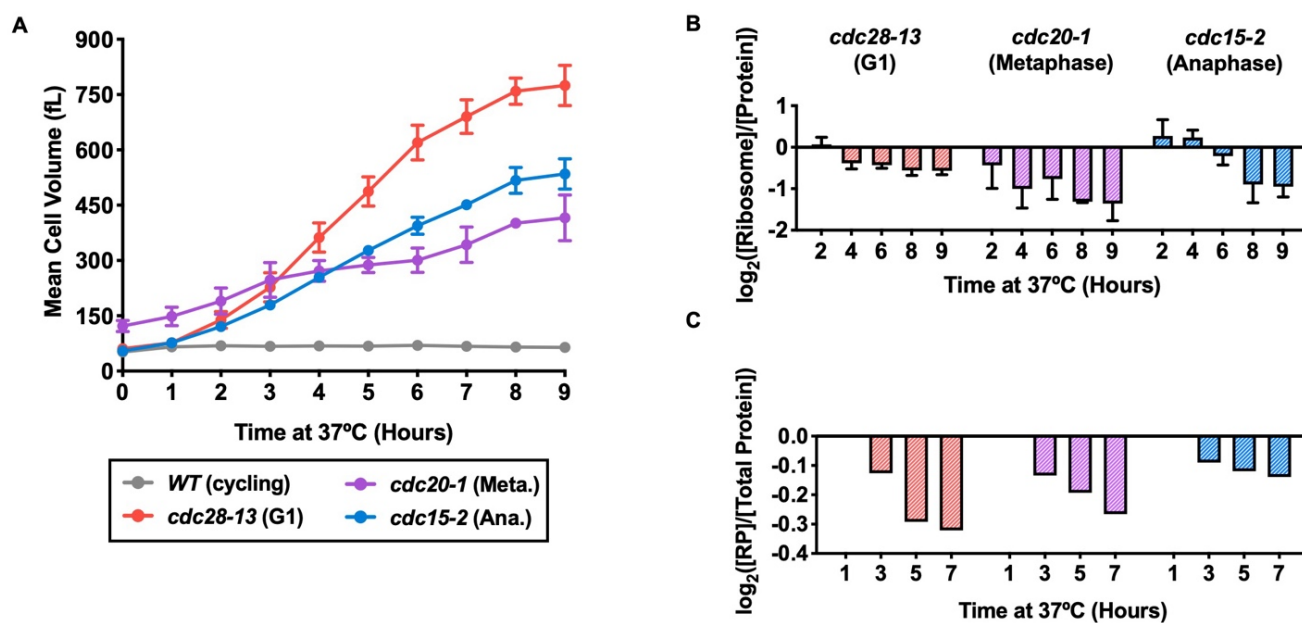
Figure 1. Ribosome concentrations decrease during prolonged cell cycle arrest.

WT (gray, A2587), *cdc28-13* (red, A39000), *cdc20-1* (purple, A937), and *cdc15-2* (blue, A2596) cells were grown to log phase in YEPD at 25ºC and then shifted to 37ºC for 9 hours. *WT* cultures were kept in log phase (cycling) at OD_{600nm} 0.2-0.8, by diluting with pre-warmed (37ºC) YEPD.

(A) Mean cell volume (fL) was measured. Error bars represent standard deviation from the mean of experimental replicates.

(B) Protein and ribosome concentrations were quantified using a quantitative ribosome purification method, described in Terhorst et al. (2020; 17). Samples of equal volume were lysed

with a French Press, and [Protein] was measured with a Bradford Assay. Intact ribosomes were purified with sucrose cushion centrifugation, and [Ribosome] was measured by rRNA absorbance at A260nm on a Nanodrop. [Ribosome]/[Protein] were determined. Values were normalized to those of the *WT* cycling samples at each time point and subsequently $\log_2$ transformed. Error bars represent standard deviation from the mean of experimental replicates. *(C)* TMT Proteomics was performed on the *cdc-ts* strains. *cdc28-13* cells were synchronized with alpha factor prior to arrest at 37ºC. The fraction of ribosomal proteins (RP) in total protein extracts ([RP]/[Total Protein]) was determined. Values were normalized to the 1-hour time point in each experiment and subsequently $\log_2$ transformed.

Protein and ribosomes are downregulated in size-attenuated *cdc-ts* arrested cells, leading to increased cytoplasmic diffusion.

Having confirmed that cell growth is attenuated during various *cdc-ts* mutant cell cycle arrests, independent of cell cycle stage in which the cells are arrested, we hypothesized that this global size control was regulated by cellular ribosome content because it is known that ribosome biogenesis is rate-limiting for growth in yeast (11). To test this hypothesis, we measured the protein and ribosome content of the *cdc-ts* mutant strains during 9-hour cell cycle arrests to determine protein and ribosome concentrations as cell growth plateaued. Cells were lysed, and protein concentration ([Protein]) of the lysates was measured with a Bradford Assay. We next measured the rRNA concentration of intact ribosomes ([Ribosome]) purified with sucrose-cushion centrifugation. To measure the ribosomal fraction of the proteome, we next calculated [Ribosome]/[Protein] from the previous measurements. Because the arrest of *cdc-ts* strains requires a temperature shift from 25ºC to 37ºC, we began protein and ribosome measurements

112

after 2 hours at 37ºC to avoid confounding effects of heat shock (19, 20). Concurrent to the arrests of the *cdc-ts* mutants, we also grew a *WT* cycling culture and normalized each *cdc-ts* time point to those of the *WT* cycling culture. Because ribosome biosynthesis rate is known to be a major determinant of cell size, we expected to see a plateau or decrease in the ribosome content of the *cdc-ts* cells compared to *WT* cycling cells (4, 11). Consistent with this prediction, [Ribosome]/[Protein] decreased dramatically over the 9-hour cell cycle arrests in all three *cdc-ts* strains, (Fig. 1*B*). We confirmed these findings by measuring the fraction of the proteome consisting of ribosomal proteins ([RP]/[Total Protein]) using TMT proteomics of whole cell lysates. Again, we saw a decrease in [RP]/[Total Protein] in all three *cdc-ts* arrests (Fig. 1*C*). The data from these two separate methods, taken together, suggest a specific downregulation of ribosomes during *cdc-ts* cell cycle arrests, which is independent of the specific cell cycle arrest, while cells continue to make other protein. We hypothesize that the resulting decreased translational capacity leads to attenuation of cell volume growth after prolonged cell cycle arrest.

Cytoplasmic ribosome concentration not only affects translational capacity but also contributes to molecular crowding and thereby indirectly influences important processes, such as phase separation and cytoplasmic diffusion (21). To determine whether cytoplasmic crowding was affected in *cdc-ts* cell cycle arrests, we used genetically encoded multimeric nanoparticles (GEMs) to probe the mesoscale diffusivity of the cytoplasm as described in Delarue et al. (2018, 21). Upon mTORC1 inactivation using rapamycin, Delarue et al. (2018, 21) reported a significant increase in the cytoplasmic effective diffusion coefficient of the GEMs, which was attributed to the presence of fewer ribosomes in the cytoplasm (21). The median effective diffusion coefficients of GEMs in *cdc-ts* and *WT* cycling cells were measured at different time points over 6 hours, at which point ribosome and protein content are downregulated in *cdc-ts*

mutants. The median effective diffusion coefficients of the *cdc-ts* and *WT* cycling cells increased considerably between 0 hours and 2 hours, during which they were shifted to 37ºC. We attribute this increase to heat shock, which has been previously shown to increase cytoplasmic diffusion (11). After the initial heat shock, the median diffusion coefficients of all three *cdc-ts* mutants remained above the median diffusion coefficient of the *WT* cycling cells, which decreased gradually after heat shock (Fig. S1*F*). As expected, *cdc20-1* cells had the highest median diffusion coefficient initially and throughout the experiment, in agreement with our observation that *cdc20-1* cells are already downregulating ribosomes at the permissive temperature. We conclude that ribosome downregulation causes decreased macromolecular crowding of the cytoplasm in *cdc-ts* cells arrested in different cell cycle phases.
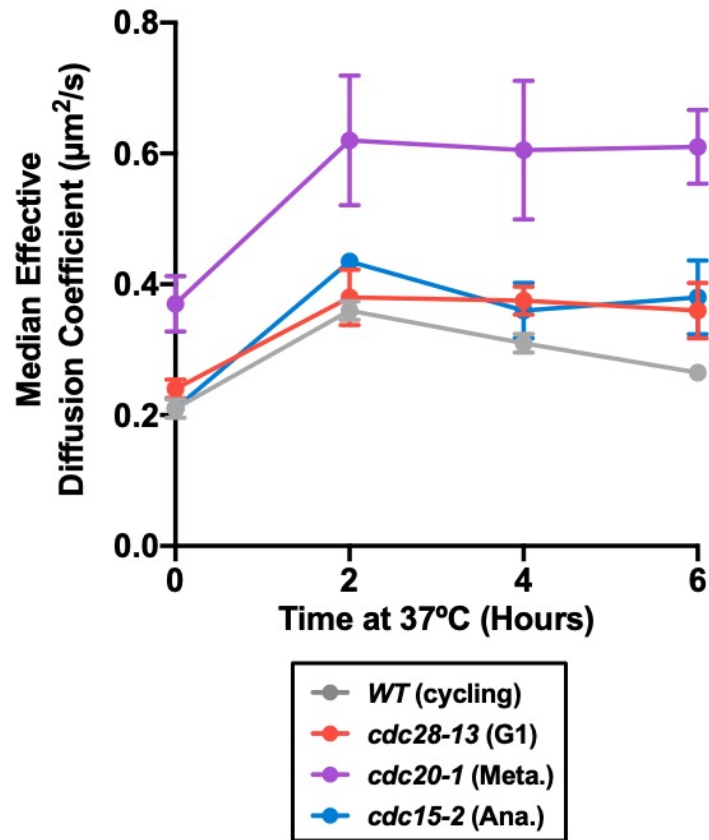
**Figure S1. Macromolecular crowding in *cdc-ts* mutants arrested in the cell cycle.**

WT (gray, A2587), *cdc28-13* (red, A39000), *cdc20-1* (purple, A937), and *cdc15-2* (blue, A2596) cells were grown to log phase in YEPD at 25ºC and then shifted to 37ºC for 6 hours. *WT* cultures were kept in log phase, termed cycling, at OD_{600nm} = 0.2-0.8, by diluting with pre-warmed (37ºC) YEPD. GEM diffusion was performed as in Delarue et al. (2018; 21) to calculate median diffusion coefficients. Error bars represent standard deviation from the mean of experimental replicates.

G1 arrests decrease ribosome content to attenuate cell growth, independent of the method used for the arrest

Whether growth attenuation caused by ribosome downregulation is a global phenomenon remained unknown, so we next studied changes in cell size and protein and ribosome content in naturally occurring cell cycle arrests. We investigated the growth of cells arrested with three different methods: alpha factor pheromone addition, TORC1 inhibition through rapamycin addition, and entry into stationary phase due to glucose depletion. Alpha factor (αf) is a pheromone secreted by mating-type alpha (*MATα*) cells that arrests mating-type a (*MATa*) in G1 before mating begins through a well-studied MAPK pathway that previous work from our lab has shown to inactivate TORC1 (22, 23). Rapamycin addition is also known to arrest cells in G1 by directly inhibiting TORC1, mimicking the effect of amino acid starvation (4, 24, 25). Depletion of glucose causes inhibition of both TORC1 and a related nutrient-sensing pathway, the Ras/PKA pathway. Cells started to enter stationary phase upon growth to saturation at OD_{600nm} of approximately 3.4 in our spectrophotometer. At this point, cells become starved for glucose, causing arrest in G1 (4, 24). These three G1 arrests function through different mechanisms and therefore, were used to determine whether ribosome downregulation only occurs in *cdc-ts* arrested cells or is independent of the method used to arrest cells.

We first measured mean cell volume throughout each cell cycle arrest. *bar1Δ* cells were used in the alpha factor experiments. These cells lack the protease that degrades alpha factor, thus ensuring that alpha factor was not degraded and that cells did not escape their cell cycle arrests. *bar1Δ* cells arrested with alpha factor (Fig. 2*A*, +αf, orange) for 9 hours reached a maximum mean cell volume of over 200 fL; in comparison to *bar1Δ* cells grown in the absence of alpha factor (Fig. 2*A*, -αf, yellow), cells arrested with alpha factor grew to be four times larger

116

(26). After 8 hours arrest, alpha factor arrested cells began to slow in cell growth at a cell volume around 200 fL, which was a smaller maximum mean cell volume than in the *cdc28-13* G1 arrested cells, suggesting the presence of size attenuation during the arrest (Fig. 2*A*). *WT* haploid cells grown into stationary phase (Fig. 2*B*, green squares) reached an OD_{600nm} of 8.5 by 10 hours and of 20.0 by 24 hours. The mean cell volume of these cells decreased as cells became starved for glucose and entered stationary phase, suggesting a potentially interesting relationship between glucose starvation and size attenuation (Fig. 2*B*). In rapamycin experiments, *WT* haploid cells were arrested with rapamycin for 5 hours (Fig. 2*C*, green circles). Although TORC1 inhibition has been shown to decrease cell size in mammalian cells (27), there was a subtle increase in mean cell volume throughout the rapamycin arrest in the W303 *S. cerevisiae* cells, reaching a final volume of approximately 130 fL, twice that of an untreated cycling *WT* haploid cell (Fig. 2*C*). The increase in mean cell volume upon rapamycin addition could be explained by growth of the vacuole, which is known to occur in *S. cerevisiae* after rapamycin addition, and the concentration of the cytoplasm specifically may be changing (28). Although the mean cell volume of rapamycin arrested cells increased, size attenuation may have prevented these cells from growing even larger. With the exception of the rapamycin experiments, cell size decreased in the naturally occurring cell cycle arrests, suggesting that growth attenuation during cell cycle arrests does not only happen in *cdc-ts* mutants and is independent of method used to arrest the cells.
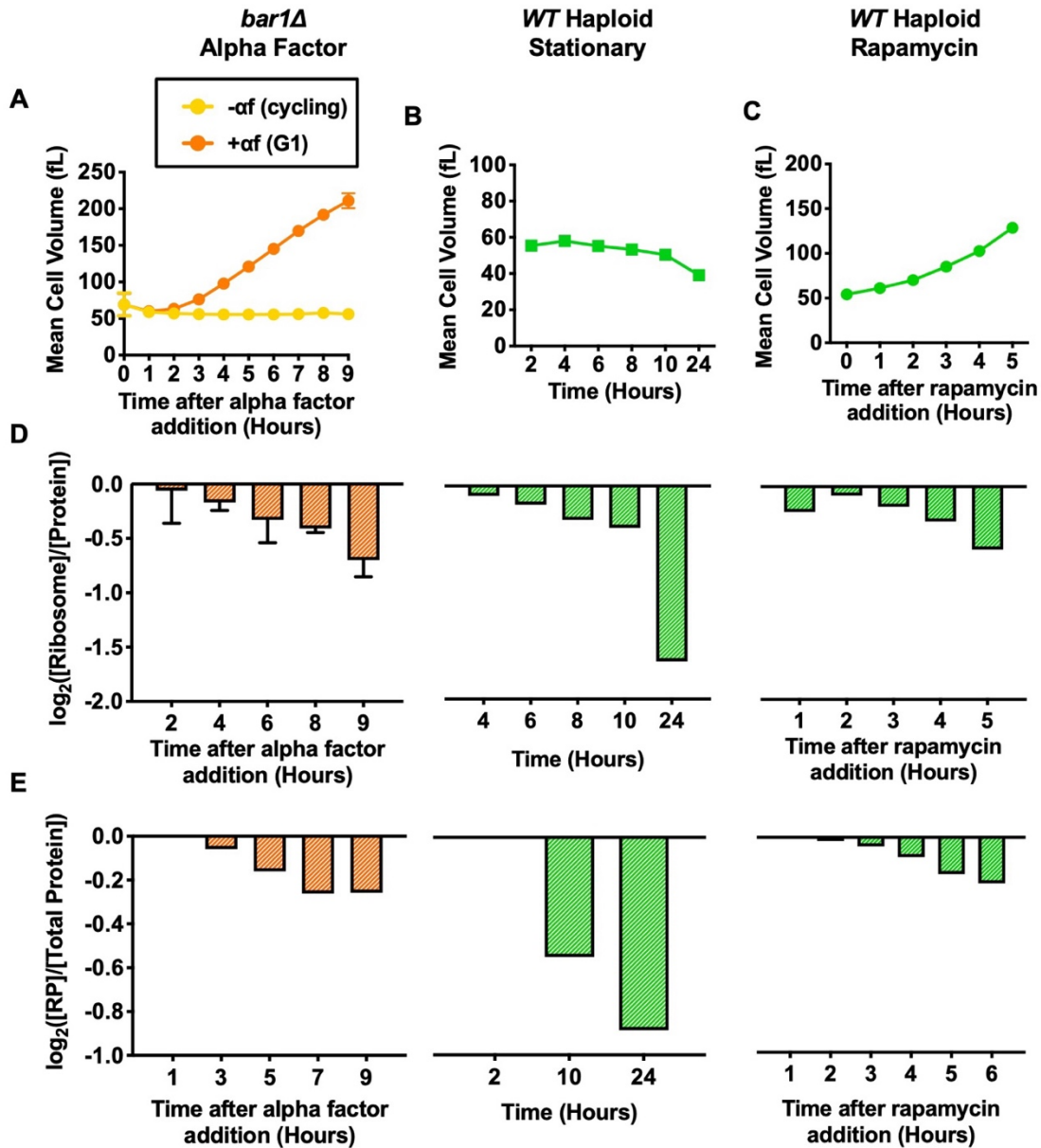
Figure 2. Protein and ribosome quantification of cells arrested in G1 with various methods.

For alpha factor experiments, *bar1Δ* (A2589) cells were grown to log phase in YEPD at 30ºC.

Cells were then divided into two cultures and grown for 9 hours at 30ºC. 5 μg/mL alpha factor

was added to one culture (+αf, orange) while the equivalent volume of DMSO was added to the

other (-αf, yellow). 2 μg/mL of alpha factor (+αf, orange) or the equivalent volume of DMSO (-

αf, yellow) was re-added every 2 hours. For stationary phase experiments, *WT* haploid (green,

A2587) cells were grown in YEPD for 24 hours at 30ºC. For rapamycin experiments, *WT* haploid (green, A2587) cells were grown to log phase in YEPD at 30ºC. 5 nM rapamycin was added, and cells were grown for 5 hours at 30ºC.

(A-C) Mean cell volume (fL) was measured for *(A) bar1Δ* cells with (+αf, orange) and without (-αf, yellow), *(B) WT* haploid cells grown into stationary phase (green squares), and *(C) WT* haploid cells with added rapamycin (green circles). Error bars represent standard deviation from the mean of experimental replicates.

(D) Protein and ribosome concentrations were quantified using the method described in Terhorst et al. (2020; 17). [Ribosome]/[Protein] was determined. Values were normalized to those of the cycling samples in each experiment (-αf in alpha factor experiments, 2-hour time point in stationary phase experiments, and 0-hour time point in rapamycin experiments) and subsequently $\log_2$ transformed. Error bars represent standard deviation from the mean of experimental replicates.

(E) TMT Proteomics was performed for each naturally occurring cell cycle arrest. The fraction of ribosomal proteins (RP) in total protein extracts ([RP]/[Total Protein]) was determined. Values were normalized to the 1-hour time point in each experiment and subsequently $\log_2$ transformed.

To investigate how cell growth was attenuated in natural cell cycle arrests, we determined whether ribosome concentration was decreasing using the method from Terhorst et al. (2020, 17). Indeed, each arrest saw a dramatic decrease in [Ribosome]/[Protein], suggesting that ribosomes are selectively downregulated during cell cycle arrests independent of the method

used to arrest cells (Fig. 2*D*). This decrease in [Ribosome]/[Protein] was confirmed with TMT

Proteomics (Fig. 2*E*). As in the *cdc-ts* measurements, the percent change was slightly different

between the two methods due to differences in normalization and [Ribosome] measuring

concentration of purified assembled ribosome, while [RP] measured the concentration of all

ribosomal proteins in whole cell lysates. Still, both experiments suggest that ribosome

downregulation occurs in cell cycle arrests independent of method used to arrest the cells.

To ensure the accuracy of our protein and ribosome measurements, the protein and

ribosome contents of *WT* haploid (closed green; Strain Table S1, A2587) and *WT* diploid (open

dark green; Strain Table S1, A33728) strains were compared, specifically in the stationary phase

and rapamycin experiments. The mean cell volume of the *WT* diploid cells was approximately

triple that of the *WT* haploid cells throughout both experiments, particularly when cells reach

stationary phase (Fig. S2*A-B*). In the stationary phase experiments, the mean cell volume *WT*

haploid cells (Fig. S2*A*, closed green squares) decreased gradually as cells entered stationary

phase, but *WT* diploid cells (Fig. S2*A*, open dark green squares) had a sharp decrease in mean

cell volume after 8 hours growth, at OD_{600nm} of 3.8. When cells were arrested with rapamycin,

the cell volume of both *WT* haploid (Fig. S2*B*, closed green circles) and *WT* diploid (Fig. S2*B*,

open dark green circles) increased exponentially throughout the G1 arrest. Each value was

normalized to the 1-hour time point of the *WT* haploid strains to better represent how the two

strains differ. In the two experiments, [Ribosome]/[Protein] was the same for *WT* haploid and

WT diploid strains at each time point, suggesting that the two have the same ribosomal fraction

of the proteome (Fig. S2*C*). Taken together, the relative measurements [Ribosome]/[Protein] in

WT haploid and *WT* diploid cells support the accuracy of our measurements.

120
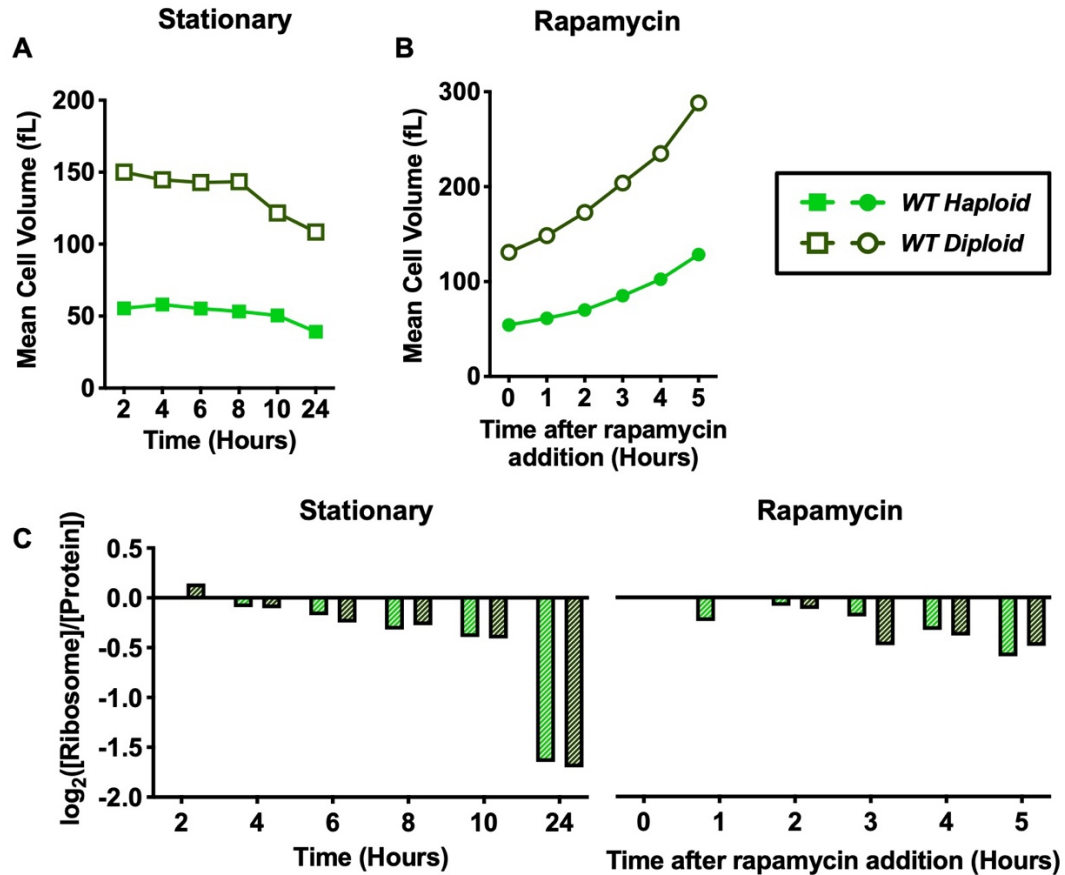
Figure S2. Comparison of protein and ribosome quantification in haploid and diploid *WT* cells.

For stationary phase experiments, *WT* haploid (green, A2587) and *WT* diploid (dark green, A33728) cells were grown in YEPD for 24 hours at 30°C. For rapamycin experiments, *WT* haploid (green, A2587) and *WT* diploid (dark green, A33728) cells were grown to log phase in YEPD at 30°C. 5 nM rapamycin was added to *WT* haploid cells, and 2.5 nM rapamycin was added to *WT* diploid cells. Cells were grown for 5 hours at 30°C in the presence of rapamycin. *(A-B)* Mean cell volume (fL) was measured for *WT* haploid (green) and *WT* diploid (dark green) cells grown *(A)* into stationary phase (squares) and *(B)* in the presence of rapamycin (circles).

(C) Protein and ribosome concentrations were quantified using the method described in Terhorst et al. (2020; 17). [Ribosome]/[Protein] was determined. Values were normalized to the 2-hour time point in stationary experiments and to the 0-hour time point in rapamycin experiments and subsequently $\log_2$ transformed.

Cell cycle arrested cells activate the Environmental Stress Response

We next wanted to understand how the cell is able to downregulate ribosomes in response to cell cycle arrests. Our previous work showed that slow growing cells activate an Environmental Stress Response (ESR) to a degree that is correlated to their growth rate (17, 29), so we collected RNASeq data to determine if the ESR is activated in our arrested cells. The ESR is a transcriptional response to a variety of stresses, such as oxidative and reductive stresses, heat shock, hyperosmotic shock, proteotoxic stress, and nutrient limitation, and was originally described by Gasch et al. (2000; 12). There are approximately 300 genes upregulated in the ESR, a gene set termed the "induced ESR" and involved in promotion of cell survival in stressful conditions by increasing autophagy, DNA damage repair, cell wall reinforcement, and protein folding and degradation. Over 600 genes are downregulated in the ESR, forming a gene set known as the "repressed ESR." The repressed ESR downregulates many genes related to size and biomass accumulation, such as ribosomal biogenesis genes, RNA production and processing genes, and protein synthesis genes (12, 13).

Previous work from our lab has shown a strong correlation between slow growth and induction of the ESR in yeast strains that have gained and/or lost one or more chromosomes, a condition termed aneuploidy (17, 29). In these aneuploid strains, we have also seen that activation of the ESR, specifically the repressed ESR, which contains many ribosomal protein

122

and biogenesis genes, correlates with a decrease in ribosome content (17). The slow growth and cell stress associated with the *cdc-ts* arrests may lead to activation of the ESR and, consequently, downregulation of ribosomal transcription.

To investigate whether the ESR is activated in cell cycle arrests, we performed RNASeq experiments and analyzed the transcriptomes using a single-sample Gene Set Enrichment Analysis (ssGSEA), described in Tarca et al. (2013, 30) and Terhorst et al. (2020, 17). This analysis calculates ssGSEA projection values for each sample to measure the changes in gene expression distribution of the ESR gene set produced by Gasch et al. (2000; 12). The ssGSEA projection values were calculated separately for the induced ESR and the repressed ESR. As a positive control of ESR activation, *WT* cells were grown in the presence of 500 mM NaCl for 40 minutes to cause hyperosmotic shock (GSE146791, accession numbers: GSM4407212, GSM4407213, and GSM4407214; Terhorst et al. (2020, 17)) (17, 31).

In all three *cdc-ts* arrests, the induced ESR (Fig. 3*A*) and the repressed ESR (Fig. 3*B*) ssGSEA projection values approach or surpass that of the positive control during the 9-hour arrests. During the cell cycle arrest, cells containing the *cdc28-13* mutation increased their induced ESR ssGSEA projection values above the positive control (Fig. 3*A*, red), while dramatically decreasing their repressed ESR ssGSEA projection values far below the positive control (Fig. 3*B*, red). *cdc20-1* mutant cells slightly exhibit both the induced ESR (Fig. 3*A*, purple) and repressed ESR (Fig. 3*B*, purple) at the beginning of the experiment, and its ssGSEA projection values near that of the positive control throughout the arrest. The early activation of the ESR at the 2-hour time points of the *cdc20-1* arrests suggest that the ESR may be already activated in *cdc20-1* cells at the permissive temperature. Cells with the *cdc15-2* mutation exhibit the ESR during their arrest as well. The induced ESR ssGSEA of *cdc15-2* cells reached the

positive control by 6 hours, while the repressed ESR ssGSEA decreased below the positive

control by 8 hours (Fig. 3*A-B*, blue). Since it is known that a large portion of the reduced ESR is

composed of ribosomal protein and ribosome biogenesis genes, the ESR activation seen in *cdc-ts*

mutants is likely responsible for the selective ribosome downregulation in these strains (12).
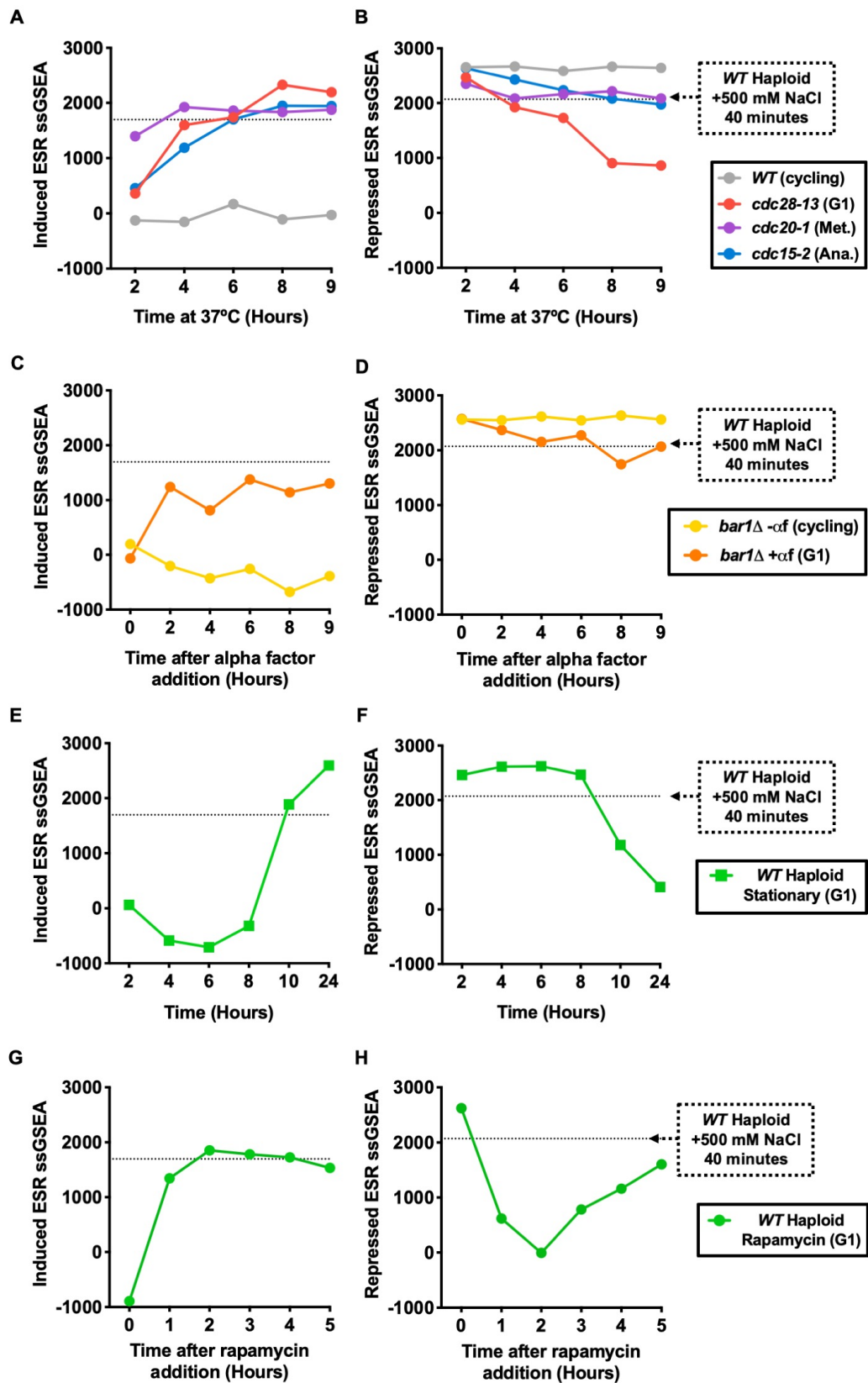
Figure 3. The Environmental Stress Response (ESR) is activated in cell cycle arrested cells.

(A-B) *WT* haploid (gray, A2587), *cdc28-13* (red, A39000), *cdc20-1* (purple, A937), and *cdc15-2* (blue, A2596) cells were grown to log phase in YEPD at 25ºC and then shifted to 37ºC for 9 hours. *WT* cultures were kept in log phase, termed cycling, at OD_{600nm} 0.2-0.8, by diluting with pre-warmed (37ºC) YEPD. RNA-Seq samples were collected, and gene expression data were analyzed by calculating ssGSEA projection values for the *(A)* induced ESR and *(B)* repressed ESR. The horizontal lines represent the induced ESR and repressed ESR ssGSEA projection values for *WT* cells (A2587) treated with 500 mM NaCl for 40 minutes, a positive control for induction of the ESR.

(C-D) *bar1Δ* (A2589) cells were grown to log phase in YEPD at 30 ºC. Cells were then divided into two cultures and grown for 9 hours at 30ºC. 5 µg/mL alpha factor was added to one culture (+αf, orange) while the equivalent volume of DMSO was added to the other (-αf, yellow). 2 µg/mL of alpha factor (+αf, orange) or the equivalent volume of DMSO (-αf, yellow) was re-added every 2 hours. RNA-Seq samples were collected, and gene expression data were analyzed by calculating ssGSEA projection values for the *(C)* induced ESR and *(D)* repressed ESR. The horizontal lines represent the induced ESR and repressed ESR ssGSEA projection values for *WT* cells (A2587) treated with 500 mM NaCl for 40 minutes, a positive control for induction of the ESR.
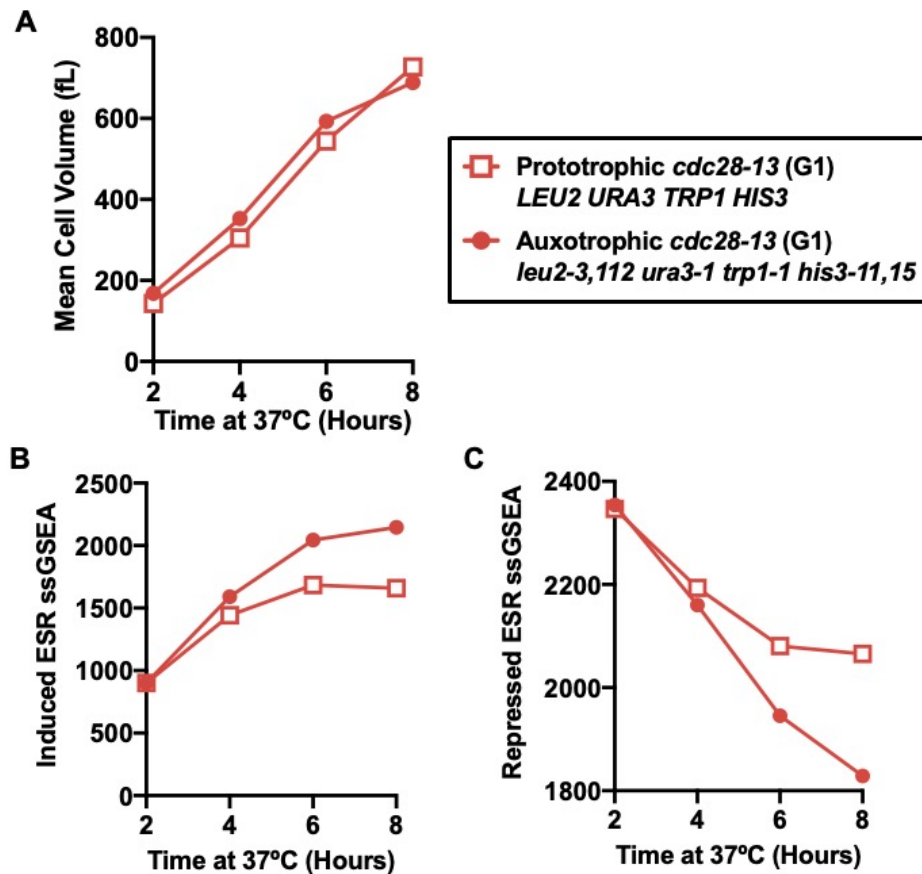
(E-F) *WT* haploid (A2587) cells were grown in YEPD for 24 hours at 30ºC. RNA-Seq samples were collected, and gene expression data were analyzed by calculating ssGSEA projection values for the *(E)* induced ESR and *(F)* repressed ESR. The horizontal lines represent the induced ESR and repressed ESR ssGSEA projection values for *WT* cells (A2587) treated with 500 mM NaCl for 40 minutes, a positive control for induction of the ESR.

(G-H) *WT* haploid (A2587) cells were grown to log phase in YEPD at 30ºC. 5 nM rapamycin was added, and cells were grown for 5 hours at 30ºC. RNA-Seq samples were collected, and gene expression data were analyzed by calculating ssGSEA projection values for the *(E)* induced ESR and *(F)* repressed ESR. The horizontal lines represent the induced ESR and repressed ESR ssGSEA projection values for *WT* cells (A2587) treated with 500 mM NaCl for 40 minutes, a positive control for induction of the ESR.

While the ESR has been thoroughly studied after rapamycin addition and growth into stationary phase, we next wanted to confirm whether the ESR occurs in our naturally occurring cell cycle arrests. In the alpha factor experiment, cells grown in the absence of alpha factor did not exhibit either the induced or repressed ESR (Fig. 3*C-D*, -αf, yellow), while cells grown in the presence of alpha factor exhibit both the induced and repressed ESR (Fig. 3*C-D*, +αf, orange). Previous work from our lab has shown that alpha factor addition causes TORC1 inhibition involving the Fus3 and Kss1 MAPK pathways, raising the possibility that TORC1 inhibition, rather than the cell cycle arrest itself, causes ESR activation in alpha factor-treated cells (23). Cells grown into stationary phase are also known to exhibit the ESR, as glucose starvation causes inhibition of the Ras/PKA pathways (17, 24). As expected, we saw ESR activation in stationary phase cells. This activation was stronger than the positive control by the 10-hour time point and dramatically stronger by the 24-hour time point (Fig. 3*E-F*, squares). Rapamycin addition, known to directly inhibit TORC1, caused ESR activation in cells as well (Fig. 3*G-H*, circles). Inhibition of either the TORC1 pathway or the Ras/PKA pathway likely caused the ESR in these naturally occurring cell cycle arrests and lead to the downregulation of their ribosomes.

To further understand the Environmental Stress Response, particularly in our W303 *cdc-ts* mutant strains, we used prototrophic and auxotrophic *cdc28-13* strains to compare the ESR in the presence and absence, respectively, of the ability of a cell to produce a subset of their amino acids. Amino acid starvation through the TORC1 pathway is known to cause activation of the ESR (12). The auxotrophic strain has mutations in genes required for the biosynthesis of leucine, uracil, tryptophan, and histidine, creating exacerbated nutrient starvation conditions, while the prototrophic strain is able to produce these amino acids. Although the two strains were generally the same size when arrested in G1 at the restrictive temperature of 37ºC (Fig. S3*A*), prototrophic *cdc28-13* cells exhibited the induced ESR (Fig. S3*B*) and the repressed ESR (Fig. S3*C*) much less than auxotrophic *cdc28-13* cells, particularly after the 4-hour time point. One explanation for the difference in ESR strength is that as the *cdc28-13* cells increase their cell volume, their surface area to cell volume ratio decreases, decreasing the cells' ability to uptake nutrients, particularly amino acids, and begin to internally starve (28, 32). Auxotrophic *cdc28-13* cells cannot produce their own amino acids and so may be more starved of nutrients than equivalent prototrophic strains. Because the auxotrophic strain exhibits the ESR more robustly than the prototrophic strain, we conclude that as auxotrophic *cdc-ts* cells become too large, the ESR is further activated potentially due to an internal nutrient starvation.

Figure S3. Comparison of ESR activation in prototrophic *cdc28-13* cells and auxotrophic *cdc28-13* cells.

Prototrophic *cdc28-13* (red squares, A41270) and auxotrophic *cdc28-13* (red circles, A17896) were grown to log phase in YEPD at 25ºC. Cells were synchronized with alpha factor then shifted to 37ºC for 6 hours.

(A) Mean cell volume (fL) was measured for prototrophic *cdc28-13* cells (red squares) and auxotrophic *cdc28-13* cells (red circles).

(B-C) RNA-Seq samples were collected, and gene expression data were analyzed by calculating ssGSEA projection values for the *(B)* induced ESR and *(C)* repressed ESR.

Cells with a hyperactive Ras/PKA pathway do not exhibit the ESR, leading to a loss of viability

To understand the role of the ESR in *cdc-ts* cell cycle arrests, we wanted to observe the effects of preventing ESR activation during these arrests. Hyperactivation of the Ras/PKA pathway dramatically changes the localization of ESR-dependent transcription factors, suggesting that Ras/PKA hyperactivation suppresses ESR activation (33). In order to hyperactivate the Ras/PKA pathway, we depleted Bcy1, a direct inhibitor of the *S. cerevisiae* PKA orthologues, Tpk1-3, using an auxin-inducible degron (AID) (34). Upon auxin addition, AID-Bcy1 is degraded by the proteasome. Previous work from our lab has further characterized this construct and shown rapid degradation of AID-Bcy1 within 90 minutes of auxin addition (35).

We set out to determine whether the ESR activation in *cdc-ts* cell cycle arrests could be suppressed by hyperactivation of PKA. ESR activation was strongly apparent in *cdc-ts* cells after 4 hours of cell cycle arrest at 37ºC (Fig. 3*A-B*). Therefore, we aimed to compare the ESR with and without BCY1 depletion at the 4-hour time point.

We concurrently grew *cdc-ts* cells without the *AID-BCY1* construct. A recent publication from our lab shows convincing data suggesting that the ESR is required to recover from the heat shock response (35), and therefore, we waited for 2 hours after heat shock before adding auxin to allow the general effects of heat-shock to resolve and thus prevent heat-shock related cell death. Auxin was re-added every two hours to maintain depletion of Bcy1 throughout the 6-hour arrest, and *WT* and *WT AID-BCY1* cells were kept in log-phase. As before, we compared iESR and rESR values to those of cells experiencing hyperosmotic shock as a positive control.

130

As before (Fig. 3*A-B*, gray), *WT* cycling cells maintained a constant iESR ssGSEA projection value below the positive control and a constant rESR ssGSEA projection value above the positive control throughout the 6-hour arrest, suggesting that ESR activation does not occur in *WT* cycling cells (iESR, Fig. 4*A-C*, gray; rESR, Fig. 4*D-F*, gray). Cycling *WT AID-BCY1* cells had lower iESR ssGSEA projection values and higher rESR ssGSEA projection values than cycling *WT* (iESR, Fig. 4*A-C*, black; rESR, Fig. 4*D-F*, black). These data suggest that hyperactivation of the Ras/PKA pathway suppress ESR activation. While we saw activation of both the iESR and rESR in *cdc28-13* cells that reached that of the positive control (iESR, Fig. 4*A*, red; rESR, Fig. 4*D*, red), *cdc28-13 AID-BCY1* cells had iESR and rESR ssGSEA projection values resembling those of the cycling *WT* cells (iESR, Fig. 4*A*, dark red; rESR, Fig. 4*D*, dark red). In *cdc20-1* cells arrested for 6 hours, iESR ssGSEA values increased to that of the positive control, and rESR ssGSEA values decreased gradually toward that of the positive control (iESR, Fig. 4*B*, purple; rESR, Fig. 4*E*, purple). When *cdc20-1 AID-BCY1* cells were arrested, iESR and rESR ssGSEA projection values were most similar to those of the cycling *WT* cells (iESR, Fig. 4*B*, dark purple; rESR, Fig. 4*E*, dark purple). *cdc15-2* cells had the most subtle activation of the ESR with its iESR and rESR ssGSEA projection values nearing but not reaching those of the positive control by 6 hours of cell cycle arrest (iESR, Fig. 4*C*, blue; rESR, Fig. 4*F*, blue). As expected, *cdc15-2 AID-BCY1* cells did not exhibit ESR activation, and iESR and rESR ssGSEA projection values were most similar to those of *WT AID-BCY1* (iESR, Fig. 4*C*, dark blue; rESR, Fig. 4*C*, dark blue). In conclusion, ESR activation was prevented in all cell cycle arrests when Ras/PKA was hyperactivated.
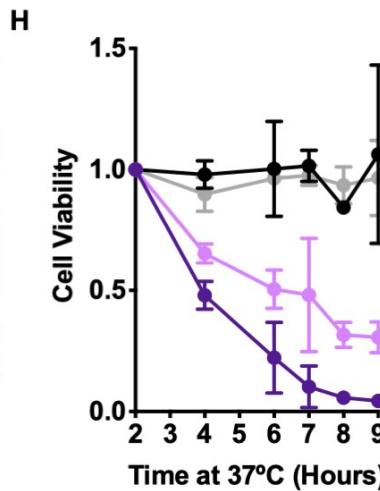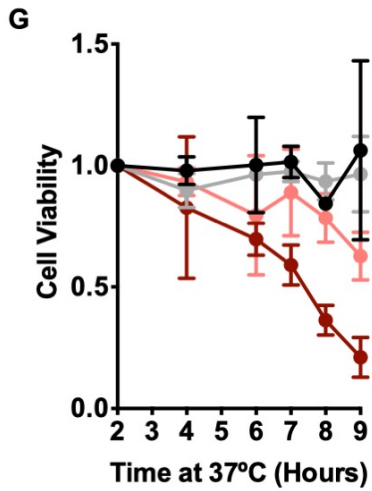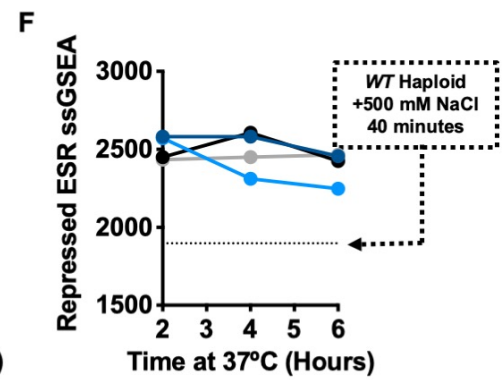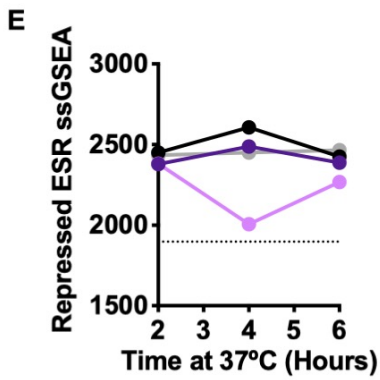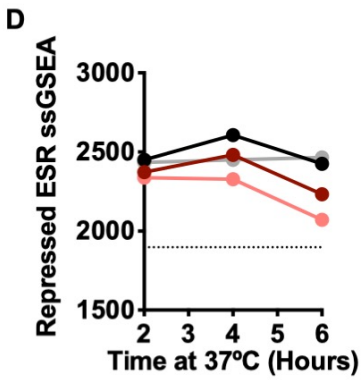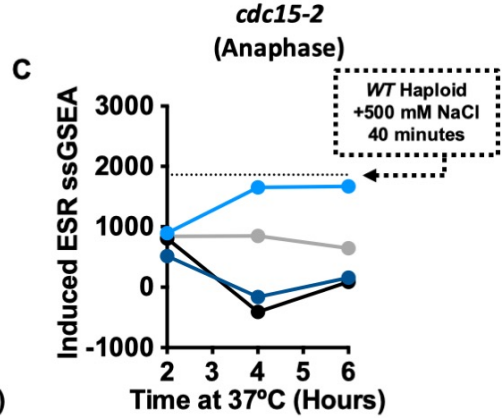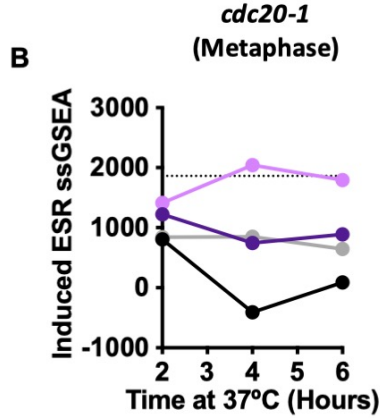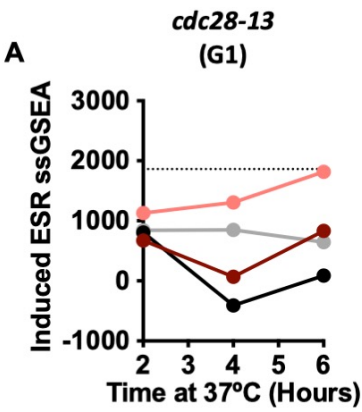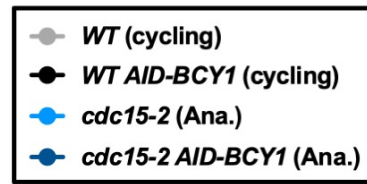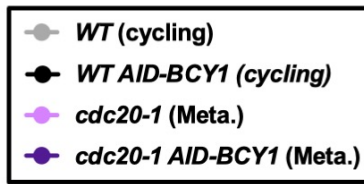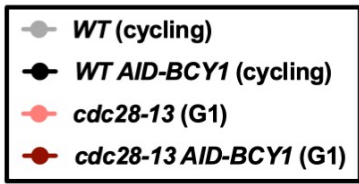
Figure 4. Hyperactivation of the Ras/PKA pathway suppresses the ESR and reduces the viability of cell cycle-arrested cells.

WT (gray, A2587), *WT AID-BCY1* (black, A40439), *cdc28-13* (red, A39000), *cdc28-13 AID-BCY1* (dark red, A40444), *cdc20-1* (purple, A937), *cdc20-1 AID-BCY1* (dark purple, A40499), *cdc15-2* (blue, A2596), and *cdc15-2 AID-BCY1* (dark blue, A40501) cells were grown to log phase in YEPD (supplemented with 138 μL glacial acetic acid for each 1 L YEPD) at 25ºC and then shifted to 37ºC for 6 hours. *WT* and *WT AID-BCY1* cultures were kept in log phase, termed cycling, at OD_{600nm} 0.2-0.8, by diluting with pre-warmed (37ºC) YEPD (supplemented with 138 μL glacial acetic acid for each 1 L YEPD). 500 μM indole-3-acetic acid was added after 2 hours and 4 hours at 37ºC.

(A-C) Induced ESR ssGSEA projection values were calculated from RNA-Seq gene expression data for *WT* (gray), *WT AID-BCY1* (black), and *(A)* *cdc28-13* (red) and *cdc28-13 AID-BCY1* (dark red), *(B)* *cdc20-1* (purple) and *cdc20-1 AID-BCY1* (dark purple), and *(C)* *cdc15-2* (blue) and *cdc15-2 AID-BCY1* (dark blue).

(D-F) Repressed ESR ssGSEA projection values were calculated from RNA-Seq gene expression data for the repressed ESR for *WT* (gray), *WT AID-BCY1* (black) and *(D)* *cdc28-13* (red) and *cdc28-13 AID-BCY1* (dark red), *(E)* *cdc20-1* (purple) and *cdc20-1 AID-BCY1* (dark purple), and *(F)* *cdc15-2* (blue) and *cdc15-2 AID-BCY1* (dark blue).

(G-H) Cell viability was measured for *WT* (gray), *WT AID-BCY1* (black) and *(G)* *cdc28-13* (red) and *cdc28-13 AID-BCY1* (dark red) and *(H)* *cdc20-1* (purple) and *cdc20-1 AID-BCY1* (dark purple). Values were normalized to the 0-hour time point of each experiment. Error bars represent standard deviation from the mean of experimental replicates.

We next asked if ESR activation was important for viability during prolonged cell cycle arrest. We grew *WT* and *cdc-ts* cells with and without the *AID-BCY1* construct for 9 hours at 37ºC and plated 300 cells on YPD plates at 25ºC, the permissive temperature, to determine the viability of cells when they return to the cell cycle. Colonies were allowed to grow for 3 days and were then counted. Cell viability was normalized to the 2-hour timepoint. Unfortunately, the sonication required to accurately determine cell concentration on the Coulter Counter appeared to separate the bud from the mother cell in *cdc15-2* cells once they began to arrest in anaphase. This caused all cells experiencing the *cdc15-2* arrest to die once sonicated, and therefore, *cdc15-2* and *cdc15-2 AID-BCY1* were not included in this analysis. *WT* and *WT AID-BCY1* did not have significantly different cell viability through the 9-hour cell cycle arrest (Fig. 4*G-H*, gray and black, respectively). In contrast, *cdc28-13* cells had a cell viability of above 0.5 during the 9-hour arrest, while *cdc28-13 AID-BCY1* cells had fewer cells survive with a cell viability below 0.3 after being arrested for 9 hours (Fig. 4*G*, red and dark red, respectively). Similarly, fewer *cdc20-1 AID-BCY1* cells survived throughout the 9-hour arrest than *cdc20-1* cells (Fig. 4*H*, dark purple and purple, respectively), but *cdc20-1* cells were less viable than *cdc28-13* cells throughout the arrest. We conclude that the inability to activate the ESR through hyperactivation of the Ras/PKA pathway leads to increased cell death in during cell cycle arrest.

Hyperactivation of the Ras/PKA pathway prevents size attenuation and ribosome downregulation in *cdc-ts* arrests

The question that remained was whether hyperactivation of the Ras/PKA pathway prevented growth attenuation through ribosome downregulation. We measured the cell volumes of our *cdc-ts AID-BCY1* strains, which we then compared to the cell volumes of *cdc-ts* mutants

without the *AID-BCY1* construct. While the mean cell volume of *cdc28-13* cells plateaued, *cdc28-13 AID-BCY1* cells continued to increase in cell volume over the 6 hours (Fig. 5*A*, red and dark red, respectively). As before, *cdc20-1* cells were larger than *WT* cells initially, but *cdc20-1 AID-BCY1* cells had an initial mean cell volume twice as large as that of *cdc20-1* and were approximately 600 fL after 6 hours of cell cycle arrest (Fig. 5*B*, purple and dark purple, respectively). Cells containing the *cdc15-2* mutant had a mean cell volume of 400 fL after 6 hours of being arrested in the cell cycle (Fig. 5*C*, blue). In comparison, *cdc15-2 AID-BCY1* strains grew to be 600 fL after a 6-hour cell cycle arrest, continuing to increase their size exponentially rather than plateauing (Fig. 5*C*, dark blue). It is worth noting that cycling *WT AID-BCY1* cells were larger than *WT* cycling (Fig. 5*A-C*, black and gray, respectively) upon auxin addition, suggesting that the increase in size may not be specific to *cdc-ts* mutants. All three *cdc-ts* strains with a hyperactive Ras/PKA pathway could no longer regulate their cell size during cell cycle arrests.
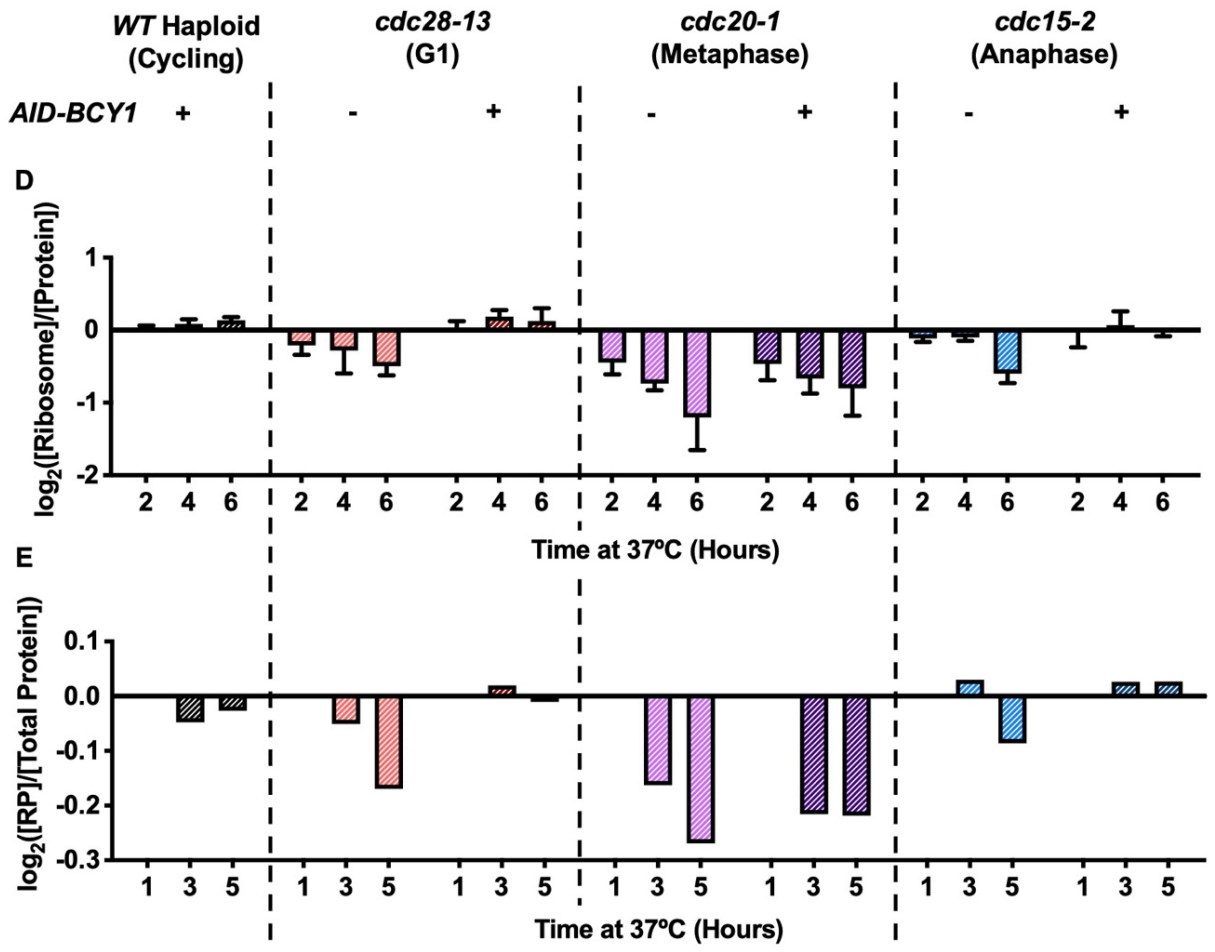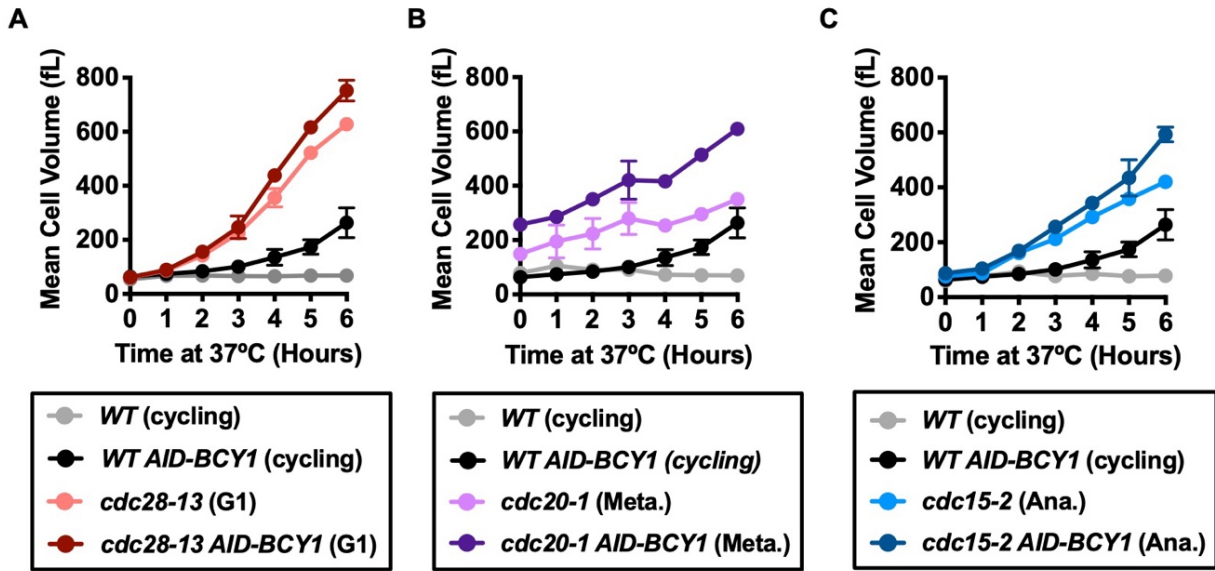
Figure 5. Hyperactivation of the Ras/PKA pathway attenuates ribosome depletion during cell cycle arrest.

WT (gray, A2587), *WT AID-BCY1* (black, A40439), *cdc28-13* (red, A39000), *cdc28-13 AID-BCY1* (dark red, A40444), *cdc20-1* (purple, A937), *cdc20-1 AID-BCY1* (dark purple, A40499), *cdc15-2* (blue, A2596), and *cdc15-2 AID-BCY1* (dark blue, A40501) cells were grown to log phase in YEPD (supplemented with 138 μL glacial acetic acid for each 1 L YEPD) at 25ºC and then shifted to 37ºC for 9 hours. *WT* and *WT AID-BCY1* cultures were kept in log phase, termed cycling, at OD_{600nm} 0.2-0.8, by diluting with pre-warmed (37ºC) YEPD (supplemented with 138 μL glacial acetic acid for each 1 L YEPD). 500 μM indole-3-acetic acid was added after 2 hours and 4 hours at 37ºC.

(A-C) Mean cell volume (fL) was measured for *WT* (gray), *WT AID-BCY1* (black) and *(A)* *cdc28-13* (red) and *cdc28-13 AID-BCY1* (dark red), *(B)* *cdc20-1* (purple) and *cdc20-1 AID-BCY1* (dark purple), and *(C)* *cdc15-2* (blue) and *cdc15-2 AID-BCY1* (dark blue). Error bars represent standard deviation from the mean of experimental replicates.

(D) Protein and ribosome concentrations were quantified using the method described in Terhorst et al. (2020; 17). [Ribosome]/[Protein] was determined. Values were normalized to those of the *WT* cycling samples at each time point and subsequently $\log_2$ transformed. Error bars represent standard deviation from the mean of experimental replicates.

(E) TMT Proteomics was performed. The fraction of ribosomal proteins (RP) in total protein extracts ([RP]/[Total Protein]) was calculated. Values were normalized to the 1-hour time point in each experiment and subsequently $\log_2$ transformed.

We next determined whether *cdc-ts* mutants with hyperactive Ras/PKA were able to selectively downregulate ribosom fraction of the proteome, through decreased [Ribosome]/[Protein] levels. *cdc28-13* exhibited a selective downregulation of ribosomes (Fig. 5*D*, red), but *cdc28-13 AID-BCY1* cells no longer decreased [Ribosome]/[Protein] (Fig. 5*D*, dark red). While ribosome downregulation appeared to occur in *cdc20-1 AID-BCY1* cells, there was more [Ribosome]/[Protein] in *cdc20-1 AID-BCY1* cells than in *cdc20-1* at each time point (Fig. 5*D*, dark purple and purple, respectively). As expected, *cdc15-2* cells decreased [Ribosome]/[Protein] over the 6-hour cell cycle arrest (Fig. 5*D*, blue), but *cdc15-2 AID-BCY1* cells no longer change [Ribosome]/[Protein] when arrested (Fig. 5*D*, dark blue). Importantly, there was also no change in [Ribosome]/[Protein] for *WT AID-BCY1* cells in comparison to *WT* cells, suggesting that hyperactivation of the Ras/PKA pathway does not cause an increase in the ribosomal fraction of the proteome in every strain we studied but instead uniquely in *cdc-ts* arrested cells (Fig. 5*D*, black). As before, we verified the changes in the ribosomal fraction of the proteome by measuring [RP]/[Total Protein] with TMT Proteomics (Fig. 5*E*). We conclude that while preventing ESR activation, *cdc-ts* mutants with hyperactive Ras/PKA pathways can no longer attenuate their size through specific ribosome downregulation.

Discussion

Previous work from our lab had thoroughly investigated the change in cell volume of *cdc-ts* mutants that were arrested in the cell cycle, but the mechanism behind cell volume plateauing in those mutant strains remained unknown (9). Here we confirmed that after prolonged cell cycle arrest, cells of three independent *cdc-ts* strains were able to regulate their cell volume and halt growth. Because ribosome synthesis has been shown to regulate cell size,

138

we studied the protein and ribosome content of the *cdc-ts* cells using two methods (4, 10). There was a selective ribosome downregulation in each strain, independent of the stage of the cell cycle arrest. Ribosome downregulation was observed upon cell cycle arrest using three different methods that mimicked naturally occurring cell cycle arrests: alpha factor addition, entrance into stationary phase, and TORC1 inhibition by rapamycin. Interestingly, while alpha factor addition and entrance into stationary phase caused cells to decrease their size, rapamycin addition led to increased cell volume in both *WT* haploid and diploid strains. Each cell cycle arrest studied activated the ESR, a transcriptional fingerprint known to downregulate ribosomal proteins and biogenesis factors. We also observed that cells exhibited a greater induction of the ESR when they were unable to make their own amino acids. When we prevented ESR activation in *cdc-ts* cells by hyperactivating the Ras/PKA pathway we observed decreased cell viability. Additionally, cells with a hyperactive Ras/PKA pathway were unable to attenuate their size through ribosomes downregulation. Taken together, we conclude that ESR activation is required for *cdc-ts* cells in order to regulate their volume and survive cell cycle arrests through downregulation of ribosome content.

Our findings uncover new questions about how *cdc-ts* mutants regulate their cell volume when arrested. The cause of ESR activation in *cdc-ts* arrests remains unknown but poses a complex question to answer because each strain studied may activate the ESR through different mechanisms, which might be related to the stage in which the cells are arrested, or the mutation itself. Therefore, it is important to continue to study multiple *cdc-ts* strains in comparison to other cell cycle arrests, as we have done here. In our studies, the ESR activation in naturally occurring cell cycle arrests, alpha factor and rapamycin addition and entrance into stationary phase, suggested three possible mechanisms of ESR activation in *cdc-ts* cells: the TORC1,

MAPK, and/or Ras/PKA pathways. Inhibiting the TORC1 pathway through rapamycin addition

caused cells to increase in size, likely due to vacuole growth (28). Goranov et al. (2013, 23)

hyperactivated the TORC1 pathway in *cdc28-4* cells, a temperature-sensitive allele of *CDC28*,

and the TORC1 hyperactivation appeared to cause cells to be even smaller than size attenuated

cdc28-4 cells during the arrest. We confirmed this finding in *cdc28-13* cells as well (data not

shown). Taken together, those results suggest that TORC1 activity is antagonistic to size

attenuation in *cdc-ts* arrests. Another group of pathways that may be involved in cell size

regulation in *cdc-ts* mutants is the MAPK pathways. ESR activation through alpha factor

addition suggests that MAPK pathways could be activated or inactivated in response to *cdc-ts*

arrests. Specifically, the cell wall integrity pathway may be activated in *cdc-ts* arrests,

particularly *cdc28-13*, since cell volume increases rapidly throughout the arrest, causing

significant stress within the cell (36). Another likely candidate is Ras/PKA pathway inactivation

since its hyperactivation prevented ESR activation and size attenuation through ribosomal

downregulation. These pathways, and many others, are highly interconnected, so it would not be

surprising if multiple pathways are involved (37).

   We also suspect that ribosomes may be disassembled, if not wholly degraded. When we

measured the ribosomal fraction of the proteome, we used two independent methods: one

involving purifying assembled ribosomes and the other involving measuring ribosomal proteins

of whole cell lysates. When we measured the rRNA concentration of purified assembled

ribosomes in the ribosome quantification method, there was a more dramatic decrease in the

ribosomal fraction of the proteome than when we measured ribosomal proteins in whole cell

lysates (Fig. 1*B-C*). As previously mentioned, this discrepancy could be simply be due to one of

the many other differences between these two methods, but an alternative, more interesting

140

explanation is that ribosomes may be disassembled when *cdc-ts* mutants are arrested in the cell cycle, and various components may be degraded downstream the disassembly. If disassembly and/or degradation were occurring upon arrest in the cell cycle, ribosomal components may be used in the synthesis of other macromolecules needed for survival as we know that ESR activation leads to increased biosynthesis of certain carbohydrates, fatty acids, and the cell wall (12). In this case, the cell's ribosomes would be used as supply key elements needed to survive cell cycle arrests.

Finally, questions remain concerning the mechanism by which cells continue to be viable after a prolonged arrest in the cell cycle. The differences in cell viability between *cdc-ts* mutants with and without a hyperactive Ras/PKA pathway were striking. When cells were no longer able to activate the ESR, cell viability decreased dramatically (Fig. 4*G-H*). We did not know which components of the ESR were responsible for cell viability or what their respective contributions to survival were. Specifically, we remain curious about the contribution of size attenuation and ribosome downregulation to cell survival in *cdc-ts* arrests. By preventing cells from growing too large and diluting their cytoplasm, ribosomes may be involved in a key mechanism in preventing cell death. Using *cdc-ts* cells as a model system, we have shown that the ESR and ribosome downregulation have profound effects on cell physiology and survival.

Materials and Methods

Yeast strains and growth conditions

Yeast strains used in this study are of the W303 background and described in Table S1. Unless otherwise noted, strains were grown in YEPD complete media. *AID-BCY1* strains were

grown in YEPD supplemented with 138 µL glacial acetic acid for each 1 L YEPD. 500 µM

indole-3-acetic acid (Sigma-Aldrich) was used as auxin in the *AID-BCY1* experiments.

Mean Cell Volume Measurements

      1 mL samples of culture were diluted 1:100 with Isoton II Diluent (Beckman Coulter)

and measured on a Beckman Multisizer 3 Coulter Counter to produce a histogram of the

population's cell volumes. Values above the half-maximal cell count were used to calculate the

mean cell volume of the culture.

Protein and Ribosome Quantification

      Protein and ribosome quantification were performed as in Terhorst et al. (2020, 17).

TMT Proteomics

      TMT Proteomics was performed by the method described in Rose et al. (2016, 40).

GEM Diffusion Measurements

      GEM diffusion measurements were performed as in Delarue et al. (2018; 21).

RNASeq

      RNASeq was performed as in Terhorst et al. (2020, 17). All sequencing was done using

an Illumina HiSeq2000.

Data Processing and Single-Sample Gene Set Enrichment Analysis

Cell Viability Measurements

1 mL samples of culture were diluted 1:100 diluted with Isoton II Diluent (Beckman Coulter) and used to determine cell concentration of the culture using a Beckman Multisizer 3 Coulter Counter. 300 cells were plated on YEPD agar plates and grown at 25ºC until colonies appeared, approximately 3-5 days. Colonies were counted by hand, and values were normalized to the 2-hour time point of each experiment.

Data Availability

RNA-Seq data will be deposited in the Gene Expression Omnibus (GEO) database upon publication.

Strain Table

Strain Table S1. Yeast strains used in this study. Description of the strain names, numbers, genotypes, and source used in this paper.

Name	Number	Genotype	Source
WT Haploid	**A2587**	*MATa, ade2-1, leu2-3, ura3, trp1-1, his3-11,15, can1-100, GAL, psi+*	**Nasmyth Lab**
cdc28-13	**A39000**	*MATa, ade2-1, leu2-3, ura3, trp1-1, his3-11,15, can1-100, GAL, psi+, cdc28-13::URA3*	**Amon Lab**
cdc20-1	**A937**	*MATalpha, cdc20-1, ura3, trp1, leu2, his3, ade2, can1*	**Nasmyth Lab**
cdc15-2	**A2596**	*MATa, cdc15-2, leu2-3, ura3, trp1-1, omns, ade1*	**Nasmyth Lab**
WT GEM	**LH4415**	*MATa, ade2-1, leu2-3, ura3, trp1-1, his3-11,15, can1-100, GAL, psi+ HIS3::pINO4-PfV-Sapphire*	**Holt Lab**
cdc28-13 GEM	**LH4416**	*MATa, ade2-1, leu2-3, ura3, trp1-1, his3-11,15, can1-100, GAL, psi+, cdc28-13::URA3 HIS3::pINO4-PfV-Sapphire*	**Holt Lab**

Data processing and ssGSEA was performed as in Terhorst et al. (2020, 17).

cdc20-1 **GEM**	**LH4417**	*MATalpha, cdc20-1, ura3, trp1, leu2, his3, ade2, can1 HIS3::pINO4-PfV-Sapphire*	**Holt Lab**
cdc15-2 **GEM**	**LH4418**	*MATa, cdc15-2, leu2-3, ura3, trp1-1, omns, ade1 HIS3::pINO4-PfV-Sapphire*	**Holt Lab**
bar1∆	**A2589**	*MATa, bar1::HisG, leu2-3, ura3, trp1-1, his3, ade2, can1-100, GAL, psi+,*	**Nasmyth Lab**
WT **Diploid**	**A33728**	*MATa/alpha, ade2-1, leu2-3, ura3, trp1-1, his3-11,15, can1-100, GAL, psi+*	**Fink Lab**
cdc28-13 **Auxotroph**	**A17896**	*MATa, cdc28-13, ADE2, leu2-3, ura3, trp1-1, his3-11,15, can1-100, GAL, psi+*	**Amon Lab**
cdc28-13 **Prototroph**	**A41270**	*MATa, cdc28-13, ADE2, URA3, TRP1, HIS3, can1-100, GAL, psi+, cdc28- 13, leu2::4xSTRE-GFP:LEU2*	**Amon Lab**
WT **AID-BCY1**	**A40439**	*MATa, ade2-1, leu2-3, ura3, trp1-1, his3-11,15, can1-100, GAL, psi+, KanMX:pRFA1:9Myc-AID-BCY1, leu2::pTEF1-osTIR::LEU2*	**Amon Lab**
cdc28-13 **AID-BCY1**	**A40444**	*MATa, ade2-1, leu2-3, ura3, trp1-1, his3-11,15, can1-100, GAL, psi+, cdc28-13::URA, KanMX:pRFA1:9Myc-AID-BCY1, leu2::pTEF1-osTIR::LEU2*	**Amon Lab**
cdc20-1 **AID-BCY1**	**A40499**	*MATa, ade2-1, leu2-3, ura3, trp1-1, his3-11,15, can1-100, GAL, psi+, cdc20-1, KanMX:pRFA1:9Myc-AID-BCY1, leu2::pTEF1-osTIR::LEU2*	**Amon Lab**
cdc15-2 **AID-BCY1**	**A40501**	*MATa, ade2-1, leu2-3, ura3, trp1-1, his3-11,15, can1-100, GAL, psi+, cdc15-2, KanMX:pRFA1:9Myc-AID-BCY1, leu2::pTEF1-osTIR::LEU2*	**Amon Lab**

References

1. Conrad, M., Schothorst, J., Kankipati, H. N., Van Zeebroeck, G., Rubio-Texeira, M., & Thevelein, J. M. (2014). Nutrient sensing and signaling in the yeast *Saccharomyces cerevisiae*. *Fems Microbiology Reviews*, *38*(2), 254–299. https://doi.org/10.1111/1574-6976.12065

2. Cadart, C., Monnier, S., Grilli, J. *et al.* Size control in mammalian cells involves modulation of both growth rate and cell cycle duration. *Nat Commun* **9,** 3275 (2018). https://doi.org/10.1038/s41467-018-05393-0

3. Dechant, R., & Peter, M. (2008). Nutrient signals driving cell growth. *Current opinion in cell biology*, *20*(6), 678–687. https://doi.org/10.1016/j.ceb.2008.09.009

4. Jorgensen P. & Tyers M. (2004). How cells coordinate growth and division. *Current Biology, 14*(23), R1014-R1027. https://doi.org/10.1016/j.cub.2004.11.027

5. Johnston, G. C., Pringle, J. R., & Hartwell L. H. (1977). Coordination of growth with cell division in the yeast *Saccharomyces cerevisiae*. *Experimental Cell Research, 105*(1), 79-98. https://doi.org/10.1016/0014-4827(77)90154-9

6. Neurohr, G. E., Terry, R. L., Lengefeld, J., Bonney, M., Brittingham, G. P., Moretto, F., Miettinen, T. P., Vaites, L. P., Soares, L. M., Paulo, J. A., Harper, J. W., Buratowski, S., Manalis, S., van Werven, F. J., Holt, L. J., & Amon, A. (2019). Excessive Cell Growth Causes Cytoplasm Dilution and Contributes to Senescence. *Cell*, *176*(5), 1083–1097.e18. https://doi.org/10.1016/j.cell.2019.01.018

7. Yang, J., Dungrawala, H., Hua, H., Manukyan, A., Abraham, L., Lane, W., Mead, H., Wright, J., & Schneider, B. L. (2011). Cell size and growth rate are major determinants of

replicative lifespan. *Cell cycle (Georgetown, Tex.)*, *10*(1), 144–155.

https://doi.org/10.4161/cc.10.1.14455

8. Hartwell, L. H., Culotti, J., & Reid, B. (1970). Genetic control of the cell-division cycle in yeast. I. Detection of mutants. *Proceedings of the National Academy of Sciences of the United States of America*, *66*(2), 352–359. https://doi.org/10.1073/pnas.66.2.352

9. Goranov, A. I., Cook, M., Ricicova, M., Ben-Ari, G., Gonzalez, C., Hansen, C., Tyers, M., & Amon, A. (2009). The rate of cell growth is governed by cell cycle stage. *Genes & Development*, *23*(12), 1408–1422. https://doi.org/10.1101/gad.1777309

10. Warner, J. R. (1999). The economics of ribosomal biosynthesis in yeast. *Trends in Biochemical Sciences 24*(11), 437-440. https://doi.org/10.1016/S0968-0004(99)01460-7

11. Metzl-Raz, E., Kafri, M., Yaakov, G., Soifer, I., Gurvich, Y., & Barkai, N. (2017). Principles of cellular resource allocation revealed by condition-dependent proteome profiling. *eLife*, *6*, e28034. https://doi.org/10.7554/eLife.28034

12. Gasch, A. P., Spellman, P. T., Kao, C. M., Carmel-Harel, O., Eisen, M. B., Storz, G., Botstein, D., & Brown, P. O. (2000). Genomic Expression Programs in the Response of Yeast Cells to Environmental Changes. *Molecular Biology of the Cell*, *11*(12), 4241–4257. https://doi.org/ 10.1091/mbc.11.12.4241

13. Ho, Y. H., Shishkova, E., Hose, J., Coon, J. J., & Gasch, A. P. (2018). Decoupling Yeast Cell Division and Stress Defense Implicates mRNA Repression in Translational Reallocation during Stress. *Current biology : CB*, *28*(16), 2673–2680.e4. https://doi.org/10.1016/j.cub.2018.06.044

14. Nasmyth K. (1993). Control of the yeast cell cycle by the Cdc28 protein kinase. *Current Opinion in Cell Biology, 5*(2), 166-179. https://doi.org/10.1016/0955-0674(93)90099-C

15. Visintin, R., Prinz, S., & Amon, A. (1997). *CDC20* and *CDH1*: A Family of Substrate-Specific Activators of APC-Dependent Proteolysis. *Science 278*(5337), 460-463. https://doi.org/10.1126/science.278.5337.460

16. Visintin, R., & Amon, A. (2001). Regulation of the mitotic exit protein kinases Cdc15 and Dbf2. *Molecular biology of the cell*, *12*(10), 2961–2974. https://doi.org/10.1091/mbc.12.10.2961

17. Terhorst, A., Sandikci, A., Keller, A., Whittaker, C. A., Dunham, M. J., & Amon, A. (2020). The environmental stress response causes ribosome loss in aneuploid yeast cells. *Proceedings of the National Academy of Sciences of the United States of America*, *117*(29), 17031–17040. https://doi.org/10.1073/pnas.2005648117

18. Werner-Washburne, M., Braun, E., Johnston, G. C., & Singer, R. A. (1993). Stationary phase in the yeast Saccharomyces cerevisiae. *Microbiological reviews*, *57*(2), 383–401.

19. Verghese, J., Abrams, J., Wang, Y., & Morano, K. A. (2012). Biology of the heat shock response and protein chaperones: budding yeast (Saccharomyces cerevisiae) as a model system. *Microbiology and molecular biology reviews: MMBR*, *76*(2), 115–158. https://doi.org/10.1128/MMBR.05018-11

20. Zakhartsev, M., & Reuss, M. (2018). Cell size and morphological properties of yeast Saccharomyces cerevisiae in relation to growth temperature. *FEMS yeast research*, *18*(6), 10.1093/femsyr/foy052. https://doi.org/10.1093/femsyr/foy052

21. Delarue, M., Brittingham, G. P., Pfeffer, S., Surovtsev, I. V., Pinglay, S., Kennedy, K. J., Schaffer, M., Gutierrez, J. I., Sang, D., Poterewicz, G., Chung, J. K., Plitzko, J. M., Groves, J. T., Jacobs-Wagner, C., Engel, B. D., & Holt, L. J. (2018). mTORC1 Controls

Phase Separation and the Biophysical Properties of the Cytoplasm by Tuning

Crowding. *Cell*, *174*(2), 338–349.e20. https://doi.org/10.1016/j.cell.2018.05.042

22. Naider, F., & Becker, J. M. (2004). The alpha-factor mating pheromone of

Saccharomyces cerevisiae: a model for studying the interaction of peptide hormones and

G protein-coupled receptors. *Peptides*, *25*(9), 1441–1463.

https://doi.org/10.1016/j.peptides.2003.11.028

23. Goranov, A. I., Gulati, A., Dephoure, N., Takahara, T., Maeda, T., Gygi, S. P., Manalis,

S., & Amon, A. (2013). Changes in cell morphology are coordinated with cell growth

through the TORC1 pathway. *Current biology:CB*, *23*(14), 1269–1279.

https://doi.org/10.1016/j.cub.2013.05.035

24. Ho, Y. H., & Gasch, A. P. (2015). Exploiting the yeast stress-activated signaling network

to inform on stress biology and disease signaling. *Current genetics*, *61*(4), 503–511.

https://doi.org/10.1007/s00294-015-0491-0

25. Martin, D. E., & Hall, M. N. (2005). The expanding TOR signaling network. *Current

opinion in cell biology*, *17*(2), 158–166. https://doi.org/10.1016/j.ceb.2005.02.008

26. Ballensiefen, W., & Schmitt, H. D. (1997). Periplasmic Bar1 protease of Saccharomyces

cerevisiae is active before reaching its extracellular destination. *European journal of

biochemistry*, *247*(1), 142–147. https://doi.org/10.1111/j.1432-1033.1997.00142.x

27. Fingar, D. C., Salama, S., Tsou, C., Harlow, E., & Blenis, J. (2002). Mammalian cell size

is controlled by mTOR and its downstream targets S6K1 and 4EBP1/eIF4E. *Genes &

development*, *16*(12), 1472–1487. https://doi.org/10.1101/gad.995802

28. Chan, Y. H., & Marshall, W. F. (2014). Organelle size scaling of the budding yeast vacuole is tuned by membrane trafficking rates. *Biophysical journal*, *106*(9), 1986–1996. https://doi.org/10.1016/j.bpj.2014.03.014

29. Sheltzer, J. M., Torres, E. M., Dunham, M. J., & Amon, A. (2012). Transcriptional consequences of aneuploidy. *Proceedings of the National Academy of Sciences of the United States of America*, *109*(31), 12644–12649. https://doi.org/10.1073/pnas.1209227109

30. Tarca, A. L., Bhatti, G., & Romero, R. (2013). A comparison of gene set analysis methods in terms of sensitivity, prioritization and specificity. *PloS one*, *8*(11), e79217. https://doi.org/10.1371/journal.pone.0079217

31. Saito, H., & Posas, F. (2012). Response to hyperosmotic stress. *Genetics*, *192*(2), 289–318. https://doi.org/10.1534/genetics.112.140863

32. Klis, F. M., de Koster, C. G., & Brul, S. (2014). Cell wall-related bionumbers and bioestimates of Saccharomyces cerevisiae and Candida albicans. *Eukaryotic cell*, *13*(1), 2–9. https://doi.org/10.1128/EC.00250-13

33. Marion, R. M., Regev, A., Segal, E., Barash, Y., Koller, D., Friedman, N., & O'Shea, E. K. (2004). Sfp1 is a stress- and nutrient-sensitive regulator of ribosomal protein gene expression. *Proceedings of the National Academy of Sciences of the United States of America*, *101*(40), 14315–14322. https://doi.org/10.1073/pnas.0405353101

34. Nishimura, K., Fukagawa, T., Takisawa, H., Kakimoto, T., & Kanemaki, M. (2009). An auxin-based degron system for the rapid depletion of proteins in nonplant cells. *Nature methods*, *6*(12), 917–922. https://doi.org/10.1038/nmeth.1401

35. Brennan, C.M., Kane, A.J., Xu, A.E., Terhorst, A., Denic, V., & Amon, A. (In Review). The environmental stress response dampens heat shock response activation in aneuploid cells.

36. Kono, K., Al-Zain, A., Schroeder, L., Nakanishi, M., & Ikui, A. E. (2016). Plasma membrane/cell wall perturbation activates a novel cell cycle checkpoint during G1 in Saccharomyces cerevisiae. *Proceedings of the National Academy of Sciences of the United States of America*, *113*(25), 6910–6915. https://doi.org/10.1073/pnas.1523824113

37. Chasman, D., Ho, Y. H., Berry, D. B., Nemec, C. M., MacGilvray, M. E., Hose, J., Merrill, A. E., Lee, M. V., Will, J. L., Coon, J. J., Ansari, A. Z., Craven, M., & Gasch, A. P. (2014). Pathway connectivity and signaling coordination in the yeast stress-activated signaling network. *Molecular systems biology*, *10*(11), 759. https://doi.org/10.15252/msb.20145120

38. Pestov, D. G., & Shcherbik, N. (2012). Rapid cytoplasmic turnover of yeast ribosomes in response to rapamycin inhibition of TOR. *Molecular and cellular biology*, *32*(11), 2135–2144. https://doi.org/10.1128/MCB.06763-11

39. An, H., & Harper, J. W. (2020). Ribosome Abundance Control Via the Ubiquitin-Proteasome System and Autophagy. *Journal of molecular biology*, *432*(1), 170–184. https://doi.org/10.1016/j.jmb.2019.06.001

40. Rose, C. M., Isasa, M., Ordureau, A., Prado, M. A., Beausoleil, S. A., Jedrychowski, M. P., Finley, D. J., Harper, J. W., & Gygi, S. P. (2016). Highly Multiplexed Quantitative Mass Spectrometry Analysis of Ubiquitylomes. *Cell systems*, *3*(4), 395–403.e4. https://doi.org/10.1016/j.cels.2016.08.009

Chapter 4: Conclusions and Future Directions

Summary of key conclusions

In eukaryotic cells, mechanisms exist to coordinate cell growth and cell cycle progression because correct cell size determines how a cell functions, survives, and reproduces (1, 2). Mutations in essential cell division cycle genes or chromosome missegregation lead to conditions under which cell cycle progression slows or halts, and cells must re-establish cell size homeostasis (3-6). In this thesis, I highlighted a mechanism through which cells can regulate their biomass accumulation during cell cycle delay or arrest: the environmental stress response. I described the role of the environmental stress response (ESR) in both aneuploid and *cdc-ts S. cerevisiae* and its effects on ribosome content and size regulation.

I first examined whether the ESR is activated in heterogeneous aneuploids populations. A previous study, Tsai et al. (2019; 7), erroneously stated that the "common aneuploidy gene-expression" (CAGE) signature, rather than the ESR, is exhibited in heterogeneous aneuploid populations. However, I showed that the CAGE signature was an artifact of a flawed analysis involving euploid control populations that had grown to confluence and entered stationary phase, a quiescent non-proliferating state. Cells grown into stationary phase exhibited the ESR once passing a certain threshold of density within the culture. When I repeated their protocol without allowing cells to enter stationary phase, activation of the ESR was apparent in heterogeneous aneuploid populations as well as slight activation of the hypo-osmolarity stress pathway, which was also described as part of the CAGE signature. As the ESR is known to cause repression of ribosome biogenesis genes (8), heterogeneous aneuploid populations had a smaller ribosomal fraction of the proteome than euploid populations, which may explain the decreased cellular density of aneuploid cells (7).

I also examined how proliferation rate affects ESR expression and ribosome downregulation by using a series of complex aneuploid strains harboring one or more additional or lost chromosomes (9). There was a correlation between degree of aneuploidy and strength of the ESR in the complex aneuploid strains, as well as between proliferation rate and ESR strength. Growth under nutrient-limiting conditions in a chemostat equalized proliferation rate, and there was no longer a correlation between degree of aneuploidy and strength of the ESR. While under normal growth conditions the ribosomal fraction of the proteome also correlated with degree of aneuploidy and proliferation rate, this correlation was also lost when cells were grown in a chemostat. These experiments in complex aneuploid strains suggested an intimate connection between degree of aneuploidy, proliferation rate, activation of the ESR, and loss of ribosomes.

I next studied three *cdc-ts* strains that arrest in various points of the cell cycle at the restrictive temperature. When arrested, *cdc-ts* cells continue to grow but eventually attenuate biomass accumulation and reach a maximum size. In all three strains, independent of the cell cycle phase in which they were arrested, the ribosomal fraction of the proteome was downregulated and the ESR was expressed to attenuate cell growth. Similarly, in three naturally occurring arrests, each of which involved inhibition of the Ras/PKA pathway and/or the TORC1 pathway, the ESR was activated, and ribosomes were consequently downregulated. In the *cdc-ts* cells, hyperactivation of the Ras/PKA pathway prevented ESR activation and caused cells to lose viability upon re-entrance into the cell cycle, potentially due to their inability to downregulate their ribosomes and attenuate their size.

Altogether, two aneuploid models and three *cdc-ts* mutants had activation of the ESR and coordinated ribosome downregulation. Preventing ESR activation led to suppression of both

ribosome downregulation and size attenuation, suggesting that the ESR may act as a coordinator

of growth and division in arrested cells. Recognizing this role of the ESR can change how we

understand cell size regulation in eukaryotes and provokes us to ask many exciting questions. In

my discussion, I will pose some of these questions and provide experimental designs that would

address them.

Coordination of cell growth and division through the ESR

My work suggests that a main role of the ESR in slow growing cells is to prevent

excessive volume growth by downregulating ribosomes. The results of this thesis lead to a model

of how the ESR can regulate cell size, shown in Figure 1.
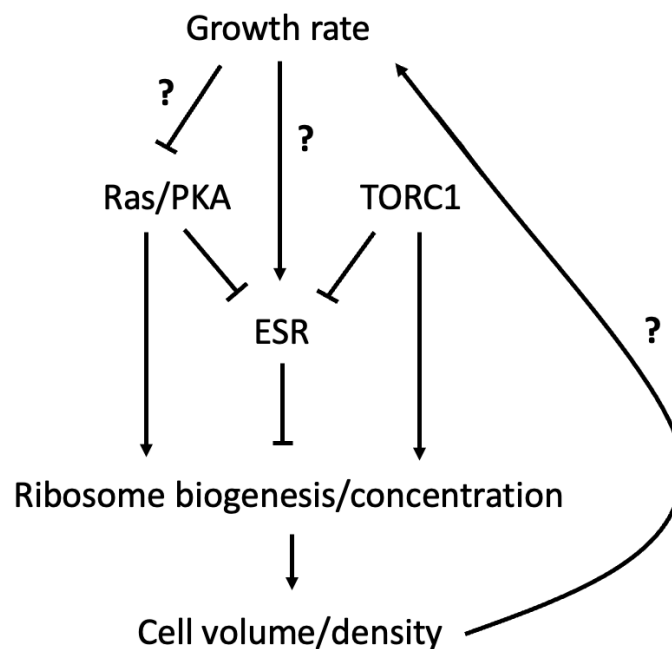
Figure 1. Model for the role of the ESR as a coordinator of cell cycle progression and cell volume. When the cell cycle is delayed or arrested, the ESR is activated, through inhibition of the Ras/PKA and/or TORC1 pathway or through an alternative unknown mechanism. The Ras/PKA and TORC1 pathways may regulate ribosome biogenesis independently of the ESR, but through ESR activation, these parallel pathways enact a dramatic downregulation of ribosome biogenesis, leading to a decreased ribosomal fraction of the proteome. By downregulating ribosomes, cells prevent excessive cell volume growth, and cell density may decrease in some circumstances. The decrease in volume growth and cell density causes slow growing cells to lose their proliferation capacity and further decrease their growth rate, potentially through inability to grow to "critical size" or through unknown mechanism.

Sensing slow growth

In this thesis, I described a relationship between growth rate and ESR strength in aneuploid cells. Under many exogeneous stresses, it is known how the ESR is activated and how the cell cycle stalls. When glucose is depleted, the Ras/PKA pathway activates the ESR and promotes entrance into the quiescent stationary phase (2, 8, 10). Rapamycin addition or depletion of amino acids inhibits the TORC1 pathway, which in turn activates the ESR and arrests cells in G1 (2, 8, 10, 11). MAP kinase (MAPK) pathways respond to stresses such as mating pheromones, hyperosmolarity, and cell wall stress, and many of these have been shown to inhibit the Ras/PKA and/or TORC1 pathways, leading to expression of the ESR and cell cycle arrest (8, 12-15). Aneuploid cells experience a host of stressors, including proteotoxic stress, DNA damage, and increased metabolic burden, that potentially activate the ESR and slow cell growth

(16-18). However, the cause of ESR activation in *cdc-ts* cells remains unknown but prompts the possibility of a potential mechanism that could set a maximum size threshold in budding yeast.

When reflecting on how the ESR may sense slow growth, a "chicken-or-egg" conundrum arises: does the strength of the ESR dictate growth rate or does the rate of growth activate the ESR to various degrees? This puzzling question is represented with the model in Figure 1. First, I will explain why the ESR likely affects growth rate. This thesis has thoroughly shown the ability of the ESR to regulate ribosome biogenesis, leading to decreased ribosome content and biomass accumulation. Without sufficient cell growth, cells spend longer in G1 until they are able to reach the "critical size" threshold (2). Decreasing ribosome content of cells also leads to decreased cell density in some specific conditions, such as in *cdc28-13* cells or in aneuploid strains, and cytoplasmic dilution is known to cause decreased proliferation capacity (7, 19). The evidence for the ESR regulating cell growth does not dismiss the possibility that cell growth affects ESR activation; the two are not mutually exclusive.

Biomass accumulation can initiate entrance into the cell cycle, as cells much reach a "critical size" threshold before Start (2). Potential sizing factors that can sense translational capacity throughout G1 are the Cln3 cyclin and its inhibitor Whi5 (20-22). Sizing factors could act similarly in cells when cell cycle progression is delayed, and candidates include proteins, metabolites, and genome content (19-22). Two potential models of how sizing factors recognize unregulated cell growth are sizing factor accumulation and sizing factor limitation, both described in Figure 2. Downstream signaling to the ESR could function through the Ras/PKA pathway and/or the TORC1 pathway or through a novel mechanism. Signaling through the Ras/PKA pathway is particularly compelling since hyperactivating the Ras/PKA pathway led to
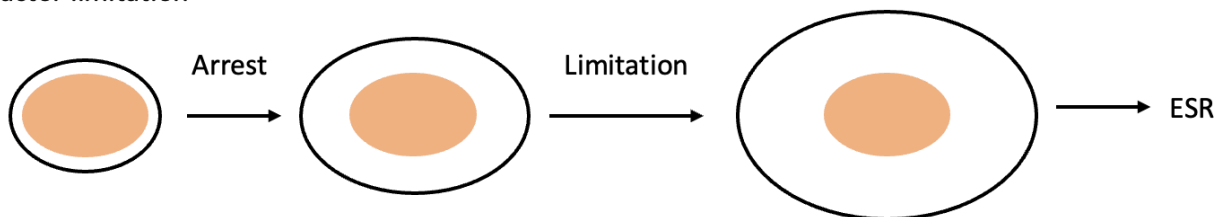
suppression of the ESR. The ability of sizing factors to recognize cell size and signal if cells become too large could provide insight into a main element of maintaining cell size homeostasis.

(a) Sizing factor accumulation
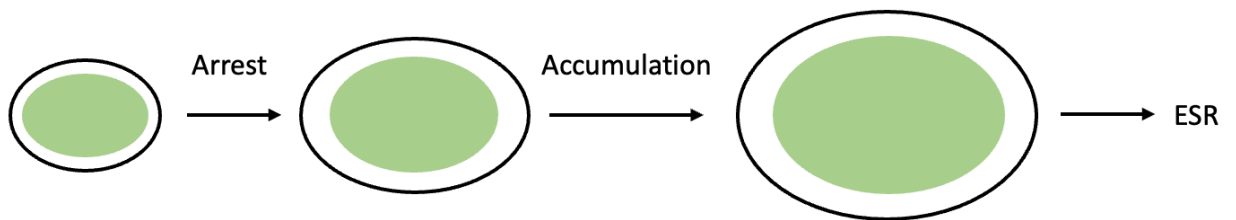
(b) Sizing factor limitation

Figure 2. Potential mechanisms for sensing cell cycle arrest in *cdc-ts* cells.

(a) Sizing factors could activate the ESR by accumulating during cell cycle arrests in *cdc-ts* cells. As cells arrest in the cell cycle but continue to accumulate biomass, sizing factors may scale with size and accumulate in the cell above a certain threshold, resulting in ESR activation.

*(b)* Sizing factors could activate the ESR by becoming limiting during cell cycle arrests in *cdc-ts* cells. When *cdc-ts* cells can no longer progress in the cell cycle, cell volume continues to increase. Sizing factors whose expression are dependent on cell cycle progress may not scale with cell volume and may become limiting, activating the ESR after decreasing below a certain threshold.

I propose that the presence and mechanisms of potential sizing factors in arrested *cdc-ts* cells could be determined with a series of screens, described in Figure 3*A-B*. To alter gene copy number, both a deletion library and an overexpression library could be used in parallel, and the effects of the changes in expression could be determined by measuring cell size and ESR strength. Comparing the effects of each gene in these two contexts could reveal whether certain genes act through sizing factor accumulation or sizing factor limitation. For a sizing factor whose accumulation activates the ESR, deletion of the gene would prevent ESR activation, and cells will continue to increase their volume because the sizing factor would never accumulate. Overexpressing the sizing factor would lead to early ESR activation and prevent growth of *cdc-ts* cells, resulting in smaller cell volume, due to pre-mature accumulation. If the limitation of a sizing factor caused ESR activation, deletion of the sizing factor would cause immediate ESR activation due to abrupt limitation, and cells would not increase in volume. By overexpressing the sizing factor, cells would continue to grow, and the ESR would not be activated because the sizing factor would never become limiting. Importantly, I would repeat these screens in a variety of *cdc-ts* strains to establish whether certain sizing factors were dependent on the cell cycle phase in which cells were arrested.

Finally, in order to ensure that the candidates identified are sizing factors, I would overexpress specific candidates in cells of varying sizes. Using cycloheximide, which prevents translational elongation and can manipulate cell size, populations of *cdc-ts* cells with different mean cell volumes could be generated (2, 19). I expect that the overexpression of sizing factors, hopefully equalizing expression in each condition, would uniquely produce a correlation between ESR strength and mean cell volume, described in Figure 3*C-D*. Through this series of

experiments, I could elucidate the cause of ESR activation in specific *cdc-ts* strains and confirm

the role of the ESR as a size regulator.
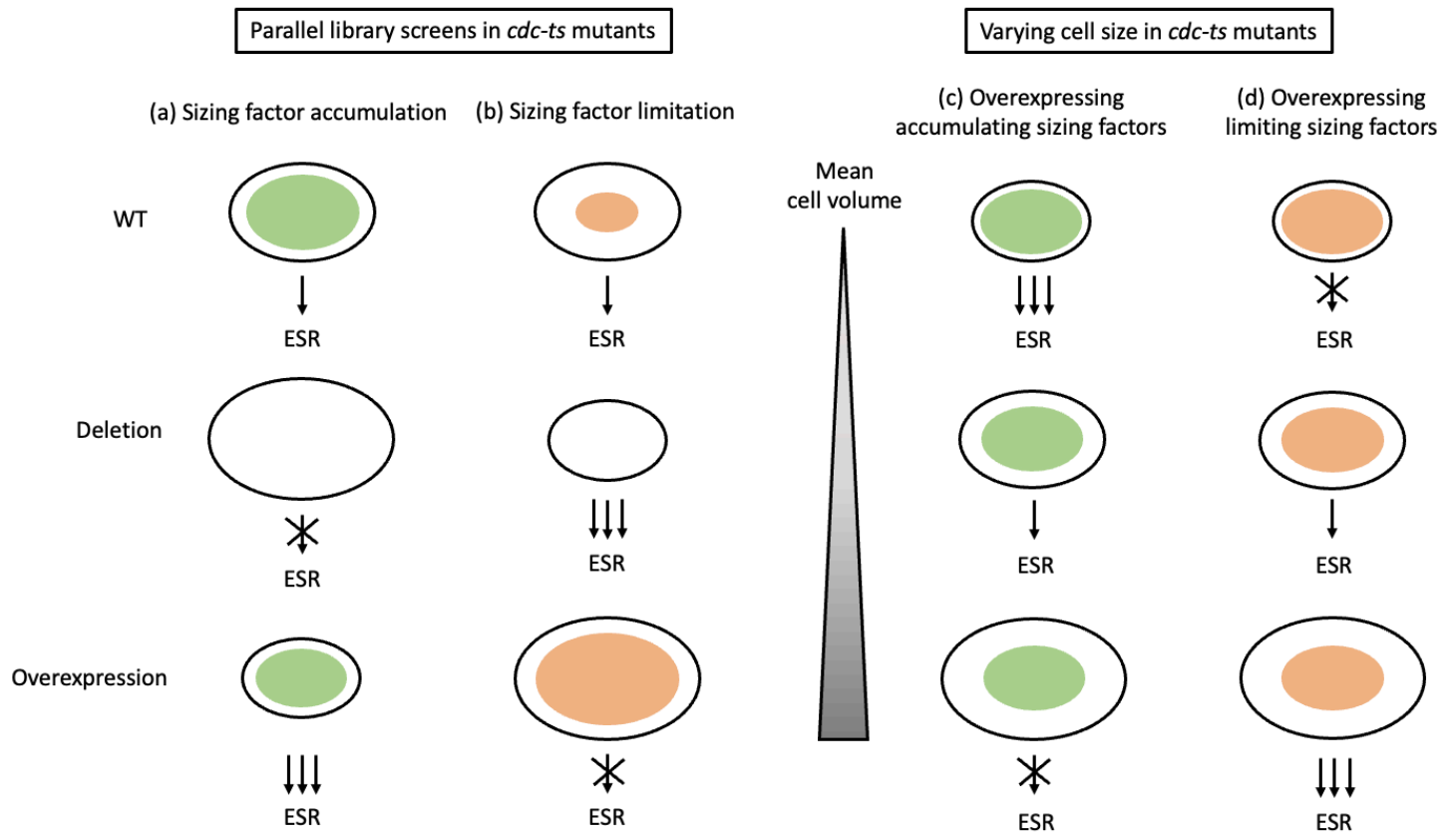
Figure 3. Experimental design to identify and characterize sizing factors.

(*A-B*) Parallel deletion and overexpression screens could reveal sizing factor candidates by

measuring cell size with a Coulter Counter and ESR strength through RNA sequencing. (*A*) If

sizing factor accumulation led to ESR activation, deletion of the sizing factor would lead to no

ESR activation and larger cell volume, while overexpression of the sizing factor would lead to

stronger expression of the ESR, resulting in cells with smaller volume. (*B*) A sizing factor that

activates the ESR through its limitation would produce different results in both screens. Deletion

of the sizing factor would cause pre-mature ESR expression and smaller cells, and

overexpression of the sizing factor would prevent ESR activation and size attenuation.

(*C-D*) Varying cell size in *cdc-ts* mutants could confirm the role of sizing factors in *cdc-ts* cells.

Populations of cells would be arrested and grown to have specific mean cell volumes, and

candidates for sizing factors would be overexpressed under the same exogenous promoter. (*C*) In

sizing factors that activated the ESR through accumulation, ESR strength would decrease with

increasing cell size. (*D*) In sizing factors that activated the ESR through limitation, ESR strength

would decrease with increasing cell size.

Aneuploidy tolerance

The ability of cells to tolerate aneuploidy varies. Cancer cells can tolerate aneuploidy

with ease and even evolve to have specific aneuploid karyotypes (23, 24). In sharp contrast,

aneuploidy in developing cells can have severe consequences on cell viability (23, 24). Only a

handful of aneuploid karyotypes are tolerated in developing human cells, but individuals

harboring cells with these karyotypes often have developmental disabilities. While there are

chromosome-specific effects in human aneuploid cells, there are also global effects, including

slow growth of developing cells, sometimes causing underdevelopment of major organs (23, 24).

Because aneuploidy has profound consequences on human physiology, determining the role of

the ESR in aneuploidy tolerance would be particularly intriguing.

UPB6 **and the ESR**

Work from our lab has found one gene that, upon its deletion, leads to significant

aneuploidy tolerance in budding yeast, *UBP6*, whose gene product is involved in de-

ubiquitination of proteins destined for the proteasome. It is thought that cells without Ubp6 are able to more effectively degrade excess proteins and that the increase in proliferation rate is a result of decreased proteotoxic stress (16, 25, 26). In many disomic strains containing one extra chromosome, known as disomes, cells harboring the *ubp6Δ* mutations had significantly faster doubling times than their wild-type disomic counterparts (25, 26). Deletion of *UBP6* also led to increased ribosome content in many of these disomes, which is likely the reason for the increased proliferation rate (25, 26). As a future direction, I would measure the relative ESR strengths in disomes with and without *UBP6*. I expect that *ubp6Δ* disomes have weaker ESR expression than their wild-type disomic counterparts. Furthermore, in the set of disomes, the changes in ESR expression would correlate to the changes in proliferation rates. By uncovering the role of the ESR in Ubp6-mediated aneuploidy tolerance, we can gain insights into understand how human cancer cells tolerate aneuploidy.

Rescuing proliferation defects

The work of this thesis can be applied to understand aneuploid tolerance by uncovering whether the ESR regulates survival and proliferation in aneuploid cells. I showed that aneuploid cells express the ESR and downregulate their ribosomes in a manner mostly independent of their karyotypes. Hyperactivation of the Ras/PKA pathway led to ESR suppression in *cdc-ts* cells, and an important next experiment would be to resolve whether hyperactivation of the Ras/PKA pathway causes similar ESR suppression in aneuploid cells. Expression of the ESR in aneuploid cells with a hyperactivate Ras/PKA pathway would suggest that the suppression of the ESR through Ras/PKA hyperactivation may be unique to *cdc-ts* cells. If aneuploid cells with a

hyperactive Ras/PKA pathway no longer exhibited the ESR, the Ras/PKA pathway would be implicated as a potentially universal ESR regulator.

Assuming ESR suppression occurred in disomes with a hyperactivated Ras/PKA pathway, I would next measure the proliferation rate in disomes with and without Ras/PKA-mediated ESR suppression. Some disomes may proliferate more slowly or potentially lose viability altogether, as seen in *cdc-ts* cells, when ESR activation is suppressed due to lack of essential ESR components. While the essential components of the ESR could be specific genes that are upregulated, ribosome downregulation itself could also be essential to cell survival in aneuploid cells. In other disomes, doubling time may decrease when ESR activation is suppressed due to lack of ribosome downregulation, suggesting that ESR activation is not essential to cell viability and is antagonistic to proliferation and aneuploidy tolerance. While the former result is more likely, these experiments could begin to uncover a novel mechanism for aneuploidy tolerance. The capability of manipulating the ESR to rescue proliferation defects in aneuploid cells could have significant implications on our understanding of aneuploidy in both cellular and organismal contexts.

Concluding remarks

Cell size regulation is complex and involves many intertwining pathways, but this thesis has highlighted the previously unrecognized significance of the environmental stress response (ESR) in coordinating cell growth and cell cycle progression. I have shown that in two separate models of delayed cell cycle progression, aneuploidy and *cdc-ts* cell cycle arrests, the ESR recognizes endogenous cellular stress and incidentally downregulates ribosome biogenesis, slowing cell growth and maintaining cell viability. Although I have studied mechanisms of cell

size control in budding yeast, my work provides substantial contributions to understanding how the regulation of biomass accumulation and cell division is maintained in all eukaryotes.

References

1. Amodeo, A. A., & Skotheim, J. M. (2016). Cell-Size Control. *Cold Spring Harbor perspectives in biology*, *8*(4), a019083. https://doi.org/10.1101/cshperspect.a019083

2. Jorgensen, P., & Tyers, M. (2004). How cells coordinate growth and division. *Current biology: CB*, *14*(23), R1014–R1027. https://doi.org/10.1016/j.cub.2004.11.027

3. Torres, E. M., Williams, B. R., Tang, Y. C., & Amon, A. (2010). Thoughts on aneuploidy. *Cold Spring Harbor symposia on quantitative biology*, *75*, 445–451. https://doi.org/10.1101/sqb.2010.75.025

4. Siegel, J. J., & Amon, A. (2012). New insights into the troubles of aneuploidy. *Annual review of cell and developmental biology*, *28*, 189–214. https://doi.org/10.1146/annurev-cellbio-101011-155807

5. Hartwell, L. H., Mortimer, R. K., Culotti, J., & Culotti, M. (1973). Genetic Control of the Cell Division Cycle in Yeast: V. Genetic Analysis of cdc Mutants. *Genetics*, *74*(2), 267–286.

6. Goranov, A. I., Cook, M., Ricicova, M., Ben-Ari, G., Gonzalez, C., Hansen, C., Tyers, M., & Amon, A. (2009). The rate of cell growth is governed by cell cycle stage. *Genes & development*, *23*(12), 1408–1422. https://doi.org/10.1101/gad.1777309

7. Tsai, H. J., Nelliat, A. R., Choudhury, M. I., Kucharavy, A., Bradford, W. D., Cook, M. E., Kim, J., Mair, D. B., Sun, S. X., Schatz, M. C., & Li, R. (2019). Hypo-osmotic-like stress underlies general cellular defects of aneuploidy. *Nature*, *570*(7759), 117–121. https://doi.org/10.1038/s41586-019-1187-2

8. Gasch, A. P., Spellman, P. T., Kao, C. M., Carmel-Harel, O., Eisen, M. B., Storz, G., Botstein, D., & Brown, P. O. (2000). Genomic expression programs in the response of

yeast cells to environmental changes. *Molecular biology of the cell*, *11*(12), 4241–4257. https://doi.org/10.1091/mbc.11.12.4241

9. Pavelka, N., Rancati, G., Zhu, J., Bradford, W. D., Saraf, A., Florens, L., Sanderson, B. W., Hattem, G. L., & Li, R. (2010). Aneuploidy confers quantitative proteome changes and phenotypic variation in budding yeast. *Nature*, *468*(7321), 321–325. https://doi.org/10.1038/nature09529

10. Conrad, M., Schothorst, J., Kankipati, H. N., Van Zeebroeck, G., Rubio-Texeira, M., & Thevelein, J. M. (2014). Nutrient sensing and signaling in the yeast Saccharomyces cerevisiae. *FEMS microbiology reviews*, *38*(2), 254–299. https://doi.org/10.1111/1574-6976.12065

11. Moreno-Torres, M., Jaquenoud, M., & De Virgilio, C. (2015). TORC1 controls G1-S cell cycle transition in yeast via Mpk1 and the greatwall kinase pathway. *Nature communications*, *6*, 8256. https://doi.org/10.1038/ncomms9256

12. Goranov, A. I., Gulati, A., Dephoure, N., Takahara, T., Maeda, T., Gygi, S. P., Manalis, S., & Amon, A. (2013). Changes in cell morphology are coordinated with cell growth through the TORC1 pathway. *Current biology: CB*, *23*(14), 1269–1279. https://doi.org/10.1016/j.cub.2013.05.035

13. Sullivan, A., Wallace, R. L., Wellington, R., Luo, X., & Capaldi, A. P. (2019). Multilayered regulation of TORC1-body formation in budding yeast. *Molecular biology of the cell*, *30*(3), 400–410. https://doi.org/10.1091/mbc.E18-05-0297

14. García, R., Bravo, E., Diez-Muñiz, S., Nombela, C., Rodríguez-Peña, J. M., & Arroyo, J. (2017). A novel connection between the Cell Wall Integrity and the PKA pathways

regulates cell wall stress response in yeast. *Scientific reports*, *7*(1), 5703.

https://doi.org/10.1038/s41598-017-06001-9

15. Gutin, J., Sadeh, A., Rahat, A., Aharoni, A., & Friedman, N. (2015). Condition-specific genetic interaction maps reveal crosstalk between the cAMP/PKA and the HOG MAPK pathways in the activation of the general stress response. *Molecular systems biology*, *11*(10), 829. https://doi.org/10.15252/msb.20156451

16. Brennan, C. M., Vaites, L. P., Wells, J. N., Santaguida, S., Paulo, J. A., Storchova, Z., Harper, J. W., Marsh, J. A., & Amon, A. (2019). Protein aggregation mediates stoichiometry of protein complexes in aneuploid cells. *Genes & development*, *33*(15-16), 1031–1047. https://doi.org/10.1101/gad.327494.119

17. Sheltzer, J. M., Blank, H. M., Pfau, S. J., Tange, Y., George, B. M., Humpton, T. J., Brito, I. L., Hiraoka, Y., Niwa, O., & Amon, A. (2011). Aneuploidy drives genomic instability in yeast. *Science (New York, N.Y.)*, *333*(6045), 1026–1030. https://doi.org/10.1126/science.1206412

18. Torres, E. M., Sokolsky, T., Tucker, C. M., Chan, L. Y., Boselli, M., Dunham, M. J., & Amon, A. (2007). Effects of aneuploidy on cellular physiology and cell division in haploid yeast. *Science (New York, N.Y.)*, *317*(5840), 916–924. https://doi.org/10.1126/science.1142210

19. Neurohr, G. E., Terry, R. L., Lengefeld, J., Bonney, M., Brittingham, G. P., Moretto, F., Miettinen, T. P., Vaites, L. P., Soares, L. M., Paulo, J. A., Harper, J. W., Buratowski, S., Manalis, S., van Werven, F. J., Holt, L. J., & Amon, A. (2019). Excessive Cell Growth Causes Cytoplasm Dilution And Contributes to Senescence. *Cell*, *176*(5), 1083–1097.e18. https://doi.org/10.1016/j.cell.2019.01.018

20. Jorgensen, P., Edgington, N. P., Schneider, B. L., Rupes, I., Tyers, M., & Futcher, B. (2007). The size of the nucleus increases as yeast cells grow. *Molecular biology of the cell*, *18*(9), 3523–3532. https://doi.org/10.1091/mbc.e06-10-0973

21. Schmoller, K. M., Turner, J. J., Kõivomägi, M., & Skotheim, J. M. (2015). Dilution of the cell cycle inhibitor Whi5 controls budding-yeast cell size. *Nature*, *526*(7572), 268–272. https://doi.org/10.1038/nature14908

22. Barber, F., Amir, A., & Murray, A. W. (2020). Cell-size regulation in budding yeast does not depend on linear accumulation of Whi5. *Proceedings of the National Academy of Sciences of the United States of America*, *117*(25), 14243–14250. https://doi.org/10.1073/pnas.2001255117

23. Ben-David, U., & Amon, A. (2020). Context is everything: aneuploidy in cancer. *Nature reviews. Genetics*, *21*(1), 44–62. https://doi.org/10.1038/s41576-019-0171-x

24. Sheltzer, J. M., & Amon, A. (2011). The aneuploidy paradox: costs and benefits of an incorrect karyotype. *Trends in genetics: TIG*, *27*(11), 446–453. https://doi.org/10.1016/j.tig.2011.07.003

25. Torres, E.M., Dephoure, N., Panneerselvam, A., Tucker, C.M., Whittaker, C.A., Gygi, S.P., Dunham, M.J., and Amon, A. (2010). Identification of aneuploidy-tolerating mutations. Cell *143*, 71–83.

26. Dephoure, N., Hwang, S., O'Sullivan, C., Dodgson, S. E., Gygi, S. P., Amon, A., & Torres, E. M. (2014). Quantitative proteomic analysis reveals posttranslational responses to aneuploidy in yeast. *eLife*, *3*, e03023. https://doi.org/10.7554/eLife.03023